Ward Identities and Mass Spectrum

of

N=1 Super Yang-Mills Theory on the Lattice

Dissertation
zur Erlangung des Doktorgrades
des Fachbereiches Physik
der Universität Hamburg

vorgelegt von
Robert Kirchner
aus Bonn

Hamburg
September 2000

Gutachter der Dissertation:	PrivDoz. Dr. I. Montvay
	Prof. Dr. G. Mack
Gutachter der Disputation:	Prof. Dr. J. Bartels
	Prof. Dr. K. Fredenhagen
Datum der Disputation:	31. 10. 2000
Dekan des Fachbereiches Physik und Vorsitzender des Promotionsausschusses:	Prof. Dr. F. W. Büßer

Abstract

We study the lattice regularization of $N = 1$ Super Yang-Mills theory. Projecting operators for the low-lying spectrum are discussed. We also consider a "baryonic" state consisting of three gluinos, and develop a numerical strategy to determine its mass in a Monte Carlo simulation. We present numerical results on the low-lying spectrum of $SU(2)$ $N = 1$ Super Yang-Mills theory with light dynamical gluinos.
The lattice regularization of $N = 1$ Super Yang-Mills theory breaks supersymmetry at any finite lattice spacing. We derive the form of the corresponding SUSY Ward identity and carry out renormalization. The ratios of the renormalization coefficients Z_T/Z_S and M_R/Z_S are determined non-perturbatively in a numerical simulation. The form of the renormalized SUSY Ward identity is confirmed numerically. We discuss how the SUSY Ward identity can be used to define a supersymmetric continuum limit, and how its approach can be monitored in numerical simulations.

Zusammenfassung

Wir untersuchen die Gitter Regularisierung von $N = 1$ Super Yang-Mills Theorien. Verschiedene Projektoren für die leichten Mitglieder des Spektrums werden vorgestellt. Außerdem untersuchen wir einen aus drei Gluinos bestehenden baryonartigen Zustand, und entwickeln die notwendigen numerischen Methoden zur Bestimmung seiner Masse in einer Monte Carlo Simulation. Wir stellen unsere numerischen Resultate über die Massen der leichten Mitglieder des Spektrums der $SU(2)$ $N = 1$ Super Yang-Mills Theorie mit leichten dynamischen Gluinos dar.
Die Gitter Regularisierung bricht die Supersymmetrie für endlichen Gitterabstand. Wir leiten die entsprechende SUSY Ward Identität her und renormieren sie. Das Verhältnis der Renormierungskonstanten Z_T/Z_S und M_R/Z_S wird in einer numerischen Simulation nicht-perturbativ bestimmt. Die Form der renormierten SUSY Ward Identität wird numerisch bestätigt. Wir beschreiben wie die SUSY Ward Identität zur Definition des supersymmetrischen Kontinuum-Limes herangezogen werden, und wie dieser Limes in numerischen Simulationen beobachtet werden kann.

As there is a Law of Gravity,
So there is a law of Love,
Working at the Heart of the Universe.

Vimala Thakar

Contents

Introduction

Since the lattice formulation of quantum field theory has been introduced by Wilson [1] in order to describe the low energy regime of strong interactions it has become a major tool in modern elementary particle physics.
Especially with the advent of modern supercomputers the numerical study of lattice-regularized theories such as lattice QCD by Monte Carlo methods has developed into a well established branch of theoretical physics.
One of the main advantages of this approach is the fact that the lattice provides currently the only known non-perturbative regulator of quantum field theory. This opens in principle the possibility to tackle problems that are outside the perturbative realm.
Besides the attempts to compute the hadron spectrum and hadronic matrix elements there are numerous other questions that have been approached either numerically or analytically through the lattice regulation. Among them is the study of the electroweak sector of the Standard Model, confinement and the role of topology in Yang-Mills theories and the study of chiral gauge theories. More recently first steps have been taken to investigate supersymmetric gauge theories numerically using the lattice formulation.
Even though no direct experimental evidence for supersymmetry could be found to this day, there are numerous reasons why the subject is still studied very actively. Softly broken $N = 1$ supersymmetry gives a natural solution to the long-standing hierarchy problem, present in the Standard Model. Furthermore the three different couplings present in a supersymmetric Standard Model become according to todays data equally strong at the scale of $m_G \approx 2 \cdot 10^{16}$ GeV, while the three running couplings of the Standard Model do not meet in one point. Another attractive feature is that once supersymmetry becomes a local gauge symmetry it inevitably becomes a theory of gravity.
In recent years there have been many new results on the non-perturbative regime of supersymmetric gauge theories which has led to a revived interest in the field. Exact solutions including confinement and chiral symmetry breaking could be found in theories with $N = 2$ and $N = 4$ extended supersymmetry [2, 3]. Subsequently some results in the phenomenologically more relevant case of $N = 1$ could be derived by introducing soft breaking terms [4]. In principle the lattice offers the possibility to confirm these results by an independent approach.
The simplest supersymmetric gauge theories are $N = 1$ supersymmetric Yang-Mills (SYM) theories. Besides the gauge field they contain massless Majorana fermions in the adjoint representation. In the case of $SU(N_c)$ gauge theories the adjoint representation has dimension $(N_c^2 - 1)$, and hence there are $(N_c^2 - 1)$ gluons and the same number of Majorana fermions called gluinos.
The general features of the low energy dynamics of $N = 1$ SYM theory have been sum-

marized in terms of low energy effective actions [5, 6]. The basic assumption about the non-perturbative dynamics of SYM theories is that there is confinement and spontaneous chiral symmetry breaking.
The confinement is realized by colorless bound states which are expected to be the relevant degrees of freedom. The mass spectrum is expected to be bounded from below by the mass gap. Furthermore on grounds of the non-vanishing of the Witten index SUSY is expected to be unbroken.
The bound states described by the effective actions belong to chiral supermultiplets. The lowest lying multiplets have a Wess-Zumino type structure. They contain a spin 1/2 fermion which is a gluino-glue bound state, and two spin 0 states with opposite parity. In the literature two different pictures for the low-lying multiplet have been conjectured [5,6]. In the older approach [5] no bound states formed out of gluons are considered, while the more recent approach succeeded in including glueballs in the low energy dynamics.
To study these and related questions directly in a non-perturbative way from first principles a lattice formulation of $N = 1$ SYM theory is needed.
Unfortunately a direct lattice regularization of supersymmetric field theories suitable for a Monte Carlo simulation is prevented by many problems. An obvious problem seems to be that it is impossible to fulfill the continuum algebra of supersymmetry transformations, as there are no lattice generators of the Poincaré group. A second problem is the balance between fermionic and bosonic degrees of freedom required by supersymmetry. The naive lattice formulation produces too many fermions, and a lattice formulation with explicit chiral symmetry and without species doubling was believed not to exist until recently [7,8]. Furthermore until some time ago no algorithm existed that could suitably meet the needs required by a numerical simulation of even the simplest supersymmetric gauge theory, namely $N = 1$ Super Yang-Mills theory.
To formulate supersymmetry on the lattice we follow the ideas of Curci and Veneziano [9]. They propose to adopt the Wilson formulation of the lattice action for a numerical study of $N = 1$ Super Yang-Mills theory. This formulation breaks supersymmetry explicitly by the introduction of a mass term for the fermion, the gluino, and the finite lattice spacing. On the basis of chiral and SUSY Ward identities it is argued that by a proper tuning of the bare gluino mass the chiral and the SUSY limit can be recovered simultaneously. Hence the conclusion is that the absence of a supersymmetric lattice regularization is qualitatively not different from the absence of a chiral regularization.
From the numerical point of view the introduction of the multi-bosonic algorithm [10] and its further development into a two-step variant with measurement correction [11] has made the numerical simulation of $N = 1$ SYM theory possible on todays supercomputers. The main difficulty of a Monte Carlo simulation is the inclusion of light dynamical gluinos. The inclusion of a gluino mass term breaks supersymmetry softly and the bare gluino mass has to be tuned numerically to its critical value which corresponds to the chiral i.e. the supersymmetric limit. For non-zero gluino mass physical quantities like the masses of the bound states are supposed to be analytic functions of the gluino mass.
Although a detailed numerical analysis of $N = 1$ $SU(2)$ SYM theory with light gluinos has been performed previously [12] the picture of the supermultiplet that emerged was incomplete. In the lightest particle group no spin 1/2 fermion was found.
In this thesis we address two questions. On one hand we compute the masses of those particles that are believed to be the building blocks of the low-lying spectrum of $N = 1$ SYM theory. Especially glueballs are included in our considerations. By investigating a

different projecting operator for the gluino-glue particle with respect to [12] a low-lying spin 1/2 state can be identified and the discrepancy of previous simulations is resolved. We also confront our results with the analytical predictions of [5, 6].
The second problem we study is the breaking of supersymmetry introduced by the lattice formulation. We do this by considering the appropriate supersymmetric lattice Ward identity.
For any global symmetry which is broken by the lattice regularization the bare Ward identities have a form which differs from their continuum counterparts by additional breaking terms. We show that in our parameter regime the ratios of the renormalization coefficients of the SUSY Ward identity pertaining to the breaking terms and to the SUSY current can numerically be determined with good precision.
By determining these ratios with the insertion of two independent operators in the Ward identity, we also show that within our numerical accuracy the renormalized SUSY Ward identity of reference [9] holds.
By a non-perturbative tuning of one parameter, the bare gluino mass, a supersymmetric limit can be obtained, which coincides with the zero gluino mass limit.
In this limit the renormalized SUSY Ward identity has the same form as the continuum identity, up to terms that vanish in the continuum limit.
We demonstrate that the approach of the supersymmetric limit defined by the SUSY Ward identity can be monitored numerically by the vanishing of the ratios of the appropriate renormalization constants, as a function of the bare gluino mass.
We will proceed as follows

- Chapter one is dedicated to a brief review of $N = 1$ SYM theory in the continuum. We mention the results of the effective action approaches to $N = 1$ SYM theory which are relevant to our work, and derive formally the supersymmetric Ward identity.

- Chapter two discusses the lattice regularization of $N = 1$ SYM theory that our numerical investigation is based on.
  The projecting operators that are used to calculate the low-lying spectrum are introduced. We also propose a wave function for a three-gluino state, and discuss how its two point correlation function can numerically be evaluated.
  Furthermore we derive the lattice form of the supersymmetric Ward identity and carry out renormalization. Finally we identify the simplest projecting operators that can be inserted in the SUSY Ward identity.

- In Chapter three we present our numerical results. A brief description of the two-step multi-bosonic algorithm is given.
  We show how the masses of the states that are part of the low-lying multiplet are calculated. For every operator we discuss seperately the projection onto the ground state. The question of the approach of the chiral limit is also investigated by means of the analog of the π mass and the η' correlator with respect to QCD.
  Finally we determine numerically the ratios of the renormalization coefficients of the SUSY Ward identity derived in Chapter two. It is shown that smeared sources are necessary to provide the accuracy needed if the tuning of the bare gluino mass to its critical value and hence the approach of the SUSY limit is to be observed numerically by the SUSY Ward identity.

- In the appendices we list the definitions and conventions we use throughout this work. We describe in detail the fit procedure employed in the determination of the ratios of the renormalization coefficients. The properties of the basic fields under the discrete symmetries $\mathcal{T}$ and $\mathcal{P}$ are listed and the explicit form of the breaking term X_S entering in the bare SUSY Ward identity is given.
  Finally we explain our form of even-odd preconditioning and the choice of smeared and local sources that have been used in the inverter.

Chapter 1

N=1 Super Yang-Mills theory

In this Chapter we introduce $N = 1$ Super Yang-Mills theory (SYM) in the continuum. We outline how the Lagrangian can be constructed with the help of superfields and give the explicit form of the SUSY transformations on the fundamental fields. The consequences of the introduction of a gluino mass term breaking supersymmetry softly are also discussed. For the structure of the low-lying spectrum different pictures have been conjectured on the basis of effective actions [5,6]. We summarize the results and point out their differences. In a later Chapter they will be compared to the numerical results we obtain for the low-lying spectrum by a Monte Carlo simulation.
Finally we formally derive the continuum form of the supersymmetric Ward identity. It will be needed in the sequel when we study the supersymmetry breaking introduced by the lattice regulator.

1.1 Introduction to the model

We now define $N = 1$, Super Yang-Mills theory, which underlies all of our following investigation. For definitions and conventions see Appendix A. The action of a $SU(N)$ Yang-Mills theory with $N = 1$ supersymmetry can be written as

$$S_{SUSY} = \mathrm{Re}\left\{ \int d^4x d^2\theta \quad \mathrm{Tr}[W^\alpha W_\alpha] \right\}.$$

The spinorial field strength superfield $W_\alpha(x, \theta, \bar{\theta})$ which depends on the four coordinates x and the anticommuting Weyl spinor variables θ_α, $\bar{\theta}_{\dot{\alpha}}$ $(\alpha, \dot{\alpha} = 1, 2)$ is given by

$$W_\alpha = -\frac{1}{8}(\bar{D}\bar{D})e^{-2V} D_\alpha e^{2V},$$

with the superspace derivative

$$\bar{D}_{\dot{\alpha}} = -\bar{\partial}_{\dot{\alpha}} - i\theta^\beta \sigma^\mu_{\beta\dot{\alpha}} \partial_\mu, \qquad D_\alpha = \partial_\alpha + i\sigma^\mu_{\alpha\dot{\beta}} \bar{\theta}^{\dot{\beta}} \partial_\mu.$$

V=$V(x, \theta, \bar{\theta})$ is the vector superfield. Written in the Wess-Zumino gauge it takes the form

$$V_{WZ}(x, \theta, \bar{\theta}) = \theta\sigma^\mu\bar{\theta}A_\mu(x) + i(\theta\theta)\bar{\theta}\bar{\psi}_w(x) - i(\bar{\theta}\bar{\theta})\theta\psi_w(x) + \frac{1}{2}(\theta\theta)(\bar{\theta}\bar{\theta})D(x).$$

The particle content can be identified as one bosonic vector field $A_\mu(x) = -igT^aA^a_\mu(x)$, its supersymmetric partner, a complex Weyl spinorfield $\psi_w = T^a\psi^a_w$, and one auxiliary scalar field D. T^a defined in Appendix A is a generator of the $SU(N)$ gauge group. We can express the action in terms of these component fields as

$$S_{SYM} = \int d^4x \quad \left\{ -\frac{1}{4}F^a_{\mu\nu}F^a_{\mu\nu} + \frac{1}{2}i\psi^a_w\sigma_\mu(D_\mu\bar{\psi}_w)^a - \frac{1}{2}i(D_\mu\bar{\psi}_w)^a\bar{\sigma}_\mu\psi^a_w + \frac{1}{2}D^aD^a \right\}, \quad (1.1)$$

where $F_{\mu\nu} = -igF^a_{\mu\nu}T^a = \partial_\mu A_\nu - \partial_\nu A_\mu + [A_\mu, A_\nu]$ is the usual field strength tensor and

$$(D_\mu\bar{\psi}_w)^a = \partial_\mu\bar{\psi}^a_w + gf_{abc}A^b_\mu\bar{\psi}^c_w \quad (1.2)$$

is the covariant derivative in the adjoint representation. The auxiliary scalar field D can be integrated out by usual Gauß integration since it has no kinetic term. The above form of the action can be rewritten in terms of one massless Majorana fermion in the adjoint representation $\lambda = ((\psi_w)_\alpha, (\bar{\psi}^{\dot{\alpha}}_w))$. After rotating to the the Euclidean we are left with the on-shell action of $N = 1$ SU(N) Super Yang-Mills theory

$$S_{SYM} = \int d^4x \quad \left\{ \frac{1}{4}F^a_{\mu\nu}(x)F^a_{\mu\nu}(x) + \frac{1}{2}\bar{\lambda}^a(x)\gamma_\mu D_\mu\lambda^a(x) \right\}. \quad (1.3)$$

As usual, expectation values of products of local fields are defined through functional derivatives of the generating functional

$$\mathcal{Z}[J] = \int D[\phi] \quad e^{-S[\phi]-S_{src}[\phi,J]}, \quad (1.4)$$

where the fields to be integrated over are collectively denoted by ϕ and $S_{src}[\phi, J] = \int d^4x\phi(x)J(x)$ is the source term. Because of the Majorana nature of the fermion the effective flavor number is $N_f = \frac{1}{2}$.
The invariance under supersymmetry transformations of the action (1.3), even though manifest by construction can explicitly be seen by applying the following transformations on the fields

$$\begin{aligned} \delta A_\mu(x) &= -2g\bar{\lambda}(x)\gamma_\mu\epsilon, \\ \delta\lambda(x) &= -\frac{i}{g}\sigma_{\mu\nu}F_{\mu\nu}(x)\epsilon, \\ \delta\bar{\lambda}(x) &= \frac{i}{g}\bar{\epsilon}\sigma_{\mu\nu}F_{\mu\nu}(x), \end{aligned} \quad (1.5)$$

where ϵ is a Grassmannian spinor parameter. Under these transformations the Lagrangian density leading to the action (1.3) changes only by a total divergence $\delta L(x) = \partial_\mu\bar{j}_\mu\epsilon$ for a suitable current j_μ. The theory described by (1.3) is an $SU(N)$ Yang-Mills theory with a massless Majorana fermion, called the gluino, in the adjoint representation. Introducing a mass term for the gluino

$$L_{mass} = m_{\tilde{g}}(\bar{\lambda}\lambda)$$

supersymmetry is broken softly, which means that important properties such as the non-renormalization theorem and the cancellation of divergencies are preserved [13].
In the massless case the action (1.3) is invariant under a global $U_A(1)$ transformation

$$\lambda \to e^{-i\phi\gamma_5}\lambda, \qquad \bar{\lambda} \to \bar{\lambda}e^{-i\phi\gamma_5}. \quad (1.6)$$

This global chiral symmetry is anomalous. For the corresponding axial current J^5_μ in case of the gauge group $SU(N_c)$ we have

$$\partial^\mu J^5_\mu = \frac{N_c g^2}{32\pi^2}\epsilon^{\mu\nu\rho\sigma} F^a_{\mu\nu} F^a_{\rho\sigma}. \tag{1.7}$$

This anomaly however leaves a $\mathbb{Z}_{2N_c}$ residual symmetry

$$\phi = \phi_k = \frac{k\pi}{N_c}, \qquad k = 0, 1, ...2N_c - 1.$$

This residual symmetry is expected to be spontaneously broken by a non-vanishing gluino condensate $\langle\bar{\lambda}\lambda\rangle$ to $\mathbb{Z}_2 = \{\phi_0, \phi_{N_c}\}$. In addition arguments have been given for a chirally symmetric phase with vanishing gluino condensate [14].
For the gauge group $SU(2)$ instanton calculations [15] indicate that two degenerate ground states exist, differing in the sign of the gluino condensate. A non-zero gluino mass breaks the degeneracy of the two ground states, such that $\langle\bar{\lambda}\lambda\rangle > 0$ for $m_{\tilde{g}} > 0$ and $\langle\bar{\lambda}\lambda\rangle < 0$ for $m_{\tilde{g}} < 0$. The symmetry breaking is linear in $m_{\tilde{g}}$, so the two ground states are exchanged at $m_{\tilde{g}} = 0$ and a first order phase transition is expected (see [16] for a numerical study).
As in QCD we expect the low-lying spectrum to consist of colorless bound states formed out of the fundamental fields, the gluons and the gluinos. These should be organized in supermultiplets at the supersymmetric point $m_{\tilde{g}} = 0$.

1.2 Effective action approaches to the low-lying spectrum

To study the low energy behavior of $N = 1$ SYM theory an effective action has been proposed by Veneziano and Yankielowicz [5]. To formulate this action they identify all degrees of freedom that they expect to govern the low energy dynamics of the theory. These are the gauge invariant and colorless composite fields

$$\begin{aligned}
&F^a_{\mu\nu} F^a_{\mu\nu},\\
&F^a_{\mu\nu} \tilde{F}^a_{\mu\nu},\\
&\bar{\lambda}^a \lambda^a,\\
&\sigma_{\mu\nu} F^a_{\mu\nu} \lambda^a.
\end{aligned} \tag{1.8}$$

The operators FF, $F\tilde{F}$ and $\bar{\lambda}\lambda$ are well known from QCD, while $\chi = \sigma F \lambda$ is a new type of composite operator, which can be formed since the gluino λ and the gauge field F are both in the adjoint representation. The fields in (1.8) can be combined to form the chiral superfield

$$S(x,\theta) = \phi(x) + \sqrt{2}\theta\chi(x) + \theta\theta F(x), \tag{1.9}$$

with the following constituents[1]:

$$\phi = \frac{\beta(g)}{2g}(\psi_w)^\alpha(\psi_w)_\alpha, \quad \sqrt{2}\chi_a = -\frac{\beta(g)}{2g}\left\{-i(\psi_w)_a D + (\sigma^{\mu\nu}\psi_w)_\alpha F_{\mu\nu}\right\},$$
$$F = -\frac{\beta(g)}{g}\left\{-\frac{1}{4}F^{\mu\nu}F_{\mu\nu} - \frac{i}{2}\psi_w\sigma^\mu\partial_\mu\bar{\psi}_w - \frac{i}{8}F^{\mu\nu}\epsilon_{\mu\nu\rho\tau}F_{\rho\tau} + \frac{i}{2}\partial^\mu J^5_\mu + \frac{1}{2}D^2\right\}.$$

[1] We follow the conventions of reference [17].

In these expressions $\beta(g)$ is the beta function of the model whose exact form is known [18]. ψ_w denotes a two component Weyl-spinor. D stands for the D component of the non-abelian vector superfield. This auxiliary field, since it has no kinetic term can be integrated out.
The effective action is formulated so that the underlying symmetries and the anomaly structure of the theory are respected.

$$L_{eff} = \frac{1}{\alpha}(S^\dagger S)^{\frac{1}{3}}|_D + \gamma\left[(S\log\frac{S}{\mu^3} - S)|_F + h.c.\right], \tag{1.10}$$
$$\text{with} \quad \mu = \mu_0 \exp\frac{8\pi^2}{3N_c g_0^2}, \qquad \alpha,\gamma > 0.$$

Expanding the effective Lagrangian around its minimum, it is found that the low-lying spectrum forming a supermultiplet of the Wess-Zumino type consists of

- a scalar boson $\phi = \bar{\lambda}\lambda$. In analogy to QCD but remembering that the gluino is in the adjoint representation we call this particle a-f_0.
- a pseudoscalar boson $\phi_p = \bar{\lambda}\gamma_5\lambda$ called a-η' in the sequel.
- a massive Majorana fermion $\chi = \sigma_{\mu\nu}F_{\mu\nu}\lambda$ which we will refer to as the gluino-glue.

As in QCD the "would be" Goldstone boson a-η' receives a mass by the chiral anomaly. By supersymmetry also the other members of the multiplet become massive. The gluonic fields $F\tilde{F}$ and FF arise only quadratically as auxiliary fields in the action and can be integrated out, so they are not a part of the particle multiplet.
Nevertheless it is not clear why glueballs should be absent in the low-lying spectrum. Furthermore they could couple to the a-η' and the a-f_0 states which in turn could have a dynamical effect on the masses. Since this model closely resembles QCD in analogy one would expect the 0^+ glueball to be the lightest glueball state [19].
The lattice formulation of $N = 1$ Super Yang-Mills theory that we will adopt later (see, Chapter 2) breaks chiral invariance and supersymmetry by the introduction of a gluino mass. It is therefore relevant to investigate how such a mass term affects the spectrum of the effective theory proposed. The introduction of a gluino mass breaks supersymmetry softly and leads to a splitting of the multiplet. If the introduced gluino mass m_0 is small the splitting is linear in m_0 and has been estimated to be [20]

$$\frac{\Delta m^{0-}_{\tilde{g}\tilde{g}}}{m_0} \div \frac{\Delta m_{\tilde{g}g}}{m_0} \div \frac{\Delta m^{0+}_{\tilde{g}\tilde{g}}}{m_0} = 5 \div 6 \div 7. \tag{1.11}$$

$\Delta m_{\tilde{g}g}$ denotes the splitting of the gluino-glue particle, and $\Delta m_{\tilde{g}\tilde{g}}$ is the splitting of the gluino-gluino meson-type particles.
The question how to include glueballs in the low energy scenario has been addressed by Farrar, Gabadadze and Schwetz [6]. In their approach they formulate an effective action respecting the symmetries and the anomaly structure, in terms of a general tensor superfield, which contains an extra term with respect to the Veneziano-Yankielowicz action. This extra term gives then dynamics to the degrees of freedom that can be identified with the glueballs. By studying the potential of the effective Lagrangian two multiplets can be

identified. For unbroken supersymmetry the masses of these two multiplets are not identical. The heavier multiplet corresponds to the Veneziano-Yankielowicz multiplet. The lighter one contains

- a 0^+ glueball $\sim F_{\mu\nu}F^{\mu\nu}$,
- a 0^- glueball $\sim F_{\mu\nu}\epsilon^{\mu\nu\rho\tau}F_{\rho\tau}$,
- a gluino-glue ground state.

Channels with the same quantum numbers such as the 0^+ channel with the a-f_0 and the 0^+ glueball, and the 0^- channel with the a-η' and the 0^- glueball can undergo mixing. Such a mixing leads to a larger splitting in mass between the two multiplets. By introducing a gluino mass term in the action, again the supersymmetry is broken softly and the multiplets themselves split up.

$$\frac{\Delta m^{0-}_{\tilde{g}\tilde{g}}}{m_0} \div \frac{\Delta m_{\tilde{g}g}}{m_0} > 1, \qquad \frac{\Delta m_{\tilde{g}g}}{m_0} \div \frac{\Delta m^{0+}_{\tilde{g}\tilde{g}}}{m_0} > 1.$$

Note that here the splitting is quantitatively different from the one predicted for the Veneziano-Yankielowicz multiplet (see, 1.11).
One of the central issues of this work that we start to address in the next Chapter is the attempt to calculate the masses for the particles making up these multiplets, non-perturbatively on the lattice.

1.3 SUSY Ward identity for N=1, SYM theory.

Let us now consider the supersymmetric Ward identity. In what follows we proceed formally, i.e. without paying attention to the proper definition of the correlation functions that occur.
In Euclidean space the expectation value of any operator $\mathcal{O}$ that is the product of local composite fields is given by the functional integral

$$\langle \mathcal{O} \rangle = \frac{1}{\mathcal{Z}[0]} \int D[\phi]\ \mathcal{O} e^{-S}. \tag{1.12}$$

$\mathcal{Z}[0]$ is the source free generating functional (1.4). The fields that are integrated over in the path integral are collectively denoted by ϕ. The action S is defined as in (1.3). Starting from this expression the general supersymmetric Ward identity can be obtained by applying the infinitesimal local supersymmetry transformations

$$\begin{aligned} \delta A_\mu(x) &= -2g\bar{\lambda}(x)\gamma_\mu \epsilon(x), \\ \delta\lambda(x) &= -\frac{i}{g}\sigma_{\mu\nu}F_{\mu\nu}(x)\epsilon(x), \\ \delta\bar{\lambda}(x) &= \frac{i}{g}\bar{\epsilon}(x)\sigma_{\mu\nu}F_{\mu\nu}, \end{aligned}$$

to the integration variables. The function $\epsilon(x)$ is smooth, Grassmannian and vanishes outside some bounded region $\mathcal{M}$. A general change of variables of the path integral will not change the expectation value (1.12)

$$\langle \mathcal{O} \rangle = \langle \mathcal{O} \rangle^{\epsilon}. \tag{1.13}$$

The right side of the above equation denotes the expectation value calculated with the transformed variables. If we now suppose that the measure is invariant under the local supersymmetry transformations we can conclude that

$$-\langle \delta S \mathcal{O} \rangle + \langle \delta \mathcal{O} \rangle = 0. \tag{1.14}$$

Note that the assumption of the invariance of the path integral measure is equivalent to assuming that the theory under consideration has no supersymmetric anomaly [21]. The supersymmetric variation of the action can be worked out straightforwardly [22] to be

$$\begin{aligned} \delta S &= -\int d^4x \quad \epsilon(x)\partial_\mu S_\mu, \\ S_\mu(x) &= -2\frac{i}{g}\mathrm{Tr}\left[\sigma_{\rho\tau}\gamma_\mu F_{\rho\tau}(x)\lambda(x)\right]. \end{aligned} \tag{1.15}$$

Since $\epsilon(x)$ can be chosen arbitrarily (with the above restrictions) we conclude that

$$\langle \partial_\mu S_\mu(x)\mathcal{O}(y) + \delta\mathcal{O}(y) \rangle = 0. \tag{1.16}$$

Under the further assumption that the product of operators $\mathcal{O}$ is localized outside the domain $\mathcal{M}$ the variation $\delta\mathcal{O}$ vanishes and equation (1.16) reduces to

$$\langle \partial_\mu S_\mu(x)\mathcal{O}(y) \rangle = 0, \tag{1.17}$$

where $y \neq x$. This avoids the occurrence of contact terms and simplifies the analysis that follows.
The lattice regularization that we are going to adopt introduces a gluino mass term and thus breaks supersymmetry. For this reason we will consider also the Ward identity that derives from the action (1.3) with an additional mass term $L_m(x) = m_0\mathrm{Tr}[\bar\lambda(x)\lambda(x)]$. This term gives rise to an additional term D_S in the Ward identity stemming from the variation of L_m. It takes the form

$$D_S(x) = 2\frac{i}{g}\mathrm{Tr}\left[\sigma_{\rho\tau}F_{\rho\tau}(x)\lambda(x)\right], \tag{1.18}$$

and the Ward identity (1.16) modifies to

$$\langle \partial_\mu S_\mu(x)\mathcal{O}(y) - m_0 D_S(x)\mathcal{O}(y) \rangle = 0. \tag{1.19}$$

Chapter 2

N=1 Super Yang-Mills theory on the lattice

In this Chapter we will formulate $N = 1$ Super Yang-Mills theory on the lattice and address the problems that arise using this regularization. The method employed by us to handle these problems is explained. We also give a detailed description of the operators and the numerical strategies used to address the two main subjects of this work, namely the calculation of the masses of the low-lying multiplet, and the study of supersymmetry breaking by Ward identities. Finally the lattice form of the SUSY Ward identity is derived and its renormalization is carried out.

2.1 Regularization of the path integral

The question whether it is possible to successfully formulate a supersymmetric theory on the lattice has been addressed by numerous authors in the past [9, 23–27]. More precisely, the question asked was whether a supersymmetric gauge theory can be formulated on the lattice in such a way that firstly, a supersymmetric limit can consistently be defined and secondly numerical simulations can be performed.

It seems clear immediately that a lattice theory will not have explicit supersymmetry at non-zero lattice spacing. The anticommutator of the infinitesimal supersymmetry transformations closes with the four momentum $\{Q_\alpha, Q_\beta\} = -2(\gamma_\mu C)_{\alpha\beta}P_\mu$, and since the lattice regularization breaks Poincaré invariance also supersymmetry is broken.

The fact that $N = 1$, SYM theory is a chiral theory and supersymmetry requires an exact balance between fermionic and bosonic degrees of freedom leads to another problem. Until recently [7, 8] it was believed that a lattice simulation with explicit chiral symmetry and without the doubling of fermion species is impossible [28] [1]. These problems reflect, on the lattice, the difficulty of defining a manifestly SUSY-invariant regularization.

The way we will deal with these problems has been proposed by Curci and Veneziano [9]. They suggest to regularize $N = 1$ Super Yang-Mills theory with the Wilson formulation for the fermionic and the gauge part of the action and let the lattice regularization spoil supersymmetry. Supersymmetry is then recovered, as chiral symmetry in QCD by an

[1] Some new ways have been pointed out in this direction, using Ginsparg-Wilson fermions [7, 8].

appropriate tuning of the bare parameters of the lattice theory. Approaching thus the continuum theory it is hoped that enough of the supersymmetry can be restored, so that its manifestation can be seen, for instance in the particle spectrum.
In our case, namely $N = 1$ Super Yang-Mills theory, the theory is equivalent to a Yang-Mills theory with a massless Majorana fermion in the adjoint representation. The only two parameters that can be tuned to define the continuum theory are the gauge coupling β and the mass of the Majorana fermion, the gluino.
In the chiral limit $m_{\tilde{g}} = 0$, which is approached through a proper tuning of the bare gluino mass (i.e. the hopping parameter $K \sim \frac{1}{m_0}$) supersymmetry is partially restored, though still broken by the finite lattice spacing.
If the gauge coupling β is in the scaling region supersymmetry should make itself manifest through the formation of multiplets in the low-lying spectrum.
On the other hand the supersymmetric limit which coincides with the chiral limit [9] can be defined with the help of the SUSY Ward identity. Additional breaking terms in the lattice Ward identity arise from the explicit breaking of supersymmetry (see Chapter 2.3). The supersymmetric limit is defined to be the point in parameter space where these breaking terms vanish and the Ward identity takes its continuum form.

2.1.1 Majorana fermions on the lattice

Let us now turn to the lattice formulation of $N = 1$ SYM theory that we will use in the sequel. As suggested by Curci and Veneziano [9] we take the Wilson action for the gluino as well as the gluon field. Basic notations and conventions can be found in Appendix A. The lattice action is

$$S_{CV}^{lattice} = S_U + S_f. \tag{2.1}$$

S_U is the standard gauge field action

$$S_U = \beta \sum_{pl} \left(1 - \frac{1}{N_c} \mathrm{Re}\left[\mathrm{Tr}[U_{pl}]\right] \right), \tag{2.2}$$

with $\beta = 2N_c/g^2$. The standard plaquette $U_{\mu\nu}$ is defined as

$$\begin{aligned} U_{\mu\nu} &= U(x, x+\hat{\nu})U(x+\hat{\nu}, x+\hat{\nu}+\hat{\mu})U(x+\hat{\mu}+\hat{\nu}, x+\hat{\mu})U(x+\hat{\mu}, x), \\ &= U_\nu^\dagger(x)U_\mu^\dagger(x+\hat{\nu})U_\nu(x+\hat{\mu})U_\mu(x). \end{aligned} \tag{2.3}$$

The fermionic action S_f, with the fermions in the adjoint representation and the fermion fields rescaled as in standard lattice QCD fashion by a factor of $\sqrt{1/2K}$ can be written as

$$\begin{aligned} S_f \;=\; & \frac{1}{2} \sum_x \Bigg\{ \bar{\lambda}_r^\alpha(x)\lambda_r^\alpha(x) \\ & -K \sum_{\mu=1}^{4} \left[\bar{\lambda}_r^\alpha(x+\hat{\mu}) V_{\mu,rs}(x)(1+\gamma_\mu)^{\alpha\beta}\lambda_s^\beta(x) + \bar{\lambda}_r^\alpha(x)(V^T)_{\mu,rs}(x)(1-\gamma_\mu)^{\alpha\beta}\lambda_s^\beta(x+\hat{\mu}) \right] \Bigg\}. \end{aligned}$$

We have fixed the Wilsonian-parameter to r=1 and the hopping parameter K is given by $K = (2m_0 + 8r)^{-1}$, with m_0 the bare gluino mass in lattice units. Note the factor $\frac{1}{2}$ relative to the QCD action with Wilson fermions stemming from the Majorana nature of the fermions. The fermions transform under the adjoint representation of the gauge group and satisfy the Majorana condition

$$\lambda = \lambda^C = C\bar{\lambda}^T. \tag{2.4}$$

The adjoint gauge field is defined as

$$V_{\mu,ab}(x) \equiv 2\mathrm{Tr}[U_\mu^\dagger(x)T^a U_\mu(x)T^b] = V_{\mu,ab}(x)^* = [V_{\mu,ab}(x)^T]^{-1}, \tag{2.5}$$

where the trace acts on color indices in the fundamental representation. Transposition and inversion act on color indices. The generators T^a are normalized in the usual way by $\mathrm{Tr}[T^aT^b] = \frac{1}{2}\delta^{ab}$. In the case of SU(2) they are given by $T^a = \frac{1}{2}\sigma^a$ with the Pauli matrices σ^a.
Introducing the fermion matrix

$$Q_{ab}^{\alpha\beta}(x,y) = \delta_{ab}\delta_{xy}\delta^{\alpha\beta} - K\sum_{\mu=1}^{4}\left[\delta_{y,x+\hat{\mu}}(1+\gamma_\mu)^{\alpha\beta}V_{\mu,ab}(x) + \delta_{y+\hat{\mu},x}(1-\gamma_\mu)^{\alpha\beta}(V^T)_{\mu,ab}(y)\right], \tag{2.6}$$

the fermionic action can be rewritten as

$$\begin{aligned} S_f &= \frac{1}{2}\sum_{x,y}\bar{\lambda}_a^\alpha(x)Q_{ab}^{\alpha\beta}(x,y)\lambda_b^\beta(y), \\ &= \frac{1}{2}\sum_{x,y}\lambda_a^\alpha(x)C^{\alpha\gamma}Q_{ab}^{\gamma\beta}(x,y)\lambda_b^\beta(y). \end{aligned}$$

The fermion Matrix Q is not hermitian, but using the property

$$Q^\dagger = \gamma_5 Q\gamma_5 \tag{2.7}$$

we can define the hermitian matrix $\tilde{Q} = \gamma_5 Q$, and we conclude that $\det Q = \det\tilde{Q}$ must be real. The fermion matrix Q furthermore fulfills the relations

$$CQC^{-1} = Q^T, \qquad C\gamma_5 Q\gamma_5 C^{-1} = Q^*, \tag{2.8}$$

from which follows that CQ is antisymmetric, and that the eigenvalues of the fermion matrix are doubly degenerate, so that the fermionic determinant is non-negative.
The theory is then defined by the generating functional

$$\mathcal{Z}[J] = \int \mathcal{D}U\mathcal{D}\lambda \;\; e^{-S_g - S_f - \sum_x J(x)\lambda(x)}, \tag{2.9}$$

where J is the source of the gluino field λ. As we are working with Majorana fermions possessing only half the degrees of freedom of Dirac fermions the fermionic integration is only over $\mathcal{D}\lambda$. The fermions can be integrated out using the change of variables

$$\begin{aligned} \lambda_a^\alpha(x)' &= \lambda_a^\alpha(x) + \sum_y J_b^\beta(M^{-1})_{ba}^{\beta\alpha}(x,y), \\ M_{ba}^{\beta\alpha}(x,y) &= [CQ]_{ba}^{\beta\alpha}(x,y). \end{aligned}$$

Substituting the above in (2.9) and simplifying the expression we obtain

$$\mathcal{Z}[J] = \int \mathcal{D}U\mathcal{D}\lambda' \quad e^{-S_g - \frac{1}{2}\sum_{x,y}[\lambda'(x)M(x,y)\lambda'(y)+J(x)M^{-1}(x,y)J(y)]}. \tag{2.10}$$

The integral

$$\int \mathcal{D}\lambda \quad e^{-\frac{1}{2}\sum_{x,y}\lambda(x)M(x,y)\lambda(y)} \tag{2.11}$$

is the Pfaffian of the antisymmetric matrix $M = CQ$. It can be defined for a complex antisymmetric matrix $M_{\alpha\beta}$ with an even number of dimensions $2N$ by the Grassmann integral

$$\mathcal{PF}[M] = \int \mathcal{D}\phi \quad e^{-\frac{1}{2}\phi_\alpha M_{\alpha\beta}\phi_\beta} = \frac{1}{N!2^N}\epsilon_{\alpha_1\beta_1...\alpha_N\beta_N}M_{\alpha_1\beta_1}...M_{\alpha_N\beta_N}, \tag{2.12}$$

where $\mathcal{D}\phi = d\phi_{2N}...d\phi_1$, and ϵ is the totally antisymmetric unit tensor. By doubling the number of integration variables one can show that

$$[\mathcal{PF}[M]]^2 = \det M. \tag{2.13}$$

Integrating out the Pfaffian, for the generating functional we finally arrive at

$$\mathcal{Z}[J] = \int \mathcal{D}U \quad \mathcal{PF}[M]e^{-S_g - \frac{1}{2}\sum_{x,y}J(x)M^{-1}(x,y)J(y)}. \tag{2.14}$$

Let us comment on a confusion concerning the sign of the Pfaffian $\mathcal{PF}[M]$.
It has been observed by Witten [29] that a $SU(2)$ Yang-Mills theory with a single Weyl fermion in the fundamental representation cannot be defined straightforwardly. The determinant of the Weyl-Dirac operator cannot be made gauge invariant without violating any other fundamental principle like locality or analyticity. By choosing a suitable gauge transformation the determinant changes sign which renders the theory ill defined.
In our case the Pfaffian of equation (2.12) is gauge invariant. No ambiguity exists and the theory is uniquely defined.
Nevertheless the numerical implementation of the Pfaffian weight in the path integral that we have chosen makes it necessary to investigate the question of the sign of the Pfaffian for the set of configurations we use to approximate the path integral. This issue is discussed in Chapter 3.1.4. It must be stressed that the question of the sign of the Pfaffian we investigate is not connected to the above mentioned Witten anomaly.
Expectation values for Majorana fermions can now be defined in the usual way by functional differentiation with respect to the source J

$$\begin{aligned}\left\langle \mathrm{T}\{\lambda(x_1)...\lambda(x_n)\bar{\lambda}(y_1)...\bar{\lambda}(y_n)\}\right\rangle &= \langle \mathrm{T}\{\lambda(x_1)...\lambda(x_n)\lambda(y_1)...\lambda(y_n)\}\rangle C...C, \\ &= 2^n\left[\frac{\delta^{2n}\ln(\mathcal{Z}[J])}{\delta J(x_1)...\delta J(x_n)\delta J(y_1)...\delta J(y_n)}\right]C...C.\end{aligned} \tag{2.15}$$

The gluino propagator for example is defined as

$$\begin{aligned}\left\langle \mathrm{T}\{\lambda(x)\bar{\lambda}(y)\}\right\rangle &= \langle \mathrm{T}\{\lambda(x)\lambda(y)\}\rangle C = 2\left[\frac{\delta^2\ln(\mathcal{Z}[J])}{\delta J(x)\delta J(y)}\right]C, \\ &= \left\langle M^{-1}(x,y)\right\rangle C = \left\langle Q^{-1}\right\rangle.\end{aligned} \tag{2.16}$$

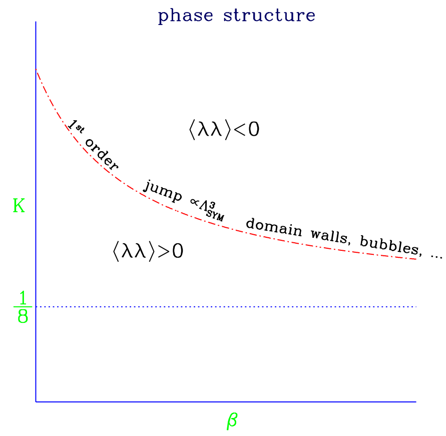

Figure 2.1: *Expected phase structure of $N = 1$ SYM theory. The line represents a first order phase transition where supersymmetry is expected.*

In the following we will denote the inverse fermion matrix Q^{-1} by $\Delta = Q^{-1}$. An important consequence of the Majorana nature of the gluino is the fact that unlike in the case of QCD Wick contractions of the form $\lambda(x)\lambda(y) = M^{-1}(x,y)$ and $\bar{\lambda}(x)\bar{\lambda}(y) = C^T M^{-1} C(x,y)$ are allowed.
A different formalism to arrive at the same results has been introduced in [11]. In this approach the Majorana fields are rewritten in terms of Dirac fields by doubling the degrees of freedom in the fermionic path integral and balancing it with a factor of $\mathcal{PF}[Q]$. Expectation values of any operator are then obtained as in QCD (see [30]). The two formalisms are equivalent and hence can both be used to calculate correlation functions of different operators. For the three-gluino propagator of Chapter 2.2.4 both formalisms were carried out to check the calculation.
As the lattice transcription of the field strength $F_{\mu\nu}$ we will use $P_{\mu\nu}$ defined as

$$P_{\mu\nu} = \frac{U_{\mu\nu} - U_{\mu\nu}^{\dagger}}{2i}. \tag{2.17}$$

2.1.2 The critical hopping parameter

As mentioned above the bare parameters of the lattice theory, β and K have to be properly tuned to arrive at the supersymmetric limit. To discuss the tuning of the bare parameters we consider the (β, K) plane spanned by the gauge coupling β and the hopping parameter $K \sim \frac{1}{m_0}$. As discussed in Chapter 1.1 for vanishing gluino mass ($K = K_{cr}$) we expect two degenerate vacua characterized by different expectation values of the gluino condensate $\langle\bar{\lambda}\lambda\rangle$. Thus on the critical line $K = K_{cr}(\beta)$ we anticipate a first order phase transition between two phases characterized by the gluino condensate $\langle\bar{\lambda}\lambda\rangle$.
The critical line corresponding to zero gluino mass $m_{\tilde{g}} = 0$ can roughly be estimated perturbatively. The expected phase structure, supported by numerical evidence from discrete chiral symmetry breaking [16] can be seen in Figure 2.1. The possible existence of a third phase with vanishing gluino condensate $\langle\bar{\lambda}\lambda\rangle$ has also been discussed [14]. The continuum limit of the theory is realized in the limit $\beta = \infty$ and at the critical hopping parameter $K = K_{cr}(\beta)$.

In the numerical simulations β is fixed at $\beta = 2.3$. From simulations of pure $SU(2)$ gauge theory this value is known to be in the lower scaling region. It is expected that the introduction of virtual dynamical gluino loops by unquenching decreases the lattice spacing due to the difference of the Callan-Symanzik β-function with and without light gluinos. Therefore $\beta = 2.3$ with light dynamical gluinos is closer to the continuum than in pure gauge theory. The critical hopping parameter K_{cr} has to be found numerically by simulations.
In practice we start on a small lattice and with K close to its perturbative value. In further simulations K is changed in small steps towards the critical K_{cr}. There exist different criteria that allow us to monitor the approach of K_{cr} and extrapolate to its real value at fixed β. A detailed numerical analysis of each of the following points can be found in Chapter 3.4.

- The mass of the a-π [2] should be small at $K \sim K_{cr}$, according to the PCAC relation

$$m_\pi^2 = A\left(\frac{1}{K} - \frac{1}{K_{cr}}\right). \tag{2.18}$$

- At zero gluino mass the a-η' is believed to remain massive [5], and thus the correlation function of the a-η' must be dominated by its disconnected contribution (see Chapter (3.3.2)).

- At $K = K_{cr}$ a first order phase transition is expected to occur, which manifests itself in a jump of the value of the gluino condensate $\langle\bar{\lambda}\lambda\rangle$.

- At the critical point the mass term in the renormalized chiral and supersymmetric Ward identity has to vanish.

Furthermore at $K = K_{cr}$ we expect the formation of supermultiplets. The consistency of the thus determined values for K_{cr} is a signal for the realization of supersymmetry in the lattice theory.

2.2 Projecting operators for bound states

The general expectation [5, 15], supported by numerical evidence [12] is that Yang-Mills theory with gluinos is confining. Thus to investigate the light bound state masses, color singlet states are considered. Furthermore the structure of the light spectrum is expected to be closest to that of single-flavor QCD with the chiral symmetry broken by the anomaly, and the presence of a mass-gap. The fundamental difference however is that in N=1 SYM theory both, the gluinos and the gluons transform under the adjoint representation of the color group. Consequently color singlet states can be constructed out of suitable combinations of gluon and gluino interpolating fields.

[2]The a-π is in the model we consider not a physical particle. It is defined by the connected part of the a-η' correlation function and can be viewed as the closest analog to the π in QCD [31] (for details see Chapter 3.3.2). Hence we expect that its mass is small in the chiral limit. This situation is analogous to partial quenching (see [32] and references therein) with respect to $N_f = 1$ adjoint QCD. In this context the pion can be defined similarly, with a well defined chiral limit in the vicinity of which its mass becomes small.

Certainly one wants to determine the masses of those particles which are the building blocks of the chiral supermultiplets (see Chapter 1.2) used in the construction of the effective actions [5, 6]. Therefore we consider various projecting operators, namely for the glueballs, well known from pure Yang-Mills theory, the gluinoballs corresponding to the mesons of QCD, and a mixed gluino-glueball which consists of a gluon and a gluino.
Before we discuss each projecting operator in detail, let us quickly review the general strategy we follow to determine the masses of the low lying states.
The masses will be computed from the asymptotic behavior of Euclidean-time correlation functions. A typical correlator can be written as

$$C(\Delta t) = \left\langle S^{\dagger}(t+\Delta t) S(t) \right\rangle, \tag{2.19}$$

where S is defined as the sum over the time-slice of the projecting operator ϕ

$$S(t, p=0) = \frac{1}{L^{\frac{3}{2}}} \sum_{\vec{x}} \phi(\mathbf{x}, \mathbf{t}), \tag{2.20}$$

thus projecting out the intermediate states with zero spatial momentum. Inserting a complete set of energy eigen-states $|n\rangle$ in (2.19) we arrive at

$$\begin{aligned} C(\Delta t) = \sum_n \Big\{ & \quad |\langle n|\mathrm{S}(t)|0\rangle|^2 e^{-\mathrm{E}_n \Delta t} \\ & \pm \quad |\langle 0|\mathrm{S}(t)^{\dagger}|n\rangle|^2 e^{-\mathrm{E}_n (T-\Delta t)} \Big\}. \end{aligned} \tag{2.21}$$

The sign ($\pm$) refers to the boundary conditions chosen in the numerical simulations. In our case we have imposed periodic boundary conditions in the three spatial directions, for the gluon and the gluino. This implies that in the Hilbert space of states supersymmetry is not broken by the boundary conditions. In the time direction antiperiodic boundary conditions for the fermion and periodic boundary conditions for the boson were adopted. The minus sign for the fermion is the one usually associated with closed fermion loops. Hence in (2.21) the ($+$) refers to periodic and the ($-$) to antiperiodic boundary conditions for the operator $\phi(x, t)$ in the time direction.
The lattice extension in the time direction is denoted by T. On a finite lattice the energy spectrum is discrete. Therefore for large T and large time separations Δt the above time-slice correlator is dominated by the lightest state $|1\rangle$ with energy E_1 that the operator $\phi(x, t)$ couples to. The sum over the time-slice projects out the zero momentum $p = 0$ state. Hence if there is a single particle state the operator $\phi(x, t)$ couples to, the lowest energy is equal to its mass and the asymptotic behavior of the correlator (2.21) can be written as

$$C(\Delta t) \overset{T\to\infty, \Delta t \to T/2}{\sim} \begin{cases} c_0 + c_1 \cosh[m_1 \left(\frac{T}{2} - \Delta t\right)] & \text{periodic boundary conditions,} \\ \\ c_1 \sinh[m_1 \left(\frac{T}{2} - \Delta t\right)] & \text{antiperiodic boundary conditions.} \end{cases} \tag{2.22}$$

The constant c_0 is different from zero iff $\langle 0|S(t)|0\rangle \neq 0$. The mass of the lowest state can be extracted from fitting the numerically determined two point function by the above form in a time interval $\Delta t \in [t_1, t_2]$.

In practice several difficulties have to be dealt with.
The operator ϕ usually displays an overlap not only with the lowest state, but also with excited ones. Thus the lowest mass can only be extracted by fitting to the form (2.22) at large time separation Δt. This may lead to large statistical errors, because the signal to noise ratio increases drastically with increasing Δt. Another possibility is to fit the available data with a form of the correlation function that contains a second mass

$$C(\Delta t) \overset{T\to\infty,\Delta t\to T/2}{\sim} \begin{cases} c_0 + c_1\cosh[m_1\left(\frac{T}{2}-\Delta t\right)] + c_2\cosh[m_2\left(\frac{T}{2}-\Delta t\right)] \\ \\ c_1\sinh[m_1\left(\frac{T}{2}-\Delta t\right)] + c_2\sinh[m_2\left(\frac{T}{2}-\Delta t\right)]. \end{cases}$$

In this way the lowest mass and the mass of the next excited state can be extracted. This however can only be carried out with a reasonable error on the masses if the signal to noise ratio of the initial data is good enough. A two mass fit does usually not solve the problem that we encounter when we try to fit with one mass at large time separation Δt. In the following, the two mass and the one mass fit will be used to display the consistency of the obtained masses if possible.
For ease of notation we will write in the following for the correlation function $C(\Delta t)$ that depends on the differences of the time coordinates t_x and t_y also simply $C(t)$. As the correlation function always depends on the difference of time coordinates this notation is not ambiguous.
When discussing our numerical results in Chapter 3.3 we will encounter both, data that allows a two mass fit with a reasonable error and data that has such a poor signal to noise ratio that only a rough estimate of the mass is possible.
To overcome the problem of a bad signal to noise ratio which renders in some cases the extraction of physical information difficult, if not impossible, in the past different smearing algorithms have been proposed and successfully been used [33–36].
The idea of the method consists in improving the overlap $\langle 1|\phi|0\rangle$ that the lowest state $\langle 1|$ has with the operator ϕ. The smearing algorithms we make use of will be discussed in Chapter 2.2.6.

2.2.1 Glueballs

The projecting operators for glueball states as well as the methods to compute their masses are well established (For a summary see [37]). The chiral multiplets put forward in the effective action of [6] contain a 0^+ and a 0^- glueball, the lighter one being the $\mathrm{J^P} = 0^+$ glueball in accordance with [19]. In this Section we will display the correlation functions that have been used in calculating the masses of these two glueballs.
A suitable operator for the $J^P = 0^+$ glueball is generated by the symmetric combination of space-like plaquettes touching one lattice point:

$$S_{0^+}(t) = \sum_{\vec{x}} \mathrm{Tr}[U_{12}(x) + U_{23}(x) + U_{31}(x)]. \tag{2.23}$$

Additionally we consider the pseudoscalar 0^- glueball. In order to create a gluonic state with these quantum numbers we need a combination of closed loops that cannot be rotated into their mirror images. One possibility would be to take the simplest lattice version of $\mathrm{Tr}[\epsilon_{\mu\nu\rho\sigma}F^{\mu\nu}F^{\rho\sigma}]$. This choice however has the disadvantage that it contains two orthogonal plaquettes so that it does not fit into one time-slice. Therefore the loop $\mathcal{C}$ shown in

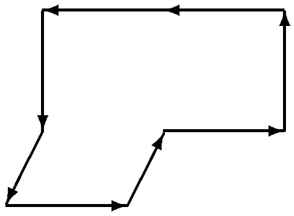

Figure 2.2: *Plaquette combination used in the construction of the time-slice operator $S_{0^-}(t)$ of the 0^- glueball*

Figure 2.2 was chosen [38], and the time-slice operator has the form

$$S_{0^-}(t) = \sum_R [\mathrm{Tr}[U(\mathcal{C})] - \mathrm{Tr}[U(\mathcal{PC})]]. \tag{2.24}$$

The sum runs over all rotations R in the cubic lattice group and $\mathcal{PC}$ is the mirror image of the loop $\mathcal{C}$.
As in pure SU(2) gauge theory smearing has to be applied to the link in order to achieve a reasonable signal. It turned out that Ape smearing was better suited than Teper blocking for the mass calculation (see Chapter 3.3).

2.2.2 Gluinoballs

We also consider color singlet states made out of two gluino fields, in analogy to flavor singlet mesons in QCD.
The first is the pseudoscalar state

$$\phi = \bar{\lambda}\gamma_5\lambda, \tag{2.25}$$

called a-η' in what follows, the a reminding us of the adjoint representation of the constituents. The η' stands for the corresponding η' meson in QCD.
The second state is the scalar

$$\phi = \bar{\lambda}\lambda, \tag{2.26}$$

called a-f_0. Both of them are found in the multiplets of [6] and [5]. For the correlation functions a straightforward calculation using (2.15) and $\Gamma \in [1, \gamma_5]$ gives

$$C_{\tilde{g}\tilde{g}}(\Delta t) = \sum_{\vec{x}} \langle \mathrm{Tr_{sc}}[\Gamma\Delta_{xx}]\mathrm{Tr_{sc}}[\Gamma\Delta_{yy}] - 2\mathrm{Tr_{sc}}[\Gamma\Delta_{xy}\Gamma\Delta_{yx}]\rangle , \tag{2.27}$$

where y is a fixed source, and the trace is in spin and color indices. Note that the factor of two originates from the Majorana character of the gluino. As in the case of flavor singlet mesons in QCD the propagator consists of a connected and a disconnected part, see Figure 2.3. The connected part which we will refer to as the a-π in the sequel corresponds in the below sense to the pion ($\Gamma = \gamma_5$) respectively the sigma ($\Gamma = 1$) in QCD. As there is only one flavor of gluinos these "states" are not physical in SYM theory. However the expectation is that analogously to QCD the mass of this unphysical a-π goes to zero in the chiral limit [31].
The vanishing of the a-π mass is then used to signal the chiral $m_{\tilde{g}} \to 0$ limit. We also expect on grounds of the axial symmetry breaking by the anomaly that the a-η' remains

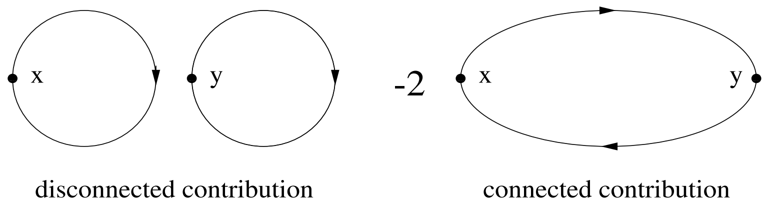

Figure 2.3: *Graphical representation of the gluinoball correlator. The connected part corresponds to the unphysical a-π and a-σ particle respectively.*

massive. This implies that approaching the supersymmetric limit the disconnected contribution for the a-η' correlator will increase relative to the connected one. A numerical analysis of these considerations can be found in Chapter 3.4 where we discuss the chiral limit.
The numerical evaluation of the time-slice for the connected part of the correlator is reduced to the calculation of the gluino propagator Q^{-1} from a few initial local sources y_s. An inversion for every lattice point would be too costly in CPU time. The sink is however summed over which projects out the $p = 0$ part.
The disconnected part is calculated using the volume source technique [39]. This method relies on the Elitzur theorem [40] which states that expectation values of non gauge invariant quantities vanish under general assumptions. This holds especially for $\mathrm{Tr}[Q^{-1}_{xy}]$ where $x \neq y$. Using this fact we can write

$$\left\langle \mathrm{Tr}[Q^{-1}_{xx}] \right\rangle = \left\langle \mathrm{Tr}[Q^{-1}_{xx}] \right\rangle + \sum_{y \neq x} \left\langle \mathrm{Tr}[Q^{-1}_{xy}] \right\rangle = \sum_{y} \left\langle \mathrm{Tr}[Q^{-1}_{xy}] \right\rangle . \tag{2.28}$$

The last term can be obtained for all lattice points x and one set of color and Dirac indices a, α, by solving $Qx = b$ (see Appendix C) with the source $b_{xa\alpha} = 1, \forall x \in V$. This method of gauge averaging will later (see Chapter 2.2.5) be used to handle more complicated terms arising in the correlator of a three-gluino particle.

2.2.3 The gluino-glueball

From the gluino fields λ and the field strength $F_{\mu\nu}$ a third type of color singlet state can be constructed. The simplest example is

$$\phi = \sigma_{\mu\nu} \mathrm{Tr}[F_{\mu\nu}\lambda]. \tag{2.29}$$

This spin $\frac{1}{2}$ Majorana fermion is one of the states appearing in [5,6] as a part of the chiral supermultiplet. In order to find the lowest state in this channel we consider the operator

$$\phi^{\alpha} = \sum_{i,j} \sigma^{\alpha\beta}_{ij} \mathrm{Tr}[P_{ij}(x)\lambda^{\beta}(x)]. \tag{2.30}$$

Recall that $P_{\mu\nu}$ is the lattice transcription of the field strength $F_{\mu\nu}$ (see 2.17). The indices i,j run only over spatial directions as to avoid contact terms from adjacent time-slices.
The correlator thus consists of plaquettes connected by a quark propagator line (see Figure 2.4) and can be written as

$$C^{\alpha\beta}(\Delta t) = -\frac{1}{4} \sum_{\vec{x}} \sum_{i,j,k,l} \sigma^{\alpha\alpha'}_{ij} \mathrm{Tr}[U_{ij}(x)\sigma^{a}] \Delta^{yb\beta'}_{xa\alpha'} \mathrm{Tr}[U_{kl}(y)\sigma^{b}] \sigma^{\beta'\beta}_{kl}. \tag{2.31}$$

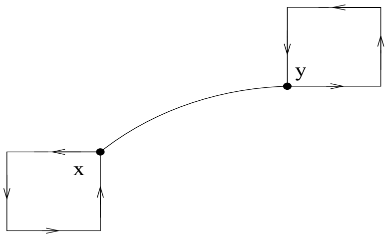

Figure 2.4: *Graphical representation of the gluino-glue correlator.*

$U_{ij}(x)$ is the simple plaquette as defined in (2.3), σ_{ij} denotes the Dirac tensor, and σ^a the Pauli matrices both defined in Appendix A. By using various symmetries of the theory we will show in Chapter 2.3.4 (see also [31]) that the correlation function (2.31) has the form

$$C^{\alpha\beta}(\Delta t) = C_1(\Delta t)\delta^{\alpha\beta} + C_2(\Delta t)\gamma_4^{\alpha\beta}. \tag{2.32}$$

Moreover using time reversal symmetry it follows that

$$\begin{aligned} C_1(\Delta t) &= -C_1(T-\Delta t), \\ C_2(\Delta t) &= C_2(T-\Delta t). \end{aligned} \tag{2.33}$$

Additionally, the coefficients C_1 and C_2 are real. Thus for antiperiodic boundary conditions C_1 is antiperiodic while C_2 is periodic on a finite lattice with time extension T. These two components can in principle be used to give an independent estimate of the lowest mass ϕ^α projects onto.
Numerically $C^{\alpha\beta}(\Delta t)$ can be evaluated by the calculation of the propagator Δ_x^y for some source y and all x of the lattice (see Appendix C). These point sources however do not lead to a satisfactory signal, and Ape as well as Jacobi smearing have to be implemented to extract the low-lying masses from the correlation functions (see Chapter 3.3).

2.2.4 Three-gluino states

Another interesting color singlet consisting of three gluinos, which is not found in the multiplets of [5,6], can be constructed in analogy to baryons in QCD [41]. This is possible for SU(2) as well as for SU(3) since the fermions are in the adjoint representation.
A possible choice for the wave function is

$$W^\alpha(x) = \epsilon_{abc}(C\gamma_4)^{\beta\gamma}\lambda(x)_a^\alpha\lambda(x)_b^\beta\lambda(x)_c^\gamma. \tag{2.34}$$

The spin content of this wave function is not completely obvious. Since two of the fields are symmetric in spin this state could in principle contain a spin $\frac{3}{2}$ and a spin $\frac{1}{2}$ component. To show this consider first a generalized wave function W_μ^α with all Lorentz components.

$$W_\mu^\alpha(x) = \epsilon_{abc}(C\gamma_\mu)^{\beta\gamma}\lambda(x)_a^\alpha\lambda(x)_b^\beta\lambda(x)_c^\gamma. \tag{2.35}$$

Indeed the spin content of this Rarita Schwinger object [42] would be purely $\frac{3}{2}$ if both of the following conditions would be satisfied:

$$\gamma_\mu W_\mu = 0,$$
$$\partial_\mu W_\mu = 0.$$

Using the Fierz identity

$$\epsilon^{abc}(\bar{\chi}(x)\gamma^\mu\lambda^a(x))(\bar{\lambda}^b(x)\gamma_\mu\lambda^c(x)) = 0 \tag{2.36}$$

which holds for arbitrary χ the first of the above conditions follows, so half of the spin $\frac{1}{2}$ components are projected out. The second one however is not satisfied and we are left with a spin $\frac{3}{2}$ and a spin $\frac{1}{2}$ component in the wave function $W^\alpha(x)$. This property makes it also a useful candidate as a projecting operator for the Ward identities. For SU(3) color additional possibilities are obtained by a symmetric color coupling

$$\begin{aligned}
\phi'^\alpha(x) &= d_{abc}(C\gamma_5)_{\beta\gamma}\lambda(x)^\alpha_a\lambda(x)^\beta_b\lambda(x)^\gamma_c, \\
\phi''^\alpha(x) &= d_{abc}(C)_{\beta\gamma}\lambda(x)^\alpha_a\lambda(x)^\beta_b\lambda(x)^\gamma_c.
\end{aligned}$$

Our analysis however will focus on the SU(2) case.
To calculate the mass of such a baryonic state the correlation function

$$C^{\alpha\beta}(\Delta t) = \left\langle W^\alpha \bar{W}^\beta \right\rangle \tag{2.37}$$

of the operator (2.34) must be calculated. The fermionic fields in the correlator can be integrated out by using either method mentioned in Chapter 2.1.1 to calculate correlation functions. Both lead to the following result:

$$\begin{aligned}
C(x,y) \;=\; & -\epsilon_{a'b'c'}\epsilon_{abc}(C\gamma_4)^{\beta'\gamma'}(C\gamma_4)^{\beta\gamma} \\
& * \{\, 2\Delta^{ya'\alpha'}_{xa\alpha}\Delta^{yb'\beta'}_{xb\beta}\Delta^{yc'\gamma'}_{xc\gamma} + 4\Delta^{yb'\beta'}_{xa\alpha}\Delta^{yc'\gamma'}_{xb\beta}\Delta^{ya'\alpha'}_{xc\gamma} \\
& +2\Delta^{xb\beta}_{xa\alpha}\Delta^{ya'\alpha'}_{xc\delta}\Delta^{yb'\beta'}_{yc'\delta'}C^{\gamma\delta}C^{\delta'\gamma'} + 4\Delta^{xb\beta}_{xa\alpha}\Delta^{xc\gamma}_{yb'\beta'}\Delta^{ya'\alpha'}_{yc'\gamma'} \\
& +\Delta^{ya'\alpha'}_{xa\alpha}\Delta^{xc\delta}_{xb\beta}\Delta^{yb'\beta'}_{yc'\delta'}C^{\gamma\delta}C^{\delta'\gamma'} + 2\Delta^{yc'\delta'}_{xa\alpha}\Delta^{xc\delta}_{xb\beta}\Delta^{ya'\alpha'}_{yb'\beta'}C^{\gamma\delta}C^{\delta'\gamma'} \,\},
\end{aligned}$$

where $\Delta = Q^{-1}$is the gluino propagator. This propagator has basically two contributions displayed in Fig. 2.5. Note that the second contribution to the correlation function arises since contractions of the form $\lambda(x)\lambda(x)$ are allowed for Majorana fermions.
Terms in the correlation function that pertain to the first type can be evaluated by the same method as the connected contribution to the mesonic correlator of (2.27). A calculation of the other terms belonging to the second, the spectacles graph as we will call it is not so straightforward. Their structure is new and hence a new method must be developed to calculate their contribution.

2.2.5 Evaluation of the spectacles graph

We now show how to evaluate the second graph of Figure 2.5. With Ω_x the gauge transformation in the fundamental representation, we see that the gauge transformation in the

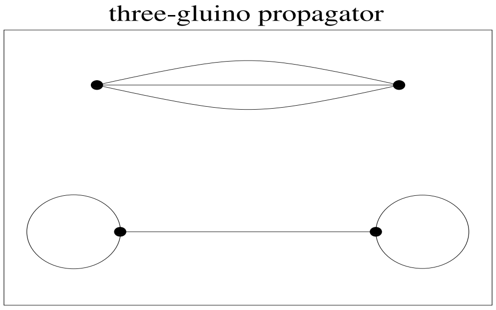

Figure 2.5: *Contributions to the propagator of a three-gluino state. The second contribution which we denote by the name "spectacles graph" arises, since contractions of the form $\lambda(x)\lambda(x)$ are allowed for Majorana fermions.*

adjoint, defined as $G_{x,ab}(\Omega) = [G^{-1}_{x,ab}]^T = 2\mathrm{Tr}[\Omega^{-1}(x)T^a\Omega(x)T^b]$, obeys

$$\int d\Omega G_{a_1b_1} = 0,$$
$$\int d\Omega G_{a_1b_1}G_{a_2b_2}G_{a_3b_3} = \frac{1}{6}\epsilon_{a_1a_2a_3}\epsilon_{b_1b_2b_3}. \qquad (2.38)$$

The propagator Δ transforms under a gauge transformation as

$$\Delta^{yb}_{xa} \to G^{-1}_{x,aa'}\Delta^{yb'}_{xa'}G_{y,b'b}. \qquad (2.39)$$

These are the necessary ingredients for an evaluation of the second graph. We have to calculate for example (spinor indices are left out for simplicity)

$$\tilde{C}(x,y) \equiv \Delta^{ya'}_{yc'}\Delta^{xc}_{yb'}\Delta^{xb}_{xa}\epsilon_{abc}\epsilon_{a'b'c'}.$$

First we compute the vector

$$W_{zb',x} = \Delta^{xc}_{zb'}\Delta^{xb}_{xa}\epsilon_{abc},$$

for a fixed site x and all sites z. Next we observe that, with the help of eqs. (2.38) and (2.39), we find the identity

$$\langle\Delta^{za'}_{yc'}W_{zb',x}\rangle = \frac{1}{6}\delta_{zy}\epsilon_{a'b'c'}\epsilon_{abc}\langle\Delta^{ya}_{yc}W_{yb,x}\rangle.$$

Composing now the "shifted" vector $W^{\mathrm{shifted}}_{xc,y}$,

$$W^{\mathrm{shifted}}_{zb',x} = W_{zb'-1,x} - W_{zb'+1,x}$$

(with $W_{x4,y} = W_{x1,y}$, $W_{x0,y} = W_{x3,y}$) it follows that

$$\sum_{y,z,c',b'}\langle\Delta^{zb'}_{yc'}W^{\mathrm{shifted}}_{zb',x}\rangle = \langle\tilde{C}(x,y)\rangle.$$

To evaluate the l.h.s. of this relation numerically only one additional inversion is needed with $W^{\mathrm{shifted}}_{zb',x}$ as the source. In this way $\langle\tilde{C}(x,y)\rangle$ is obtained from a given x to all y by two inversions of the fermion matrix Q.

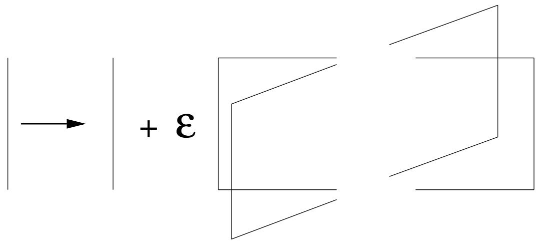

Figure 2.6: *Illustration of Ape smearing.*

2.2.6 Ape and Jacobi smearing

In our numerical simulations Ape as well as Jacobi smearing [34, 36] have been implemented, in order to improve the projection onto the ground state and the signal to noise ratio of correlation functions. In a former analysis [43] these algorithms have been shown to achieve results on the operators considered that were superior to other algorithms such as Teper blocking [33] or Wuppertal smearing [35].
Ape smearing was performed on gluonic operators used in the calculation of the glueball masses and the gluino-glue. For the latter also Jacobi smearing as fermionic smearing algorithm was used.
Both smearing algorithms have also been used in the numerical analysis of the Ward identity, since the inserted operators are of the gluino-glue type.
Ape smearing substitutes every link by the sum of itself and the weighted space-like staples perpendicular to the direction of the original link. This is illustrated in Figure 2.6. The result is projected back onto $SU(2)$. Such smeared links are defined by the following relation:

$$\begin{aligned} \overline{U}_\mu(x) &= U_\mu(x) + \epsilon \sum_{\substack{\alpha=\pm 1 \\ |\alpha|\neq\mu}}^{\pm 4} U_\alpha(x) U_\mu(x+\hat{\alpha}) U_\alpha(x+\hat{\mu})^\dagger, \\ U^s_\mu(x) &= \frac{\overline{U}_\mu(x)}{\left(\frac{1}{2}\mathrm{Tr}\overline{U}_\mu(x)^\dagger \overline{U}_\mu(x)\right)^{1/2}}. \end{aligned} \tag{2.40}$$

U^s is the resulting smeared link. It is easily checked that the smearing algorithm defined in this way is gauge invariant. The algorithm is usually applied to the whole lattice and can be carried out N number of times. Nevertheless not too many smearing steps can be applied as not to wash out the signal of interest.
For small values of ϵ this procedure corresponds to solving a diffusion equation. The diffusion or smearing radius is given by

$$R_s = N\epsilon.$$

Comparing the smearing radius where masses can be extracted to the lattice size allows then an estimate whether the used volume is sufficient to contain the particle wave function.
Since Ape smearing acts on the gauge fields only, even for N of the order of 20 the CPU time necessary is negligible with respect to the inversion of the fermion matrix. Usually both parameters have to be tuned numerically to find values which allow a reasonable

estimate of the mass or some other matrix element.
Let us now turn to Jacobi smearing. The idea is to construct, guided by physical intuition, new fermionic operators that resemble more closely than the point-like sources the true physical state of the fermion. To construct this new operator the fermion field is smeared out by a suitable operator $F(x,x')$ acting on a fixed time-slice

$$\tilde{\lambda}_b^\beta(x,t) = \sum_{x'a\alpha} F_{ba}^{\beta\alpha}(x,x')\lambda_a^\alpha(x'). \tag{2.41}$$

The time-slice is held fixed since we are interested in the value of correlation functions as a function of time. Smearing in the time direction would spoil the signal we wish to study. Both Jacobi and Ape smearing usually allow two parameters to be tuned. As the Jacobi algorithm is recursive the operator F carries an index N_J indicating how many times a certain iterative procedure is carried out. The other parameter, referred to as K_J is responsible for the convergence of this iteration. In the Jacobi smearing procedure that we have adopted F is chosen to be

$$\begin{aligned} F_{ba}^{\beta\alpha}(x,x') &= \delta_{xx'}\delta_{ba}\delta^{\beta\alpha} + \\ & \delta^{\beta\alpha}\sum_{i=1}^{N_J}\left(K_J\sum_{\mu=1}^{3}\left[\delta_{x',x+\hat{\mu}}V_{\mu,ba}(x) + \delta_{x'+\hat{\mu},x}(V^\dagger)_{\mu,ba}(x)\right]\right)^i . \end{aligned}$$

For a suitably small K_J and $N_J \to \infty$ this is the solution kernel of the three dimensional Klein-Gordon equation

$$\begin{aligned} & K_{aa'}(x,x')F_{a'b}(x',y) = \delta_{xy}\delta^{ab} \\ & K_{aa'}(x,x') = \delta_{xx'}\delta_{aa'} - K_J\sum_{\mu=1}^{3}\left[\delta_{x',x+\hat{\mu}}V_{\mu,aa'}(x) + \delta_{x'+\hat{\mu},x}(V^\dagger)_{\mu,aa'}(x)\right] . \end{aligned}$$

The trivial spinor indices α and β have been omitted. The so defined smearing algorithm is gauge covariant. Numerically also for values of K_J where the iteration does not converge a wave function is obtained which leads to good results in the expectation values, i.e. to an improved signal to noise ratio. As in the case of APE smearing a smearing radius R_J can be defined

$$R_J^2 = \frac{\sum_x |x|^2|F(x,0)|^2}{\sum_x |F(x,0)|^2}.$$

A calculation of this smearing radius could then be used to establish whether or not the ground state wave function fits onto the lattice at the optimized smearing parameters.
Smearing the sources only on one time-slice is not very time consuming. On the sink, however, this procedure as it has to be performed on every time-slice of the lattice is for N_J of the order of 10 as costly in CPU time as an inversion of the fermion Matrix.
For each set of simulation parameters β and K the smearing parameters N_{APE},ϵ_{APE},N_J and K_J have to be retuned to achieve an optimal projection onto the ground state. The optimal smearing parameter K_J is usually not equal to the value of the hopping parameter K of the simulation.

2.3 Ward identities on the lattice

The introduction of a space-time lattice as a regulator of the path integral breaks the symmetries associated with continuous space-time, i.e. Poincaré invariance and supersymmetry. In the Wilsonian approach of lattice fermions also chiral symmetry is broken. This is the lattice version of the general problem of defining a manifestly SUSY-invariant regularization. In the path integral formulation these symmetries are expressed through the Ward identities associated with the respective symmetry transformation. The breaking of these symmetries by the lattice formulation introduces new terms in the Ward identities. Provided that there are no SUSY-anomalies the lattice form of the Ward identities can be used, by imposing that their continuum form should be recovered when removing the lattice regulator, to define the continuum limit of the lattice theory [9].
Hence Ward identities can be used to formulate the problem of supersymmetry and chiral symmetry breaking and their restoration on the lattice. This is completely analogous to the problem of non-singlet chiral symmetry breaking in lattice QCD and its restoration described by Ward identities [44, 45].
It is an essential observation that, provided there are no supersymmetric anomalies the symmetry breaking effects introduced by the lattice that survive the continuum limit can be eliminated by renormalization. In this case the renormalization amounts to a proper tuning of the bare gluino mass.
In the supersymmetric Ward identities the supersymmetry restoration manifests itself in the vanishing of the subtracted gluino mass, and the continuum form of the SUSY Ward identity is recovered.
It is in this way that the supersymmetric limit can be formulated through Ward identities, and obtained by tuning a single parameter, the bare gluino mass. Furthermore the SUSY limit coincides with the zero gluino mass limit [9].
For a numerical study of $N = 1$ SYM theory it is of high interest to determine the critical value of the bare gluino mass where symmetry restoration takes place.
Such a study can give insight into the question of supersymmetric anomalies. Also at this point in parameter space the formation of supermultiplets is expected. Furthermore by discrete chiral symmetry breaking a first order phase transition is expected to occur [16].
We start our analysis by deriving the bare lattice Ward identity from lattice SUSY transformations. Afterwards we carry out renormalization of the bare Ward identity.
On the lattice the renormalized identity holds only up to order $O(a)$. Thus there is a freedom in choosing the lattice form of the SUSY current. We discuss two forms that we hope are suited for a numerical investigation.
Finally we analyze what kind of operator we can insert in the Ward identity. For the simplest possible choice of this operator we determine an independent set, which will later be used in the numerical determination of the ratios of the renormalization coefficients.

2.3.1 Lattice SUSY transformations

Although supersymmetry is broken by the lattice regularization, we can still define lattice SUSY transformations. Under these transformations the action (2.1) is not invariant for any finite lattice spacing a, and additional breaking terms of the order $O(a)$ arise. The form of these lattice transformations is only restricted by the condition that their continuum form (1.5) should be recovered (apart from overall factors) in the continuum limit. Furthermore we also want the supertransformations to commute with the parity $\mathcal{P}$ time-reversal $\mathcal{T}$ and charge conjugation $\mathcal{C}$ transformation on the lattice. The simplest choice that fulfills these requirements is [46]

$$\begin{aligned}
\delta U_\mu(x) &= -\frac{ig}{2}(\bar{\theta}(x)\gamma_\mu U_\mu(x)\lambda(x) + \bar{\theta}(x+\hat{\mu})\gamma_\mu\lambda(x+\hat{\mu})U_\mu(x)),\\
\delta U_\mu^\dagger(x) &= \frac{ig}{2}(\bar{\theta}(x)\gamma_\mu\lambda(x)U_\mu^\dagger(x) + \bar{\theta}(x+\hat{\mu})\gamma_\mu U_\mu^\dagger(x)\lambda(x+\hat{\mu})),\\
\delta\lambda(x) &= \frac{1}{2}P_{\mu\nu}(x)\sigma_{\mu\nu}\theta(x),\\
\delta\bar{\lambda}(x) &= -\frac{1}{2}\bar{\theta}(x)\sigma_{\mu\nu}P_{\mu\nu}(x),
\end{aligned} \tag{2.42}$$

where $\bar{\theta}$ and θ are infinitesimal fermionic parameters that satisfy the Majorana condition (2.4). The lattice transcription of the field strength $F_{\mu\nu}(x)$ is chosen as in (2.17), but with the simple plaquette $U_{\mu\nu}(x)$ replaced by the clover plaquette.

$$\begin{aligned}
P_{\mu\nu}(x) &= \frac{1}{4}\sum_{i=1}^{4}\frac{1}{2ig}\left(U_{\mu\nu}^{(i)}(x) - U_{\mu\nu}^{(i)\dagger}(x)\right),\\
U_{\mu\nu}^{(1)}(x) &\equiv U_{\mu\nu}(x) = U_\nu^\dagger(x)U_\mu^\dagger(x+\hat{\nu})U_\nu(x+\hat{\mu})U_\mu(x),\\
U_{\mu\nu}^{(2)}(x) &= U_\mu^\dagger(x)U_\nu(x-\hat{\nu}+\hat{\mu})U_\mu(x-\hat{\nu})U_\nu^\dagger(x-\hat{\nu}),\\
U_{\mu\nu}^{(3)}(x) &= U_\nu(x-\hat{\nu})U_\nu(x-\hat{\nu}-\hat{\mu})U_\mu^\dagger(x-\hat{\nu}-\hat{\mu})U_\mu^\dagger(x-\hat{\mu}),\\
U_{\mu\nu}^{(4)}(x) &= U_\mu(x-\hat{\mu})U_\nu^\dagger(x-\hat{\mu})U_\mu^\dagger(x+\hat{\nu}-\hat{\mu})U_\nu(x).
\end{aligned} \tag{2.43}$$

The reason for this choice is that $P_{\mu\nu}$ defined in this way transforms under parity and time reversal in the same way as $F_{\mu\nu}$ does in the continuum. As we will see in the following these properties are crucial for the numerical analysis.
The so defined lattice supertransformations can now be used to derive a lattice form of the SUSY Ward identity. We proceed in the same way as was done in the continuum in Chapter 1.3 by transforming vacuum expectation values of some operator $\mathcal{O}$

$$\langle\mathcal{O}\rangle = \int \mathcal{D}U\mathcal{D}\lambda \;\; \mathcal{O}e^{-S_g - S_f}. \tag{2.44}$$

Carrying out this transformation explicitly we find the SUSY Ward identity on the lattice to be

$$\left\langle\left(\nabla_\mu^r S_\mu(x)\right)\mathcal{O}(y)\right\rangle = m_0\left\langle D_S(x)\mathcal{O}(y)\right\rangle + \left\langle X_S(x)\mathcal{O}(y)\right\rangle - \left\langle\frac{\delta\mathcal{O}(y)}{\delta\bar{\theta}(x)}\right\rangle. \tag{2.45}$$

The lattice derivative ∇_μ^r in direction μ is in lattice units defined as

$$\nabla_\mu^r f(x) = f(x) - f(x-\hat{\mu}). \tag{2.46}$$

The supercurrent S_μ and the gluino mass term D_S have the following form[3]

[3]Notice that the lattice form of S_μ, and the operators T_μ and D_S defined in the following differ by a factor of $2i/g$ from their continuum counterparts.

$$S_\mu(x) = -\frac{1}{2}\sum_{\rho\sigma}\sigma_{\rho\sigma}\gamma_\mu \mathrm{Tr}\Big[P_{\rho\sigma}(x)U^\dagger_\mu(x)\lambda(x+\hat{\mu})U_\mu(x) + P_{\rho\sigma}(x+\hat{\mu})U_\mu(x)\lambda(x)U^\dagger_\mu(x)\Big], \tag{2.47}$$

$$D_S(x) = \sum_{\rho\sigma}\sigma_{\rho\sigma}\mathrm{Tr}\left[P_{\rho\sigma}(x)\lambda(x)\right]. \tag{2.48}$$

The bare identities derived in this way have a form which differs from their continuum counterparts by additional terms X_S arising from the explicit breaking of the symmetries by the lattice regulator. X_S is a sum of operators with dimension 9/2 whose explicit form is not needed in the following but can be found in Appendix B. Note that the gluino mass term (2.48) comes from the variation of the Wilson mass term in the action. The explicit form of the current (2.47) and the breaking terms X_S depends certainly on the form of the lattice supersymmetry transformations chosen. The breaking term X_S introduced by the lattice regulator can now give rise to non-trivial contributions. At tree level the breaking term is of the order $O(a)$ and the continuum form of the SUSY Ward identity is recovered in the $a \to 0$ limit [46].
At higher orders however the breaking terms give finite contributions and the symmetry restoration is non-trivial. This is the origin of renormalization of the SUSY current and the gluino mass. In case of the axial Ward identity this is the source of the anomalous contribution. It is a basic question whether an anomaly appears in the SUSY Ward identity. If the answer is yes it would mean that SUSY is intrinsically broken and cannot be realized in the framework of a supersymmetric Standard Model. In order to analyze this situation we have to renormalize the above Ward identity (2.45).

2.3.2 Renormalization

In the process of renormalization[4] we identify all gauge invariant operators O_i of equal or lower dimension with the same quantum numbers as X_S, and define a finite $\bar{X}_S$ [9,47]. In the naive continuum limit X_S is proportional to the lattice spacing a times a dimension 11/2 operator Y_S

$$X_S = aY_S. \tag{2.49}$$

We define the subtracted $\bar{X}_S$ to be

$$\bar{X}_S = a\bar{Y}_S = a[Y_S + \sum_i Z_i O_i], \tag{2.50}$$

where the O_i are all gauge invariant operators of lower or equal dimension than 11/2. The renormalization condition imposed is that matrix elements of $\bar{X}_S$ between physical states are of order $O(a)$, so

$$\langle\alpha|\bar{X}_S|\beta\rangle \overset{a\to 0}{=} 0. \tag{2.51}$$

By power counting we know that the renormalization coefficients Z_i of the dimension 11/2 operators are at most of the order $Z_i \sim \ln(a\mu)$. Since this is multiplied by another factor of a their contribution vanishes in the continuum limit. We now have to evaluate all gauge

[4] In this Section we follow references [9,31].

invariant operators of equal or lower dimension than 9/2 with the same quantum numbers as $\partial_\mu S_\mu$. We will do so in the continuum notation and return to the lattice formulation afterwards.
The basic fields we have at hand to construct operators of any dimension are the gluino fields λ and the gauge fields $F_{\mu\nu}$. They have dimension 3/2 and 2, respectively. Furthermore we have to construct operators of spin 1/2 and the same behavior under parity as $\partial_\mu S_\mu$, X_S and D_S appearing in (2.45). This restricts the number of gluino fields to one or three. We start our investigation by considering operators built from three gluinos as in Chapter 2.2.4. The most general gauge invariant color singlet operator with spin 1/2 built from three gluinos with dimension 9/2 can be written as

$$W(x)^\gamma = \epsilon_{abc}\left(\lambda_a^\alpha C^{\alpha\beta'}\Gamma^{\beta'\beta}\lambda_b^\beta\right)\ \Gamma'^{\gamma\gamma'}\lambda_c^{\gamma'}. \tag{2.52}$$

Γ and Γ' is any 4×4 Dirac matrix. It is sufficient to consider

$$\Gamma,\quad \Gamma' \ \in \{\mathbb{1},\gamma^5,\gamma^\mu,\gamma^5\gamma^\mu,\sigma^{\mu\nu}\}. \tag{2.53}$$

Note that the combination $C\Gamma$ must be symmetric, since ϵ_{abc} is antisymmetric. Otherwise the operator $W(x)$ vanishes identically. This leaves us with γ^μ and $\sigma^{\mu\nu}$ as possible choices for Γ. Furthermore $W(x)$ must transform as a spin 1/2 object under the Lorentz group, so any free Lorentz index appearing in Γ must be contracted with one in Γ'. Considering also the behavior under parity $\mathcal{P}$ the inclusion of $\Gamma'=\gamma^5\gamma^\mu$ and similar constructions with the $\epsilon^{\mu\nu\rho\sigma}$ tensor are forbidden. So in conclusion we can have one of the two possibilities

$$\begin{aligned} &a)\quad \Gamma = \gamma^\mu, \qquad \Gamma' = \gamma^\mu;\\ &b)\quad \Gamma = \sigma^{\mu\nu}, \qquad \Gamma' = \sigma^{\mu\nu}. \end{aligned}$$

By taking into account the Fierz identities reported in Appendix B we find that $W^\gamma = 0$ in all cases. This concludes our analysis of three-gluino operators.
Let us now investigate those dim 9/2 operators containing one gluino field. Since they have to be color singlets they can, apart from the gluino, contain either an $F_{\mu\nu}$ field with a (covariant) derivative (defined in equation (1.2)), or combinations of covariant derivatives (the trace is in color)

$$\begin{aligned} &a)\quad \mathrm{Tr}\left[D_\mu D_\nu D_\rho \Gamma_{\mu\nu\rho}\lambda(x)\right],\\ &b)\quad \mathrm{Tr}\left[D_\mu F_{\nu\rho}(x)\Gamma_{\mu\nu\rho}\lambda(x)\right],\\ &c)\quad \partial_\mu \mathrm{Tr}\left[F_{\nu\rho}(x)\Gamma_{\mu\nu\rho}\lambda(x)\right]. \end{aligned} \tag{2.54}$$

The covariant derivative acting on any field $\omega(x)$ transforming according to the adjoint representation ($D_\mu\omega(x) = \partial_\mu\omega(x) + i[A_\mu(x),\omega(x)]$) can in b) act on any of the two fields $\lambda(x)$ or $F_{\mu\nu}(x)$ or on the product of both. The tensor $\Gamma_{\mu\nu\rho}$ is a 4×4 Dirac matrix. As the trace of a commutator vanishes we can use the relation

$$\mathrm{Tr}[D_{\mu_1}...D_{\mu_n}\omega(x)] = \partial_{\mu_1}...\partial_{\mu_n}\mathrm{Tr}[\omega(x)] \tag{2.55}$$

to show that operators that are of type a) vanish identically. Type c) can be traced back to type b). We have now shown that the possible choices for operator mixing with a dimension 9/2 field are expressed by the type b) fields of (2.54).

Let us now consider the tensor $\Gamma_{\mu\nu\rho}$. To determine its structure dictated by symmetry it is sufficient to determine all independent matrices that can be build using the tensors $\delta_{\mu\nu}$ and $\epsilon_{\mu\nu\rho\sigma}$ and the different elements of (2.53). Since both of the tensors $\delta_{\mu\nu}$ and $\epsilon_{\mu\nu\rho\sigma}$ have an even number of indices Γ of (2.53) must have an odd number of indices. The only possibilities are hence γ_μ and $\gamma_5\gamma_\mu$. Note that combinations with an odd number of indices, as $\sigma_{\mu\nu}\gamma_\rho$ and $\gamma_\mu\sigma_{\nu\rho}$ are not independent. By making use of

$$\begin{aligned}[][\gamma_\mu, \sigma_{\rho\tau}] &= 2(\delta_{\mu\rho}\gamma_\tau - \delta_{\mu\tau}\gamma_\rho), \\ \{\gamma_\mu, \sigma_{\rho\tau}\} &= -2\epsilon_{\mu\rho\tau\nu}\gamma_\nu\gamma_5\end{aligned}$$

they can be expressed in terms of γ_μ, $\gamma_5\gamma_\mu$, $\delta_{\mu\nu}$ and $\epsilon_{\mu\nu\sigma\rho}$.
We first consider the case of γ_μ. The Γ matrix can now take the form $\Gamma_{\mu\nu\rho} = \delta_{\mu\nu}\gamma_\rho$ or $\Gamma_{\mu\nu\rho} = \epsilon_{\mu\nu\rho\sigma}\gamma_\sigma$. The second possibility is excluded by parity. This leaves us with the following operator

$$\mathrm{Tr}\left[D_\mu F_{\mu\nu}(x)\gamma_\nu\lambda(x)\right]. \tag{2.56}$$

Remember that this is shorthand for the three different combinations of fields D_μ can act on

$$\begin{aligned}&\mathrm{Tr}\left[D_\mu\left(F_{\mu\nu}(x)\gamma_\nu\lambda(x)\right)\right], \\ &\mathrm{Tr}\left[\left(D_\mu F_{\mu\nu}(x)\right)\gamma_\nu\lambda(x)\right], \\ &\mathrm{Tr}\left[F_{\mu\nu}(x)\gamma_\nu D_\mu\left(\lambda(x)\right)\right].\end{aligned} \tag{2.57}$$

The Leibniz rule telling us that the first line is the sum of the remaining two leaves us with two of the above three operators. Let us consider the first two as independent. We now make use of the equation of motion

$$D_\mu F^a_{\mu\nu}(x) = -ig\bar{\lambda}^b(x)\gamma_\nu\lambda^c(x)\epsilon_{abc} \tag{2.58}$$

to rewrite the second expression of (2.57) and arrive at

$$\mathrm{Tr}[(\bar{\lambda}(x)\gamma_\nu\lambda(x))\gamma_\nu\lambda(x)] = 0. \tag{2.59}$$

Here we have made use of the Fierz identities (Appendix B) as in the case of the three-gluino operators. Using the equations of motion for the Green functions introduces extra terms proportional to a delta function. In the numerical simulation we will always keep sources and sinks apart so that these terms vanish. Finally we are left with the following type of operator

$$\mathrm{Tr}[D_\mu(F_{\mu\nu}(x)\gamma_\nu\lambda(x))] \equiv \partial_\mu \mathrm{Tr}[F_{\mu\nu}(x)\gamma_\nu\lambda(x)] \equiv \frac{g}{2i}\partial_\mu T_\mu(x). \tag{2.60}$$

The case of $\gamma_5\gamma_\sigma$ can be handled in very much the same way. Out of the two possible tensors $\delta_{\mu\nu}$ and $\epsilon_{\mu\nu\rho\sigma}$ only the latter one is relevant. The first is again excluded by parity. We are now left with the combination

$$\Gamma_{\mu\nu\rho} = \epsilon_{\mu\nu\rho\sigma}\gamma_5\gamma_\sigma = -\sigma_{\nu\rho}\gamma_\mu + (\delta_{\mu\nu}\gamma_\rho - \delta_{\mu\rho}\gamma_\nu). \tag{2.61}$$

Using this identity we see that only the first part is new, while the second part in parentheses gives rise to an operator of the same form as (2.56). The new term is

$$\mathrm{Tr}[D_\mu F_{\nu\rho}(x)\sigma_{\nu\rho}\gamma_\mu\lambda(x)]. \tag{2.62}$$

Again D_μ acts on any of the two fields or on the product. The Leibniz rule can again be employed to reduce the number of independent operators to two. These two remaining possibilities are

$$\begin{aligned} &\mathrm{Tr}[F_{\mu\nu}(x)\sigma_{\mu\nu}\not{D}\lambda(x)], \\ &\mathrm{Tr}[D_\mu(F_{\nu\rho}(x)\sigma_{\nu\rho}\gamma_\mu\lambda(x))]. \end{aligned} \tag{2.63}$$

Using now the equation of motion $(\not{D}+m_0)\lambda = 0$ we find for the first of the above operators

$$\mathrm{Tr}[F_{\mu\nu}(x)\sigma_{\mu\nu}\not{D}\lambda(x)] = -m_0\mathrm{Tr}\left[F_{\mu\nu}(x)\sigma_{\mu\nu}\lambda(x)\right] = -\frac{g}{2i}m_0 D_S, \tag{2.64}$$

where D_S is as in (1.18) and m_0 is the bare gluino mass. We see furthermore that the bottom operator of (2.63) is proportional to the divergence of the SUSY current in (1.15)

$$\mathrm{Tr}[D_\mu(F_{\nu\rho}(x)\sigma_{\nu\rho}\gamma_\mu\lambda(x))] = -\frac{g}{2i}\partial_\mu S_\mu(x). \tag{2.65}$$

In conclusion we are left with three gauge invariant operators of dimension 9/2 that contribute to the mixing

$$\partial_\mu S_\mu(x) = -2\frac{i}{g}\partial_\mu \mathrm{Tr}[F_{\nu\rho}(x)\sigma_{\nu\rho}\gamma_\mu\lambda(x)], \tag{2.66}$$

$$\partial_\mu T_\mu(x) = 2\frac{i}{g}\partial_\mu \mathrm{Tr}[F_{\mu\nu}(x)\gamma_\nu\lambda(x)], \tag{2.67}$$

$$m_0 D_S(x) = m_0\frac{2i}{g}\mathrm{Tr}\left[F_{\mu\nu}(x)\sigma_{\mu\nu}\lambda(x)\right]. \tag{2.68}$$

The next possible lower dimensional operators have dimension 7/2. They necessarily contain only one gluino field. Again combinations with the gauge field and covariant derivatives can be formed. The different possibilities are

$$\begin{aligned} &\text{a)}\quad \mathrm{Tr}[D_\mu D_\nu\Gamma_{\mu\nu}\lambda(x)], \\ &\text{b)}\quad \mathrm{Tr}[F_{\mu\nu}\Gamma_{\mu\nu}\lambda(x)], \end{aligned}$$

where the notation is the same as for the dimension 9/2 case. Operators of type a) are identically zero because of (2.55). $\Gamma_{\mu\nu}$ must be an antisymmetric tensor with even parity, so the only choice is $\sigma_{\mu\nu}$ and we find the operator

$$\mathrm{Tr}[F_{\mu\nu}\sigma_{\mu\nu}\lambda(x)] = \frac{g}{2i}D_S(x). \tag{2.69}$$

This is the only operator relevant for mixing with the dimension 7/2. Its presence generates a mass subtraction $\bar{m}(K,\beta,m_0)$.

For the next lower dimensions 5/2 and 3/2 the only possible operators are of the form $\mathrm{Tr}[D_\mu\Gamma_\mu\lambda(x)]$ and $\mathrm{Tr}[\Gamma\lambda(x)]$. Both vanish identically.

This exhausts the analysis of operators that take part in the mixing in the process of renormalization. Thus for the properly renormalized SUSY Ward identity we obtain

$$\langle Z_S\partial_\mu S_\mu(x)\mathcal{O}(y) + Z_T\partial_\mu T_\mu(x)\mathcal{O}(y)\rangle = (m_0-\bar{m})\langle D_S(x)\mathcal{O}(y)\rangle\,, \tag{2.70}$$

where contact terms have been omitted. We can also define a renormalized SUSY current $\hat{S}_\mu$ [9]

$$\hat{S}_\mu = Z_S S_\mu + Z_T T_\mu, \tag{2.71}$$

and the renormalized Ward identity takes the form

$$\nabla_\mu \left\langle \hat{S}_\mu(x)\mathcal{O}(y) \right\rangle = (m_0 - \bar{m}) \left\langle D_S(x)\mathcal{O}(y) \right\rangle, \tag{2.72}$$

where m_0 is the bare gluino mass, which is connected to the hopping parameter K of the lattice regularization by $K = (2m_0 + 8)^{-1}$. The renormalization coefficients are of the form

$$Z_S = 1 + O(g_0^2), \quad Z_T = O(g_0^2), \quad \bar{m} = \bar{m}(K, \beta, r) \tag{2.73}$$

and it can be shown [9] in the framework of the lattice regularization that at the critical value of the gluino mass $m_{cr} \propto 1/K_{cr}$ the continuum form of the supersymmetric Ward identity (1.16) is recovered, in the sense that $\bar{m}(K_{cr}, \beta, r) = m_0(K_{cr})$. Hence at the critical mass $m_{cr} = m_0(K_{cr})$ the combination $(m_0(K) - \bar{m}(K, \beta, r))$ vanishes.
We will refer to $(m_0 - \bar{m}) = M_R$ as the subtracted mass. By renormalizing M_R multiplicatively one can make the connection to some standard definition of the gluino mass, e.g. the "current" gluino mass (see [9]):

$$M_R = Z_{D_S}^{-1} m_{\tilde{g}}. \tag{2.74}$$

Here Z_{D_S} is the renormalization of the operator D_S which is expected to diverge in the continuum limit.
The magnitude of the factor M_R and its evolution in numerical simulations at different values of the hopping parameter tells us how the chiral and the supersymmetric limit is approached in the simulation. Indeed it has been shown in [9] that the SUSY limit and the chiral limit coincide. Notice that this implies by the Nielsen-Ninomiya theorem [28] that in the Wilson formulation of $N = 1$ Super Yang-Mills theory on the lattice SUSY is necessarily broken.
The breaking term X_S has had several effects. The gluino mass term D_S acquires an additive renormalization. Second a new operator T_μ along with a multiplicative renormalization Z_T is introduced by mixing. And last the current S_μ is renormalized multiplicatively by Z_S.

2.3.3 Lattice formulation of the renormalized SUSY Ward identity.

We now turn to the explicit lattice formulation. A proper definition of the SUSY current S_μ and the breaking term D_S derived from lattice SUSY transformations (2.42) has been given in (2.47) and (2.48) . In principle the lattice definition of $T_\mu(x)$ can be chosen in different ways, with the only requirement that as $a \to 0$ the continuum form is approached. Various definitions will then differ by discretization effects of order $O(a)$.
For the numerical analysis that follows it is however important that $\nabla^r_\mu S_\mu$, $\nabla^r_\mu T_\mu$ and D_S behave in the same way under time reversal $\mathcal{T}$ for finite lattice spacing a and not only in the continuum limit. This is necessary since numerically we are going to analyze the integrated Ward identity on the time-slice. A different behavior under $\mathcal{T}$ would add extra

$O(a)$ effects on each time-slice.
The first choice that comes to mind for the operator T_μ is the simplest discretization

$$T_\mu^{ps}(x) = \sum_\nu \mathrm{Tr}[P_{\mu\nu}(x)\gamma_\nu\lambda(x)]. \tag{2.75}$$

However with this choice $\nabla_\mu^r T_\mu$ and $\nabla_\mu^r S_\mu$ do not behave the same under $\mathcal{T}$ and we have to adopt another definition of T_μ which is equivalent up to order $O(a)$ terms. Inspired by S_μ in (2.47) we choose an analogous point-split form for T_μ

$$T_\mu^{ps}(x) = \sum_\nu \gamma_\nu \mathrm{Tr}\Big[U_\mu(x)P_{\mu\nu}(x)U_\mu^\dagger(x)\lambda(x+\hat\mu) + U_\mu^\dagger(x)P_{\mu\nu}(x+\hat\mu)U_\mu(x)\lambda(x)\Big]. \tag{2.76}$$

The above T_μ has now the right behavior under time reversal $\mathcal{T}$. In the following we will refer to (2.47) and (2.76) as point-split current and mixing operator respectively. They will carry the superscript ^{ps}. For the gluino mass term D_S we stay with the definition (2.48). To summarize, we arrive at the Ward identity

$$Z_S^{ps}\left\langle \nabla_\mu^r S_\mu^{ps}(x)\mathcal{O}(y)\right\rangle + Z_T^{ps}\left\langle \nabla_\mu^r T_\mu^{ps}(x)\mathcal{O}(y)\right\rangle = (m_0-\bar m)\left\langle D_S(x)\mathcal{O}(y)\right\rangle + O(a), \tag{2.77}$$

where T_μ^{ps} is defined in (2.76), and S_μ^{ps} is given by

$$S_\mu^{ps}(x) = -\frac{1}{2}\sum_{\rho\sigma}\sigma_{\rho\sigma}\gamma_\mu \mathrm{Tr}\Big[P_{\rho\sigma}(x)U_\mu^\dagger(x)\lambda(x+\hat\mu)U_\mu(x) + P_{\rho\sigma}(x+\hat\mu)U_\mu(x)\lambda(x)U_\mu^\dagger(x)\Big] \tag{2.78}$$

as in (2.47). The renormalization coefficients Z_S^{ps} and Z_T^{ps} depend specifically on the discretization of S_μ and T_μ. Note that the above Ward identity holds for every lattice size, and no finite volume effects are present in the order $O(a)$ terms.
The order $O(a)$ term in (2.77) stems from the mixing that takes place under renormalization with operators of dimension higher than 9/2.
The method of deriving the exact form of the lattice current S_μ^{ps} is admittedly tedious. We can also proceed in a different manner. If we choose a lattice-regularized version of the SUSY current S_μ which goes to its continuum counterpart (1.15) in the $a \to 0$ limit it will differ only by $O(a)$ terms from the point-split current (2.78). Nevertheless the renormalization that we have carried out above remains valid. Choosing a different current S_μ and a different operator T_μ, certainly always with the correct continuum limit alters only the order $O(a)$ effects and the numerical value of the renormalization constants Z_S and Z_T.
For the numerical simulation it is also of interest how noisy the signal is when the relevant expectation values are calculated. It can be argued that a local version of the current S_μ^{ps} will behave better in a numerical simulation and that its implementation is easier anyhow. Another nontrivial point is that with a local current the determination of the renormalization coefficients in 1-loop perturbation theory is technically much easier.
For this reason we also introduce a local current S_μ^l along with the local operator T_μ^l [22,47]

$$S_\mu^l(x) = -\sum_{\rho\sigma}\sigma_{\rho\sigma}\gamma_\mu \mathrm{Tr}\Big[P_{\rho\sigma}(x)\lambda(x)\Big], \tag{2.79}$$

$$T_\mu^l(x) = 2\sum_\nu \gamma_\nu \mathrm{Tr}\Big[P_{\mu\nu}(x)\lambda(x)\Big]. \tag{2.80}$$

As above, for the gluino mass term D_S we stay with the definition (2.48).
In order not to break parity and time reflection symmetry we introduce the symmetric lattice derivative. In lattice units it takes the form

$$\nabla_\mu^{symm} f(x) = \frac{1}{2}(f(x+\hat{\mu}) - f(x-\hat{\mu})). \tag{2.81}$$

With the local version of the current and the operator T_μ the lattice SUSY Ward identity can be written as

$$Z_S^l \left\langle \nabla_\mu^{symm} S_\mu^l(x) \mathcal{O}(y) \right\rangle + Z_T^l \left\langle \nabla_\mu^{symm} T_\mu^l(x) \mathcal{O}(y) \right\rangle = (m_0 - \bar{m}) \left\langle D_S(x) \mathcal{O}(y) \right\rangle + O(a). \tag{2.82}$$

The renormalization coefficients pertaining to the local operators are here denoted by Z_S^l and Z_T^l. Note that in general they will differ from Z_S^{ps} and Z_T^{ps} belonging to the point-split operators.
Both forms of the SUSY Ward identity (2.77) and (2.82) will be subject of our numerical investigation presented in Chapter 3.5.
Numerically it is convenient to consider the integrated Ward identity where the integration is performed over all three-space. The resulting identity will then hold on every time-slice. Without loss of generality we can consider the operator $\mathcal{O}(y)$ at the origin $y = 0$ (or any other fixed point in our space-time lattice), and divide by the renormalization coefficient Z_S^d. As we will see below this is for our purposes the more suitable form of the Ward identity, and we finally arrive at

$$\nabla_4^d \sum_{\vec{x} \in V} \left\{ \left\langle (S_4^d)^\alpha(x) \mathcal{O}^\beta(0) \right\rangle + \frac{Z_T^d}{Z_S^d} \left\langle (T_4^d)^\alpha(x) \mathcal{O}^\beta(0) \right\rangle \right\} = \frac{(m_0 - \bar{m})}{Z_S^d} \sum_{\vec{x} \in V} \left\langle D_S^\alpha(x) \mathcal{O}^\beta(0) \right\rangle + O(a). \tag{2.83}$$

The superscript d stands for the different lattice discretizations of the current S_μ, the mixing operator T_μ and the lattice derivative.
This identity is a homogeneous system of equations consisting of 4×4 matrices in Dirac space. By calculating numerically the expectation values of the above expression we can in principle solve this system of equations for the ratios Z_T^d/Z_S^d and $(m_0 - \bar{m})/Z_S^d$.
It has been observed in [9] that by a proper tuning of the bare gluino mass m_0 the subtracted mass $(m_0 - \bar{m}) = M_R$ vanishes. Furthermore it has been shown that at this point in parameter space the continuum form of the chiral lattice Ward identity is also recovered. This situation is commonly described by stating that the chiral and the supersymmetric limit coincide.
It is highly interesting to determine the critical value of the bare gluino mass at which $(m_0 - \bar{m}) = M_R$ vanishes, because this is the point in parameter space which realizes the supersymmetric and simultaneously the chiral limit as defined by the Ward identities.
In principle we can determine numerically from (2.83) and the above definitions the critical value of the bare mass, or equivalently the critical hopping parameter. Keeping β fixed in the simulations, by calculating the renormalization coefficients and the subtracted mass one can monitor for which $K = K_{cr}$ the subtracted mass M_R approaches zero [5].
Since the system of equations defined by (2.83) is homogeneous a non-perturbative study at non zero distance ($x \neq y$) only allows to determine ratios of the renormalization coefficients and M_R.

[5]Note that Z_S and Z_T depend only on the bare coupling β, and do not diverge in the continuum limit.

We will solve for Z_T/Z_S and M_R/Z_S (see equation (2.83)) since perturbatively it is estimated that Z_S is of the order of $(1+O(g_0^2))$ [9]. Thus at $K = K_{cr}$ we still expect the ratio M_R/Z_S to vanish.
Vice versa we can perform different simulations approaching the K_{cr} as determined by discrete chiral symmetry breaking [16] and calculate M_R/Z_S numerically as a function of K. If a supersymmetric limit can consistently be defined, approaching K_{cr} we should observe that M_R/Z_S goes to zero. Close to the critical hopping parameter M_R/Z_S should vanish linearly.
In practice it may however be difficult to determine M_R/Z_S accurately enough in a numerical simulation to use it for the tuning of the bare gluino mass.
It is one of the results of this work, presented in Chapter 3.5 that with some numerical effort the ratios of the renormalization coefficients can at $\beta = 2.3$ and $K = 0.1925$ be determined with sufficient accuracy.
In the above discussion we have always assumed that (2.83) is valid, hence that no supersymmetric anomaly exists. An independent determination of the ratios of the renormalization constants and the subtracted mass by inserting different operators $\mathcal{O}$ in the expectation values of (2.83) serves also to verify numerically this assumption.
If on the other hand (2.83) does not hold, this should be signaled by a clear incompatibility of the different ratios as determined by independent operators.
Before we can turn to the numerical determination of the expectation values in the above identity we first have to discuss which operators are to be inserted for $\mathcal{O}$. An important task is to determine an independent set of them so that the above system of equations can at least be solved. If we can determine enough independent operators so that the system becomes overdetermined we can check numerically if the above form of the Ward identity holds.
As mentioned before a possible scenario might be the appearance of anomalies that have not been considered and would add extra terms to the Ward identity (2.83). This would be signaled by the impossibility of finding a good solution to the overdetermined system of equations.
The general strategy will be to determine as many independent operators as possible, calculate the expectation values numerically, and perform a linear fit on every time-slice to the above form of the Ward identity. For every time coordinate t we obtain an estimate of the two ratios Z_T/Z_S and $(m_0 - \bar{m})/Z_S$. If (2.83) holds then a plateau in t should be observed which can serve as a best estimate for these ratios.

2.3.4 Investigating the simplest projecting operators

Possible operators $\mathcal{O}$ that can be inserted in the expectation values of (2.83) have to have the same quantum numbers as D_S, $\partial_\mu S_\mu$ and $\partial_\mu T_\mu$. In particular they have to carry spin $\frac{1}{2}$, otherwise the expectation values vanish. With these conditions at hand we can systematically determine a set of independent operators that can be used as suitable insertions.
We observe that the operators D_S, $\partial_\mu S_\mu$ and $\partial_\mu T_\mu$ have spin 1/2 [6]. Hence to start with we look for a local, gauge invariant operator $\mathcal{O}$ which is a spin 1/2 object. The lowest

[6] The operator $D_S(x)$ transforms under rotation like a Dirac spinor, hence it carries spin 1/2. S_μ is the product of a four vector and a spinor. The Lorentz index μ is contracted with the partial derivative, and $\partial_\mu S_\mu$ transforms like a Dirac spinor. The same holds for T_μ.

dimensional operators of this kind are the dim 7/2 operators that have the general form $P_{\mu\nu}\lambda$, containing a gluino and a gauge field. For this reason we limit ourselves to finding the independent local operators of this kind. Non-local operators, or those containing a higher number of gluino fields will not be considered. Nevertheless in a future investigation it might be interesting to consider also a three-gluino operator as a candidate for insertion in the SUSY Ward identity.
Without loss of generality we will confine our considerations to the time-slice correlation

$$C_{D_S}(t) = \sum_{\vec{x}} \langle D_S(x)\mathcal{O}(0)\rangle = \sum_{\vec{x}} \langle \mathrm{Tr}[P_{\mu\nu}(x)\sigma_{\mu\nu}\lambda(x)]\mathcal{O}(0)\rangle . \tag{2.84}$$

We are going to show now that for the integrated Ward identity (2.83) only two independent operators can be formed that have the general structure $P_{\mu\nu}\lambda$. One operator can be formed with the time-like (electric) part of the field strength P_{4i}, the other uses the spatial (magnetic) sector, P_{ij}. This results from the different footing on which space and time are treated in our numerical analysis. Summing over all 3-space in (2.83) we project out the corresponding $\mathbf{p} = \mathbf{0}$ states.
We start by considering the operators

$$\mathcal{O}_1(y) = \mathrm{Tr}[\bar{\lambda}(y)P_{ij}(y)], \quad (ij) \in \{(12), (13), (23)\} \tag{2.85}$$

The expectation value (2.84) can now be written

$$C^{\alpha\beta}_{D_S}(t) = \sum_{\vec{x}} \left\langle D^{\alpha}_S(x)\mathcal{O}^{\beta}_1(0)\right\rangle = \sum_{\vec{x}} \left\langle \mathrm{Tr}[P_{\mu\nu}(x)\sigma^{\alpha\alpha'}_{\mu\nu}\lambda^{\alpha'}(x)] \;\; \mathrm{Tr}[\bar{\lambda}^{\beta}(0)P_{ij}(0)]\right\rangle = c_n(t)\Gamma^{\alpha\beta}_n, \tag{2.86}$$

where (ij) is held fixed, Γ_n is one of the 16 gamma matrices, $\Gamma_n \in \{\mathbb{1}, \gamma_i, \gamma_5, \gamma_5\gamma_i, \sigma_{\mu\nu}\}$ and spinor indices $(\alpha, \alpha', \beta, \beta')$ have been written explicitly. Using now invariance of the vacuum under parity $\mathcal{P}$ and the transformation properties of the fundamental fields (see Appendix B) we find

$$C_{D_S}(t) = \gamma_4 C_{D_S}(t)\gamma_4. \tag{2.87}$$

This even behavior under parity leaves us with $\Gamma_n \in \{\mathbb{1}, \gamma_4, \gamma_5\gamma_i, \sigma_{ij}\}$. The condition

$$\Delta = \gamma_5 C^{-1}\Delta^* C\gamma_5, \tag{2.88}$$

(see 2.8) leads to the further constraint that the coefficients $C_n(t)$ are real. Next we consider rotations of the cubic group. Let us define Λ^c to be a cubic rotation that rotates $P_{ij}(x,t)$ into $-P_{ij}(x',t)$, $x' = \Lambda^c x$ for fixed (ij)

$$\begin{aligned} P'_{ij}(x',t) &= (\Lambda^c)^{-1}_{ik} P_{kl}(x',t)\Lambda^c_{lj} = -P_{ij}(x',t), \\ P'_{lm}(x',t) &= (\Lambda^c)^{-1}_{lj} P_{jk}(x',t)\Lambda^c_{km} \quad \forall (lm) \neq (ij). \end{aligned} \tag{2.89}$$

Furthermore we define $S(\Lambda^c)$ to be the spinor $(1/2, 1/2)$ representation of Λ^c in Dirac space. Using the invariance of the vacuum under such a rotation we find for the time-slice correlator (2.86)

$$C_{D_S}(t) = -S^{-1}(\Lambda^c)C_{D_S}(t)S(\Lambda^c). \tag{2.90}$$

This condition excludes further the identity $\mathbb{1}$ and γ_4, and we are left with the two matrices $\Gamma_n \in \{\gamma_5\gamma_k, \sigma_{ij}\}$, where k is such that $\epsilon_{ijk} \neq 0$. Making further use of rotations in the above way we can see that the three different operators $\mathrm{Tr}[P_{ij}(y)\lambda(y)]$ can all be rotated into one another and we have really only one independent operator with space-like indices. However, we would like to use a combination of fields that, as projecting operator, is rotationally invariant. We expect that such a choice is less noisy in the numerical simulation since it has a higher degree of symmetry. For this reason we will use the spatial part of D_S as projecting operator

$$\mathcal{O}_1^\alpha(y) = \bar{\chi}_s^\alpha(y) = \sum_{ij} \mathrm{Tr}[P_{ij}(y)\overline{\lambda}^\beta(y)]\sigma_{ij}^{\beta\alpha}, \tag{2.91}$$

which is the same as the projecting operator for the gluino-glue (2.30). Instead of $\Gamma_n \in \{\gamma_5\gamma_k, \sigma_{ij}\}$ this operator when inserted in (2.84) develops the components $\Gamma_n \in \{1\!\!1, \gamma_4\}$, and the correlation function takes the form

$$C_{D_S}(t) = C_1(t)1\!\!1 + C_2(t)\gamma_4, \qquad C_1(t) = C_1(t)^*, \;\; C_2(t) = C_2(t)^*. \tag{2.92}$$

Time-reversal $\mathcal{T}$ which we have not considered yet can be used to determine the symmetry properties of the coefficients C_1 and C_2 as functions of the time t. Using the properties of the fundamental fields under time reversal as listed in Appendix B we find that

$$C_{D_S}(t) = \gamma_4\gamma_5(-C_{D_S}(T-t))\gamma_5\gamma_4, \tag{2.93}$$

where T is the lattice extension in the time direction. The negative sign in front of the transformed correlator in the above relation comes from the antiperiodic boundary conditions for the gluino in the time direction. Considering now the general form of the time-slice correlator $C_{D_S}(t)$ in (2.92) we find

$$C_1(t) = -C_1(T-t), \;\; C_2(t) = C_2(T-t). \tag{2.94}$$

This general form of the time-slice correlator also holds for the gluino-glue correlator (2.31). Summing in the former also over the time-like coordinates in one of the operators $\sigma_{\mu\nu}F_{\mu\nu}\lambda$ does not change the transformation properties in any of the above cases. Furthermore the above conclusions also hold for the other expectation values in (2.83) as can easily be verified.

A second operator independent from the one defined by (2.91) can be constructed from the time-like (electric) components of $P_{\mu\nu}(x)$ and takes the form

$$\mathrm{Tr}[\bar{\lambda}(x)P_{4i}(x)], \quad i \in \{1,2,3\} \tag{2.95}$$

This kind of operator is really independent from (2.91). Certainly a rotation (boost in Minkowsky space) can be found that takes a time-like component of (2.95) into a space-like component of (2.85), but since we consider time-slice correlation functions integrated over 3-space (see (2.83)) this is not a symmetry operation.

The form of the correlator $C_{D_S}(t)$ defined in (2.84) with the operator insertion (2.95) can now be investigated in the same way as was done for the insertion of (2.85). The cubic rotation defined by (2.89) acts on P_{4k} for k fixed such that $\epsilon_{ijk} \neq 0$ as follows

$$P'_{4k}(x',t) = (\Lambda^c)^{-1}_{4l} P_{lm}(x',t)\Lambda^c_{mk} = -P_{4k}(x',t),$$
$$P'_{4i}(x',t) = (\Lambda^c)^{-1}_{4l} P_{lm}(x',t)\Lambda^c_{mi}, \quad \forall i \neq k,$$

and hence we can proceed exactly as for the insertion (2.85) in (2.84). In this manner we find that the correlator (2.84) with the insertion (2.95) has the components $\Gamma_n \in \{\gamma_k, \sigma_{4k}\}$. As before we include the matrix σ_{4k} in the operator for symmetry reasons and sum over the spatial index. Note that the different spatial components are not independent. Thus the projecting operator we consider reads

$$\mathcal{O}_2^\alpha(y) = \bar{\chi}_t^\alpha(y) = \sum_k \mathrm{Tr}[P_{4k}(y)\bar{\lambda}^\beta(y)\sigma_{4k}^{\beta\alpha}]. \tag{2.96}$$

The expectation values of (2.84) have with this insertion the two independent components $\Gamma_n \in \{1\!\!1, \gamma_4\}$ and we find

$$\begin{aligned} W_{D_S}(t) &= \sum_{\vec{x}} \langle D_S(x)\mathcal{O}_2(0)\rangle = \big\langle \mathrm{Tr}[P_{\mu\nu}(x)\sigma_{\mu\nu}\lambda(x)]\mathrm{Tr}[P_{4k}(0)\bar{\lambda}(0)\sigma_{4k}\big\rangle \\ &= W_1(t)1\!\!1 + W_2(t)\gamma_4. \end{aligned} \tag{2.97}$$

Using time reversal we find for the coefficients $W_1(t)$ and $W_2(t)$

$$W_1(t) = -W_1(T-t), \qquad W_2(t) = W_2(T-t). \tag{2.98}$$

In conclusion we have found two independent operators (2.91) and (2.96) that can be used as projecting operators in the Ward identity (2.83). Each of these operators has two components, so that we have a total of four independent operators at hand.

Chapter 3

Numerical simulation of N=1 SYM theory

In this Chapter we will describe the numerical part of this work. We start with a brief account of the algorithm that has been used to produce gauge configurations. The run parameters that have been chosen in the algorithm are described, and the autocorrelations of some key quantities are calculated. We then turn to the evaluation of the masses, obtained from the correlation functions and techniques that are discussed in Chapter 2.2. The chiral limit, i.e. the extrapolation to the critical hopping parameter through the different methods as described in Chapter 2.1.2 will also be investigated. Finally we discuss in detail how we determine numerically the ratios of the renormalization coefficients in the supersymmetric Ward identity.

3.1 The algorithm

To study $N = 1$ Super Yang-Mills theory numerically at first the algorithm that is most suitable for this task has to be chosen. The Curci-Veneziano action (2.1) with an effective flavor number of $N_f = \frac{1}{2}$ is very demanding in this respect. The frequently used Hybrid Monte Carlo algorithm cannot be applied since only multiples of four Majorana flavors can be simulated. A so called R-algorithm pertaining to the family of the Hybrid Molecular Dynamics algorithms has been tested for the Curci-Veneziano action [48]. However, as in the Langevin algorithm an extrapolation to step size $\Delta t = 0$ of the integration is necessary, which is difficult and rather demanding in computer time.
On the basis of the multi-bosonic algorithm [10] a modified two-step algorithm has been developed [11] to cope with the difficulties a numerical simulation making use of the Curci-Veneziano action presents. In previous works [43, 49–51] this algorithm has been further developed in detail and thoroughly tested. The results obtained show [12] that the two-step algorithm can meet the demands of such a numerical simulation and a lattice study of $N = 1$ Super Yang-Mills theory becomes possible.

3.1.1 Basic concepts of the multi-bosonic algorithm

The basic problem in unquenched lattice simulations is how to incorporate numerically the fermionic factor in the path integral. Consider on the lattice the expectation value of any operator $\mathcal{O}$ [1] that is the product of local fields

$$\langle \mathcal{O} \rangle = \int \mathcal{D}[U] \;\; \mathcal{PF}[M] \;\; \mathcal{O}(U) e^{-S_g}. \tag{3.1}$$

Following [10] the first step to implement the Pfaffian numerically consists in bosonizing the fermion determinant. Since

$$(\mathcal{PF}[M])^2 = (\mathcal{PF}[CQ])^2 = \det CQ \tag{3.2}$$

we consider instead of the Pfaffian $\mathcal{PF}[M]$ of the fermion matrix the absolute value of the square root of the fermion determinant $|\sqrt{\det CQ}| = |\sqrt{\det Q}|$. This can in principle lead to a sign problem, because effectively by substituting the Pfaffian with the positive absolute value of the square root of the determinant we have fixed the sign of the Pfaffian to be positive [2]. Thus we assume that one can restrict the Monte Carlo simulation to gauge configurations where $\mathcal{PF}[CQ] = +|\sqrt{\det Q}|$. Note that because of (2.8) $\det(Q)$ is always positive. For what follows we will consider the above assumption to be valid and defer a discussion to Chapter 3.1.4.

Furthermore we introduce the hermitian product $Q^\dagger Q = \tilde{Q}^2$, and since $\sqrt{\det(\tilde{Q}^2)} = \det(Q)$ we consider the weight

$$|(\det \tilde{Q}^2)^{\frac{1}{4}}| e^{-S_g} \tag{3.3}$$

for our numerical simulation. Introducing $\tilde{Q}^2$ is necessary since it is positive definite (and bounded), which is an important property for the bosonization.

If we consider that

$$\det(\tilde{Q}^2) = \frac{1}{\det[(\tilde{Q}^2)^{-1}]}, \tag{3.4}$$

and introduce the polynomial P_n of degree n which approximates the function $\frac{1}{x}$ in the sense that $\lim_{n\to\infty} P_n = x^{-1}$ in some positive interval $x \in [\epsilon, \lambda], (0 < \epsilon < \lambda < \infty)$ we can write

$$\det(\tilde{Q}^2) = \frac{1}{\det[(\tilde{Q}^2)^{-1}]} \approx \frac{1}{\det(P_n(\tilde{Q}^2))} = \int \mathcal{D}[\phi] \exp\left\{ -\sum_{j=1}^{n} \sum_{xy} \phi^\dagger_{j,x} P_n(\tilde{Q}^2_{xy}) \phi_{j,y} \right\}. \tag{3.5}$$

In our case as we are interested in the simulation of one adjoint Majorana flavor we have to approximate $|\det(\tilde{Q}^2)|^{1/4}$ and the polynomial must be chosen such that

$$\lim_{n\to\infty} P_n = (x)^{-\frac{1}{4}} \qquad \forall x \in [\epsilon, \lambda]. \tag{3.6}$$

The interval $[\epsilon, \lambda]$ in which the approximation should be valid is dictated by the smallest and the largest eigenvalue of Q. In the case of N_f degenerate quark flavors polynomials

[1] The fermionic fields have been integrated out and the operator $\mathcal{O}$ contains the propagator Δ.

[2] By sign problem we refer to a large cancellation that could take place when calculating expectation values stemming from a rapid sign change in the Pfaffian as we go from configuration to configuration. As we consider only the absolute value of the Pfaffian such a sign change is not accounted for in our simulation.

that approximate $x^{-\frac{N_f}{2}}$ have to be chosen [3]. The polynomial P_n can always be expressed as a product of monomials

$$P_n(\tilde{Q}^2) = c_0 \prod_{i=1}^{n} (\tilde{Q}^2 - z_i). \tag{3.7}$$

The roots come in complex conjugate pairs, so we can make use of the equivalent forms

$$P_n(\tilde{Q}^2) = r_0 \prod_{j=1}^{n} [(\tilde{Q}^2 \pm \mu_j)^2 + v_j^2] = r_0 \prod_{j=1}^{n} (\tilde{Q} - \rho_j^*)(\tilde{Q} - \rho_j), \tag{3.8}$$

where $z_j = (\mu_j + i\nu_j)^2$ and $\rho_j = \mu_j + i\nu_j$. In terms of complex scalar fields (pseudofermion fields) ϕ_{jx} we can express the determinant factor as

$$\begin{aligned} \frac{1}{\det(P_n(\tilde{Q}^2))} &= \det(r_0)^{-1} \prod_{j=1}^{n} \det[(\tilde{Q} - \rho_j^*)(\tilde{Q} - \rho_j)]^{-1}, \\ &\propto \int \mathcal{D}[\phi] \exp\left\{ -\sum_{j=1}^{n} \sum_{xy} \phi_{j,x}^{\dagger} [(\tilde{Q} - \rho_j^*)(\tilde{Q} - \rho_j)]_{xy} \phi_{j,y} \right\}. \end{aligned}$$

The expectation value (3.1) in terms of the Curci-Veneziano action can thus be written as

$$\begin{aligned} \langle \mathcal{O} \rangle &= \int \mathcal{D}[U]\mathcal{D}[\lambda] \;\; \mathcal{O}(U,\lambda) e^{-S_{CV}(U,\lambda)} \overset{n \to \infty}{=} \int \mathcal{D}[U]\mathcal{D}[\phi] \;\; \mathcal{O}(U) e^{-S_{CV}^n[U,\phi]}, \\ S_{CV}^n(U,\phi) &= \beta \sum_{pl} \left(1 - \frac{1}{N_c} \mathrm{Re}\,[\mathrm{Tr}[U_{pl}]]\right) + \sum_{j=1}^{n} \sum_{xy} \phi_{j,x}^{\dagger} \left[(\tilde{Q} - \rho_j^*)(\tilde{Q} - \rho_j)\right]_{xy} \phi_{j,y}. \end{aligned} \tag{3.9}$$

This is how the fermion determinant is represented in the path integral by a local bosonic action. In this form configurations $[U]$ approximately distributed according to the weight (3.3) can be produced making use of the usual heatbath, overrelaxation and Metropolis algorithms.

It is however nontrivial to implement the multi-bosonic algorithm in practice.

A priori the polynomial approximation can be carried out in a number of ways, using different polynomials, that approach the limit $\lim_{n\to\infty} P_n(x) = (1/x)^{\frac{1}{4}}$ differently. Certainly polynomials should be chosen which converge fast, so that for small orders of n already a good approximation is obtained. This is crucial since on one hand the expenditure for calculating the bosonic action (3.9) and the required memory increase with the polynomial order n. On the other hand tests have shown [52] that the autocorrelation of the algorithm increases linearly with increasing n. By introducing a two-step polynomial approximation the situation regarding both problems can be improved.

In the original work [10] Chebyshev polynomials have been proposed, which minimize the maximal error in the interval of convergence. However for our purposes we consider quadratically optimized polynomials [11, 53]. These polynomials minimize the deviation of the approximation in an average sense. One of their advantages is that certain regions

[3] It is an advantage of the multi-bosonic algorithm that theories with an arbitrary number of flavors can be simulated.

of optimization can be chosen, taking into account the distribution of eigenvalues of the fermion matrix. Furthermore they can be used for the two step approximation to be discussed in the next Section.

For a finite polynomial order n the approximation (3.5) is not exact and in principle an extrapolation to $n \to \infty$ is necessary. For practical purposes it is however sufficient to investigate the n-dependence, and to show that the systematic error introduced by the finiteness of n is negligible compared to the statistical error.

The general strategy, of modeling the weight (3.3), will be that we proceed in different approximation steps. We start with a quadratically optimized polynomial of relatively low order ($n \approx 30$). The configuration produced with this polynomial is in a second step subjected to a global accept-reject step refining the first approximation. In a third step at the level of the measurement of observables the approximation is corrected by reweighting the expectation values.

The advantage of introducing the measurement correction lies in the fact that there is no need to perform several simulations with increasing order n of the polynomial. It is sufficient to observe that the introduction of the measurement correction does not change the value of observables substantially. In this case the systematic errors introduced by the finite order n are negligible in comparison to the statistical errors.

3.1.2 Two-step approximation

Quadratically optimized polynomials typically approximate rather well over a broad range of the interval $[\epsilon, \lambda]$. However towards the small end of the interval they give a value which is systematically too small, leading to an enhancement of configurations with small eigenvalues. This represents a problem in particular for fermionic quantities that are sensitive to the smallest eigenvalue of $\tilde{Q}$ as for example the correlation function of the gluinoball (2.27). Pure gauge quantities like the plaquette are expected to be less influenced by small eigenvalues. This problem becomes more severe for small fermion masses in large physical volumes, as both the largest and the smallest eigenvalue of the fermion matrix increase and decrease respectively.

This problem cannot be solved by simply lowering the value of ϵ and increasing that of λ such that the eigenvalues of the fermion matrix lie in a region of the interval $[\epsilon, \lambda]$ where P_n is a good approximation. Since the quadratically averaged error made by the approximation behaves according to [53]

$$\delta_n(\epsilon, \lambda) \simeq \exp\left\{-Cn\sqrt{\frac{\epsilon}{\lambda}}\right\}, \tag{3.10}$$

decreasing the lower end of the interval $[\epsilon, \lambda]$ increases the error exponentially.

In principle to reduce the error we could increase n until the approximation fits our needs. However, for the previously mentioned reasons of linearly increasing autocorrelations, and the demand of computer resources the order n of the approximating polynomial can not be increased at will.

This situation can substantially be improved by introducing a two-step approximation [11], in which the error introduced by the finite order of the polynomial $P^1_{n_1}$ is corrected in a global noisy correction step.

One starts with a relatively low order of n_1 (~ 30) for the polynomial $P^1_{n_1}$ used in the multi-bosonic algorithm as explained in the last Section. The update for n_1 scalar pseudofermionic fields is carried out by heatbath and overrelaxation sweeps. For gauge fields Metropolis sweeps are employed. A second polynomial $P^2_{n_2}$ is introduced, such that

$$|(\det \tilde{Q}^2)^{\frac{1}{4}}| \simeq \frac{1}{\det P^1_{n_1}(\tilde{Q}^2) \det P^2_{n_2}(\tilde{Q}^2)}. \tag{3.11}$$

While the multi-bosonic representation is only used for the polynomial $P^1_{n_1}$, the additional approximation by the second polynomial is realized by a global stochastic noisy correction step. This means that the gauge field that has been updated with the help of $P^1_{n_1}$ is in a second step subjected to a global accept-reject condition, which introduces the additional approximation of $P^2_{n_2}$ in (3.11). The hope is that with a high acceptance rate for the noisy correction step the autocorrelation is practically not influenced. In that way even with a low order first polynomial an arbitrarily exact algorithm can in principle be set up. We now explain how this global accept-reject step is realized in the algorithm.
The second polynomial $P^2_{n_2}$ is introduced, so that (3.6) is replaced by

$$\lim_{n_2 \to \infty} P^1_{n_1}(x) P^2_{n_2}(x) = x^{-\frac{1}{4}}, \quad x \in [\epsilon, \lambda]. \tag{3.12}$$

Thus the two steps have to generate the distribution

$$w[U] = \frac{e^{-S_g[U]}}{\det P^1_{n_1}(\tilde{Q}^2) \det P^2_{n_2}(\tilde{Q}^2)} \tag{3.13}$$

for the gauge configurations. This is the case if the algorithm employed fulfills the condition of detailed balance for $w[U]$.
Denote the transition probability of going from the gauge field $[U]$ to the field $[U']$ by

$$P(U' \leftarrow U) = P_A(U' \leftarrow U) P_B(U' \leftarrow U). \tag{3.14}$$

P_A is the transition probability of the combined various updaters that are part of the first step generating the distribution

$$w_{P_1}[U] = \frac{e^{-S_g[U]}}{\det P^1_{n_1}(\tilde{Q}^2)} = e^{-S^{n_1}_{CV}[U,\phi]}. \tag{3.15}$$

P_B represents the probability that in the global accept-reject step the change from $[U]$ to $[U']$ is accepted.
The condition of detailed balance for $P(U' \leftarrow U)$ reads now

$$\frac{P(U' \leftarrow U)}{P(U \leftarrow U')} = \frac{w[U']}{w[U]} = \frac{e^{-S^{n_1}_{CV}[U',\phi]} \det\left(P_{n_2}(\tilde{Q}[U]^2)\right)}{e^{-S^{n_1}_{CV}[U,\phi]} \det\left(P_{n_2}(\tilde{Q}[U']^2)\right)} \tag{3.16}$$

where we have made use of (3.15). Since for the probability P_A detailed balance holds, for P_B we find that

$$\frac{P_B(U' \leftarrow U)}{P_B(U \leftarrow U')} = \frac{\det\left(P^2_{n_2}(\tilde{Q}[U]^2)\right)}{\det\left(P^2_{n_2}(\tilde{Q}[U']^2)\right)} \tag{3.17}$$

must hold. This can be realized for example by the standard Metropolis acceptance

$$P_B(U' \leftarrow U) = \min\left\{1, \frac{\det\,(P^2_{n_2}(\tilde{Q}[U]^2))}{\det\,(P^2_{n_2}(\tilde{Q}[U']^2))}\right\}. \tag{3.18}$$

Numerically it is too costly to implement such a Metropolis step directly. For this reason the transition probability P_B is realized in a stochastic noisy correction step.
The idea is to generate a random vector η according to the normalized Gaussian distribution

$$\frac{e^{-\eta^\dagger P^2_{n_2}(\tilde{Q}[U]^2)\eta}}{\int d[\eta]e^{-\eta^\dagger P^2_{n_2}(\tilde{Q}[U]^2)\eta}}. \tag{3.19}$$

If the transition $[U] \to [U']$ is accepted with the probability

$$P_B = \min\left\{1, A(\eta, U' \leftarrow U)\right\} \tag{3.20}$$

where

$$A(\eta, U' \leftarrow U) = e^{-\eta^\dagger P^2_{n_2}(\tilde{Q}[U']^2)\eta - \eta^\dagger P^2_{n_2}(\tilde{Q}[U]^2)\eta}, \tag{3.21}$$

the condition of detailed balance (3.17) is fulfilled. The distribution (3.19) can in turn be generated from the simple Gaussian distribution

$$\frac{e^{-\eta'^\dagger\eta'}}{\int d[\eta']e^{-\eta'^\dagger\eta'}}. \tag{3.22}$$

To this end we define the Gaussian vector η and the new polynomial $P^{\frac{1}{2}}_{n_2}(\tilde{Q})$

$$\eta = (P^{\frac{1}{2}}_{n_2}(\tilde{Q}))^{-1}\eta'. \tag{3.23}$$

By substituting (3.23) in (3.22) and comparing with (3.19) we see that

$$P^2_{n_2}(\tilde{Q}^2) = P^{\frac{1}{2}}_{n_2}(\tilde{Q})^\dagger P^{\frac{1}{2}}_{n_2}(\tilde{Q}) \tag{3.24}$$

must hold. Indeed if we use the second decomposition in (3.8) and define

$$P^{\frac{1}{2}}_{n_2} = \sqrt{r_0}\prod_{j=1}^{n_2}(\tilde{Q} - \rho_j) \tag{3.25}$$

we see that (3.24) is satisfied. Since a simple Gaussian vector is easy to generate we now face the question of how to calculate $(P^{\frac{1}{2}}_{n_2}(\tilde{Q}))^{-1}$.
By using (3.24) $P^{\frac{1}{2}}_{n_2}$ can be inverted by inverting $P^2_{n_2}$

$$P^{\frac{1}{2}}_{n_2}(\tilde{Q})^{-1} = P^{\frac{1}{2}}_{n_2}(\tilde{Q})^\dagger[P^2_{n_2}(\tilde{Q}^2)]^{-1}. \tag{3.26}$$

The inversion of $P^2_{n_2}$ can be carried out in different ways. One possibility is an iterative scheme like the conjugate gradient, which can be applied since $P^2_{n_2}(\tilde{Q}^2)$ is hermitian. However, tests have shown [43,49] that an inversion which uses again quadratically optimized polynomials is more convenient, since less matrix multiplications have to be performed to

attain a given precision. To approximate $P^2_{n_2}(\tilde{Q}^2)^{-1}$ we introduce a third polynomial $P^3_{n_3}$ superior in order to $P^1_{n_1}$ and $P^2_{n_2}$ which approximates $1/x$. In this way the distribution (3.19) can be generated.
The global accept-reject step for the gauge field has in our simulations been performed after full sweeps over the gauge field links[4]. Choosing the length of the first polynomial is a delicate matter and tests have to be performed [43, 54] to decide which parameter combination for the multi-bosonic sweeps and the noisy correction step leads to optimal correlation lengths. If n_1 is chosen too large the correction step looses its influence and the correlation length grows. If on the other hand it is chosen too low the noisy correction step influences too much the dynamics of the updater and the correlation length can grow again.
The order n_1 of the first polynomial has been chosen such that the acceptance rate for the noisy correction is around 90%. However a recent QCD study [54] seems to indicate that fixing n_1 at a lower value does in fact decrease the autocorrelation of the plaquette substantially. The question of an optimal polynomial length n_1 is currently investigated in the DESY-Münster-Rome collaboration.

3.1.3 Measurement correction

The two-step approximation is certainly a progress compared to the original algorithm. Nevertheless, also the two-step variant will introduce systematical errors, especially near the lower end of the spectrum of the inverse fermion matrix. This problem becomes more severe when we go to smaller fermion masses and larger physical volumes.
The multi-bosonic algorithm becomes exact only for $n_2 \to \infty$ in (3.12). Instead of increasing n_2 and investigating the dependence of key quantities, i.e. observables on the polynomial order by performing several simulations, it is more practicable to fix a large n_2 for the simulation and perform yet another correction on the "measurement" of expectation values. This is realized by a reweighting of the configurations in the expectation value of the different quantities under investigation. In the case of $N_f = 2$ flavors this kind of reweighting has been used in the framework of the polynomial hybrid Monte Carlo scheme [55]. For a general flavor number N_f the measurement correction was introduced in [51]. For finite n_1 and n_2 we have that

$$|(\det(\tilde{Q}^2))^{\frac{1}{4}}| \simeq \frac{1}{\det[P^1_{n_1}(\tilde{Q}^2)P^2_{n_2}(\tilde{Q}^2)]}. \tag{3.27}$$

Introducing a fourth polynomial $P^4_{n_4}(x)$, such that

$$P^4_{n_4}(x)P^1_{n_1}(x)P^2_{n_2}(x) \overset{n_4 \to \infty}{=} x^{-\frac{1}{4}}, \tag{3.28}$$

the fermionic factor can be written as

$$\begin{aligned} |(\det \tilde{Q}^2)^{-\frac{1}{4}}| &\overset{n_4 \to \infty}{=} \frac{1}{\det[P^1_{n_1}(\tilde{Q}^2)P^2_{n_2}(\tilde{Q}^2)]\det[P^4_{n_4}(\tilde{Q}^2)]} \\ &= \frac{R[U]}{\det[P^1_{n_1}(\tilde{Q}^2)P^2_{n_2}(\tilde{Q}^2)]}. \end{aligned}$$

[4]As mentioned before those full sweeps consist of overrelaxation, heatbath and Metropolis updates.

The correction factor $R[U]$ can now be calculated through the bosonic path integral

$$R[U] = \frac{1}{\det\left[P^4_{n_4}(\tilde{Q}^2)\right]} = \frac{\int d[\eta] e^{-\eta^\dagger\eta} \;\; e^{\eta^\dagger[1-P^4_{n_4}(\tilde{Q}^2)]\eta}}{\int d[\eta] e^{-\eta^\dagger\eta}}, = \left\langle \exp\{\eta^\dagger[1-P^4_{n_4}(\tilde{Q}^2)]\eta\}\right\rangle_\eta ,$$

making use of the simple Gaussian noise estimator η. The reweighted expectation value $\langle\mathcal{O}\rangle$ is then given by

$$\langle\mathcal{O}\rangle = \frac{\left\langle \mathcal{O}\exp\{\eta^\dagger[1-P^4_{n_4}(\tilde{Q}^2)]\eta\}\right\rangle_{U,\eta}}{\left\langle \exp\{\eta^\dagger[1-P^4_{n_4}(\tilde{Q}^2)]\eta\}\right\rangle_{U,\eta}}. \tag{3.29}$$

$\langle ...\rangle_{U,\eta}$ denotes the expectation value with respect to the gauge configurations $[U]$ and a sequence of independent Gaussian vectors $\{\eta_i\}$. The length of the sequence of the $\{\eta_i\}$ has to be optimized to obtain sufficiently small errors.

In practice the correction factor $R[U]$ is calculated for each configuration of the sample, and the numerical estimate $\hat{\mathcal{O}}$ for the expectation value $\langle\mathcal{O}\rangle$ is then

$$\hat{\mathcal{O}} = \frac{\sum_U R[U]\mathcal{O}[U]}{\sum_U R[U]}, \tag{3.30}$$

where $\mathcal{O}[U]$ is the value of the local operator $\mathcal{O}$ on the configuration U. If the approximation by the first two steps is already good enough the correction factors do not change the expectation values ($R[U] \simeq 1$) and can be used to confirm the results obtained by the two-step approximation.

Figure 3.1 shows such a set of correction factors. Indeed including this correction factor in the mass calculation of the gluinoballs and the gluino-glueball does not result in any perceivable change in the mass values. The same is true for the ratios of the renormalization coefficients of the Ward identity (2.83) calculated in Chapter 3.5.

The measurement correction becomes particularly important for quantities that are sensitive to the small eigenvalues of the fermion matrix. As mentioned earlier this comes about since the approximation of the fermion factor by quadratically optimized polynomials enhances gauge configurations with small eigenvalues. Those configurations can give values for purely fermionic quantities which are orders of magnitude larger than the mean. This makes it impossible to extract physical information from the sample without further correction. The influence of these so-called exceptional configurations with very small eigenvalues must then be suppressed by reweighting.

However for exceptional configurations with the smallest eigenvalues in the range of 10^{-7} to 10^{-12} also a reweighting as described above is not sufficient. No polynomial $P^4_{n_4}$ with reasonable order n_4 can be generated which has acceptable errors in this range.

Furthermore on those configurations the value of $R[U]$ on one set of $\{\eta_i\}$ will be very noisy. This noise in turn is transmitted to the expectation value (3.30).

This problem can be avoided by fixing some ϵ' and calculating directly the eigenvalues of the matrix $\tilde{Q}$ that are smaller than ϵ'. The polynomial is then chosen such that a satisfactory approximation in the interval $[\epsilon', \lambda]$ is achieved. The number of eigenvalues smaller than a suitable ϵ' is usually of the order of 10, so their explicit calculation is feasible. The smallest eigenvalues ω that are determined explicitly, by a conjugate gradient

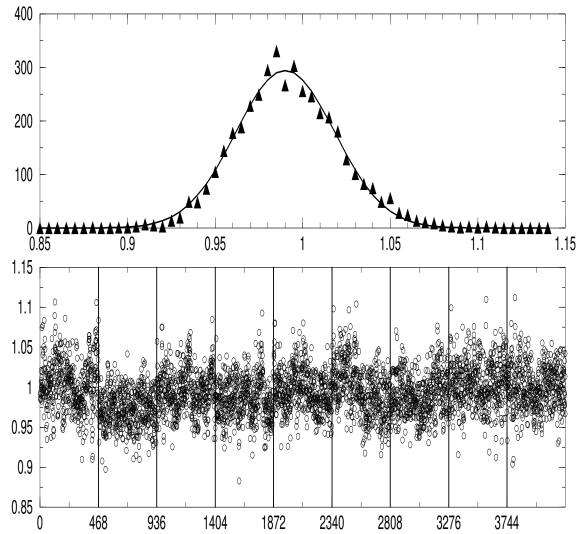

Figure 3.1: *Below: Correction factors of configurations separated by* 50 *updating sweeps produced on a* $12^3 \times 24$ *lattice at* $\beta = 2.3$ *and* $K = 0.1925$. *The vertical lines divide nine independent lattices.*
Above: A Gaussian fit to the distribution of the correction factors is shown.

for example, are reweighted by the factor $P^1_{n_1}(\lambda)P^2_{n_2}(\lambda)\lambda^{\frac{1}{4}}$ and the whole correction factor takes the form

$$R[U] \simeq \prod_{\omega<\epsilon'} P^1_{n_1}(\omega)P^2_{n_2}(\omega)\omega^{\frac{1}{4}} \prod_{\omega>\epsilon'} P^4_{n_4}(\omega)^{-1}. \tag{3.31}$$

To implement the second factor of the above equation numerically in (3.29) the eigenspace of the set of smallest eigenvalues has to be projected out from the noisy vectors $\{\eta_i\}$.
Let us comment on the interplay between the different approximations that we have discussed so far.
The reweighting is a comfortable method to explore the effect of different approximations to the fermion determinant. Omitting it would make different simulations with changing n_2 needed which is more costly. On the other hand leaving out the noisy correction step in favor of the measurement correction by reweighting would not be practical either. A first polynomial only, with relatively low order does not suppress sufficiently the configurations with small eigenvalues. Consequently the reweighting would be carried out with small correction factors, reducing in this way considerably the effective statistics. The effect of a proper reweighting can best be seen by considering quantities that actually diverge for zero eigenvalues. As an example we show in Figure 3.2 the a-π propagator on a $6^3 \times 12$ lattice at $\beta = 2.3$ and $K = 0.195$.

3.1.4 The Pfaffian and its sign

Let us now turn to the sign problem that arises in our numerical implementation of the Pfaffian. In Chapter 2.1.1 it was discussed that the question of the positivity of the Pfaffian has been settled in the continuum theory. The sign problem that we discuss now results from our lattice regularization of $N = 1$ SYM theory. As explained in the last Chapter not

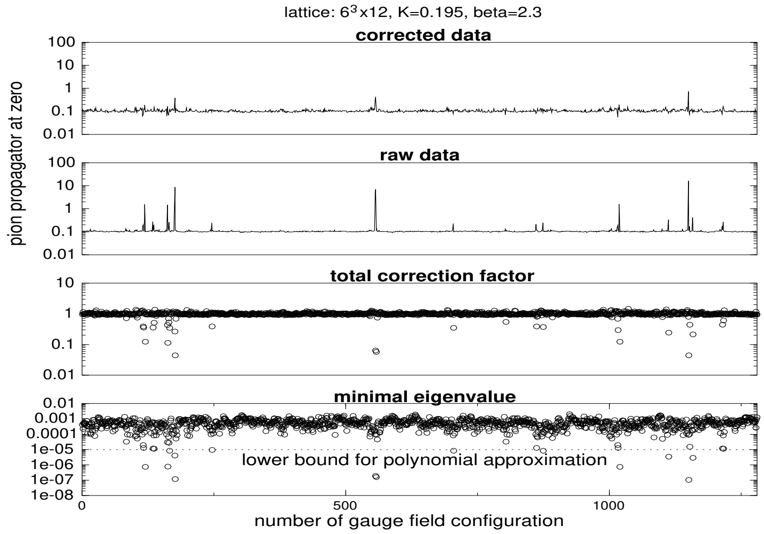

Figure 3.2: *Measurement correction of the a-π propagator at zero distance. The contribution of exceptional configurations on the raw data is up to two orders of magnitude larger than the mean value. After the correction their contribution is of normal size.*

the actual fermionic weight $\mathcal{PF}[M]$ appearing in the path integral (3.1), but its absolute value

$$|\mathcal{PF}[M]| = |(\det \tilde{Q}^2)^{-\frac{1}{4}}| \tag{3.32}$$

has been considered in the numerical simulation. The omitted sign can in principle be taken into account by reweighting the expectation values according to

$$\langle \bar{\mathcal{O}} \rangle = \frac{\langle \mathcal{O}\mathrm{sign}(\mathcal{PF}[M]) \rangle}{\langle \mathrm{sign}\mathcal{PF}[M] \rangle}. \tag{3.33}$$

The question is whether in our simulations a considerable number of configurations contributes with the wrong sign, so that when a reweighting according to (3.33) is performed large cancellations will take place altering the expectation value (3.30).
The exact numerical determination of the Pfaffian and its sign can be carried out by decomposing the N dimensional antisymmetric matrix M into a block diagonal matrix J and a triangular matrix P, so that

$$M = P^T J P, \qquad \mathcal{PF}[M] = \det(P). \tag{3.34}$$

The difficulty is to construct the matrix P explicitly, which can only be done on small lattices such as $4^3 \times 8$ [51] [5]. This is so since a full $N \times N$ matrix has to be stored, where N is the number of lattice points times the number of color and spinor indices, which equals $4(N_c^2 - 1)$ for the adjoint representation of $SU(N_c)$. In a thorough analysis [51] on a $4^3 \times 8$ lattice at $\beta = 2.3$ and $K = 0.1925$ no negative Pfaffians were found, which indicates that they are at least very rare and hence have a small statistical weight.
To calculate the sign necessary for a reweighting according to (3.33) on larger lattices we must use another method. The idea is to monitor sign changes in $\mathcal{PF}[M]$ as a function of

[5] The necessary RAM on such a small lattice exceeds already 16 MB.

the hopping parameter K.
Take a fixed gauge configuration U that has been produced at a certain $\hat{K}$. Consider now $\mathcal{PF}[M = CQ(U)]$ as a function of K. Since at $K = 0$ we have $\mathcal{PF}[CQ] = 1$. The sign of $\mathcal{PF}[CQ]$ at $\hat{K}$ where the actual dynamical fermion simulation is carried out is determined by the number of sign changes that take place as we vary K from 0 to $\hat{K}$.
The sign changes can be determined by the flow of the eigenvalues of $\tilde{Q}$ through zero. We already know from the last Section that $\tilde{Q} = \gamma_5 Q$ has doubly degenerate real eigenvalues. So

$$\det(M) = \det(\tilde{Q}) = \prod_{i=1}^{N/2} \tilde{\omega_i}^2, \tag{3.35}$$

where $\tilde{\omega_i}$ are the eigenvalues of $\tilde{Q}$. This implies for the absolute value of the Pfaffian

$$|\mathcal{PF}(M)| = \prod_{i=1}^{N/2} |\tilde{\omega}_i|. \tag{3.36}$$

Considering that the Pfaffian is a smooth polynomial in K we conclude that

$$\mathcal{PF}[M] = \prod_{i=1}^{N/2} \tilde{\omega}_i. \tag{3.37}$$

Therefore if any eigenvalue of $\tilde{Q}$ changes sign as a function of K, or any odd number of eigenvalues, the sign of $\mathcal{PF}$ changes too.
The sign of the Pfaffian on configurations of a $6^3 \times 12$ lattice has been monitored by this spectral flow method [12]. In all cases the deviations from the positive sign were smaller than 3% and hence on the average their effect is smaller than the statistical error (see Table 3.1).

K	# configs.	# of $Pf(M) < 0$	fraction
0.19	3840 (60x64)	0	< 0.0003
0.196	5248 (82x64)	14	0.0027
0.2	2304 (36x64)	69	0.03

Table 3.1: *The fraction of Pfaffians with negative sign at $\beta = 2.3$ on $6^3 \times 12$ lattice for different hopping parameters K.*

We see that for smaller values of K there are less configurations with a negative sign of the Pfaffian. This behavior is qualitatively clear, since for smaller values of K the spectrum is farther away from 0. Hence we conclude that at $K = 0.1925$ there are very few configurations with a negative sign of the Pfaffian.
For our simulation taking place on a $12^3 \times 24$ lattice at $\beta = 2.3$ and $K = 0.1925$ we do not expect to find a significant number of configurations with a negative sign of the Pfaffian. Consider the distribution of correction factors displayed in Figure 3.1, with respect to the distribution of correction factors for the $6^3 \times 12$ lattice at $\beta = 2.3$ and $K = 0.195$ shown in Figure 3.2. The correction factors of the $12^3 \times 24$ lattice are narrowly distributed around

their mean of about 0.98. There are no correction factors found with a large deviation from this mean value.
This in turn is an argument that in the course of updating not a lot of configurations have changed their sign. In the case of a sign change we would expect to find a larger number of smaller eigenvalues that are reminiscent of a crossing through zero, and the correction factor for these configurations would show a large deviation from the mean value. This situation can for example be observed on the $6^3 \times 12$ lattice at $\beta = 2.3$ and $K = 0.195$ which is displayed in Figure 3.2.
Thus we conclude that the appearance of negative Pfaffians at all parameter values considered in this work is negligible. Therefore the absolute value of the Pfaffian gives a good approximation of the path integral for the parameter region considered. There also exist theoretical positivity arguments based on another lattice formulation of $N = 1$ SYM theory using domain wall fermions [56]. In this formalism a positive definite Pfaffian arises naturally.

3.2 Run parameters and autocorrelations

3.2.1 Run parameters

The numerical simulations this work is based on, were done on a $12^3 \times 24$ hypercubical lattice. The boundary conditions chosen were periodic in the spatial directions for both the gluino and the gauge field. This implies that in the Hilbert space of states supersymmetry is not broken. In the time direction antiperiodic conditions were used for fermions, and periodic conditions for bosons. This is a direct consequence of the definition of the transfer matrix in the Hilbert space. The gauge coupling was fixed at $\beta = 2.3$, which from quenched simulations is believed to be in the scaling region. The hopping parameter of our simulation was chosen to be $K = 0.1925$. Based on previous experience [43, 51] this value seemed a good choice for a further approach of the chiral, i.e. the supersymmetric limit.
The polynomial degrees are fixed by performing a number of trial runs with increasing value. During these runs a number of quantities, such as the eigenvalues and autocorrelations are observed so as to fix the polynomial degrees to their optimal values and to find the interval $[\epsilon, \lambda]$, where the eigenvalues of the inverse fermion matrix are located.
However, the parameters we used are not yet optimized for the autocorrelation lengths. They were found in previous works [43, 49] to give satisfactory results for the updating and the autocorrelations.
A recent study of QCD [54] using the same algorithm seems to indicate that indeed the parameters so far used are not yet optimal. It has been found that contrary to prior expectations lowering the order of the first polynomial n_1 the autocorrelation of the plaquette decreases by a factor of two. Currently in the context of a new simulation this question is studied in the DESY-Münster-Rome collaboration.
In the simulation the final value of n_1 was fixed by ensuring a high acceptance rate ($80\% \simeq 90\%$) in the noisy correction step. The order of the second polynomial n_2 is fixed so that reweighting the expectation values of the physical quantities by the correction factors introduces a correction smaller than the statistical error. Typical examples of the polynomials can be seen in Figure 3.3. In the upper part the relative deviation of $P^1_{n_1}$

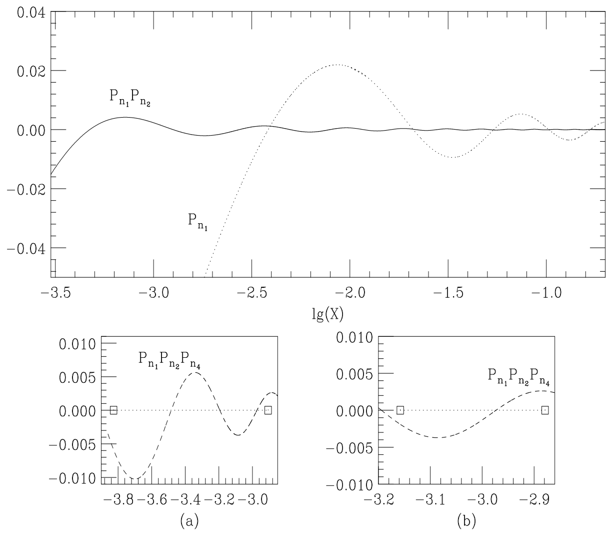

Figure 3.3: *Relative deviation of the polynomial approximation of $x^{-\frac{1}{4}}$ in the range of eigenvalues of the simulation on the $12^3 \times 24$ lattice at $\beta = 2.3$ and $K = 0.1925$. In (a) the range of the fluctuating smallest eigenvalue is shown, while (b) displays the range of the largest eigenvalue which was determined explicitly.*

and $P^1_{n_1} P^2_{n_1}$ from $(1/x)^{\frac{1}{4}}$ is shown. In the lower part the product of all three polynomials $P^1_{n_1} P^2_{n_1} P^4_{n_4}$ is displayed. The left of the lower Figures shows the approximation in the region where the smallest eigenvalue is fluctuating, while the right graph shows the same Figure, but in the range where the largest of the explicitly calculated eigenvalues is found. The degree of the third polynomial is fixed by considering the probability $P(U \leftarrow U)$ of the system to accept the updated configuration if actually no updating has taken place. In the limit of $n_3 \to \infty$ the probability $P(U \leftarrow U)$ goes to one. In the actual simulation n_3 was fixed as soon as $P(U \leftarrow U) \simeq 0.99$ was reached. That this is acceptable can be seen by monitoring expectation values. Finally n_4 is fixed by observing its effect on the expectation values.

In the process of one multi-bosonic sweep there are different updates involved for the scalar and the gauge field. The scalar field is updated by overrelaxation and scalar-heatbath sweeps, while the N-hit Metropolis was chosen for the gauge field. As mentioned earlier the combination of these three updaters that has been used is not the result of an extensive optimization, but rather what has been found to be convenient in former works [43, 49]. A complete multi-bosonic update consists now of the following combination

1 step scalar-heatbath $\to$ 3 steps scalar-overrelaxation $\to$ 1 step 20-hit Metropolis.

The parameters of the numerical simulation this work is based on are summarized in Table 3.2. The configurations were produced on 9 lattices run in parallel. Every 50 sweeps a configuration was saved, so that we have a total of 4320 configurations at hand.

Let us comment on another nontrivial point. For performing the noisy correction step as described in Chapter 3.1.2 the roots of the polynomial $P^2_{n_2}$ are needed. The ordering of these roots when the second representation of (3.8) is used is important. Choosing the order naively leads to over and underflow problems because very different orders of magnitude are involved. For a discussion of this point see [12, 53].

lattice: L, T	β	K	ϵ	λ	n_1	n_2	n_3	n_4	updates	N_c	N_{lat}
12,24	2.3	0.1925	0.0003	3.7	32	150	220	400	216000	4320	9

Table 3.2: *Parameters of the numerical simulations. N_c is the number of configurations saved, and N_{lat} is the number of lattices run in parallel.*

3.2.2 Autocorrelation lengths

The Markov process producing our configurations is characterized by its autocorrelation time τ. Qualitatively this is the time requested for the process to loose the memory of its current sample. Let $\mathcal{O}$ be any operator, and define the normalized autocorrelation function by

$$C_{\mathcal{O}\mathcal{O}}(t) = \frac{\langle \mathcal{O}(n)\mathcal{O}(n+t)\rangle}{\langle \mathcal{O}(n)\mathcal{O}(n)\rangle}. \tag{3.38}$$

Typically $C_{\mathcal{O}\mathcal{O}}(t)$ decays exponentially according to

$$C_{\mathcal{O}\mathcal{O}}(t) \propto e^{-|t|/\tau}, \tag{3.39}$$

for large t. This leads to the definition of the exponential autocorrelation time τ_{exp}

$$\tau_{exp,\mathcal{O}} = \lim_{t\to\infty} \sup \frac{t}{-\log|C_{\mathcal{O}\mathcal{O}}(t)|}. \tag{3.40}$$

Hence $\tau_{exp,\mathcal{O}}$ is the relaxation time of the slowest mode that couples to the operator $\mathcal{O}$. Nevertheless the true variance of the sample average $\bar{\mathcal{O}}$ is controlled by the integrated autocorrelation time $\tau_{int,\mathcal{O}}$

$$\tau_{int,\mathcal{O}} = \frac{1}{2} + \sum_{t=1}^{\infty} C_{\mathcal{O}\mathcal{O}}(t), \tag{3.41}$$

in the sense that

$$\sigma^2_{\bar{\mathcal{O}}} \overset{N\to\infty}{=} (\bar{\mathcal{O}}^2 - (\bar{\mathcal{O}})^2)\frac{2\tau_{int,\mathcal{O}}}{N}, \tag{3.42}$$

where N is the number of samples the average is taken over. This means that a sample of length N contains $N/(2\tau_{int,\mathcal{O}})$ effectively independent configurations.
Thus τ_{int} is of higher practical importance in a Monte Carlo simulation than τ_{exp}. Unfortunately as we will see below it is not always possible to give a reliable estimate of the integrated autocorrelation time. The problem is that the number of configurations at hand is too low, and in most cases we can only determine τ_{exp}.
We start the analysis by considering the short range exponential autocorrelation time τ_{exp} of three different quantities, namely

- the a-η' propagator.
- the gluino-glue propagator.
- the plaquette.

Only in the last case has the statistics been sufficient to give an estimate of the integrated autocorrelation. Our analysis is carried out on the configurations of Table 3.2. Note that we work with nine independent lattices run in parallel. Results for smaller lattices and at different K values can be found in [16, 43].
First of all we calculate the autocorrelation function $C(t)$ for all of the above quantities. In case of the a-η' we calculated the autocorrelation of the propagator at time distance $t = 1$, considering every 150'th configuration of the updating series. This was done separately on

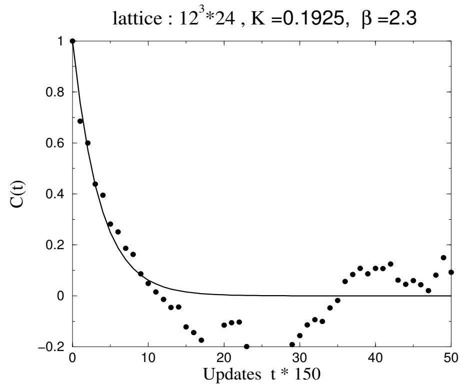

Figure 3.4: *Typical autocorrelation of the gluino-glue propagator on one of the nine lattices run in parallel.*

each of the lattices run in parallel. By averaging over the correlation functions obtained in this way we observed that the mean correlation function $\bar{C}^{a-\eta'}(t)$ was at $t = 1$ already compatible with zero ($\bar{C}^{a-\eta'}(1) = 0.028(19)$), which led to the conclusion that $\tau_{exp}^{a-\eta'} \leq 150$ updates.
Estimating the exponential autocorrelation τ_{exp} of the gluino-glue propagator we proceeded similarly as in the a-η' case. On all nine lattices that were run in parallel we determined independently the autocorrelation of the propagator at time distance $t = 1$ on every 150'th configuration of our total history. The exponential autocorrelation time was then estimated by fitting an exponential of the form $\exp(-t/\tau_{exp})$ to the first points of the curve for each lattice.
A typical autocorrelation function with the exponential fit can be seen in Figure 3.4. By finally taking the average of τ_{exp} over all lattices we arrived at the result displayed in Table 3.3. It has to be understood that τ_{exp} determined in this way displays a mode between the true short range exponential and the integrated autocorrelation, since only every 150'th sweep has been considered. To estimate the integrated autocorrelation time τ_{int} of the plaquette we proceeded in a different manner.
On the basis of prior analysis [16, 43] we expect the order of magnitude of τ_{int} to be $10^2 \sim 10^3$. Since for each lattice we have a total of about 24000 configurations in equilibrium we expect our time history to have a length of at most $\sim 100\tau_{int}$. This leads to the conclusion that standard methods to determine τ_{int} [57, 58] are not reliable since they require statistics that are at least of the order of several hundred τ_{int}.
Therefore, to estimate the order of magnitude of τ_{int} we proceeded as follows. For each lattice run in parallel we calculated the autocorrelation function $C^{plaq}(t)$ of the plaquette for the complete history of 24000 configurations. We fitted an exponential decay to

$C^{plaq}(t)$ in a small interval (typically $[0, 300]$) at the beginning where the fastest decay mode should be dominant. For longer distance the exponential typically decayed faster than $C^{plaq}(t)$. This expected behavior could usually be observed up to a point $\hat{t}$ where $C^{plaq}(t)$ started to be dominated by its noise.

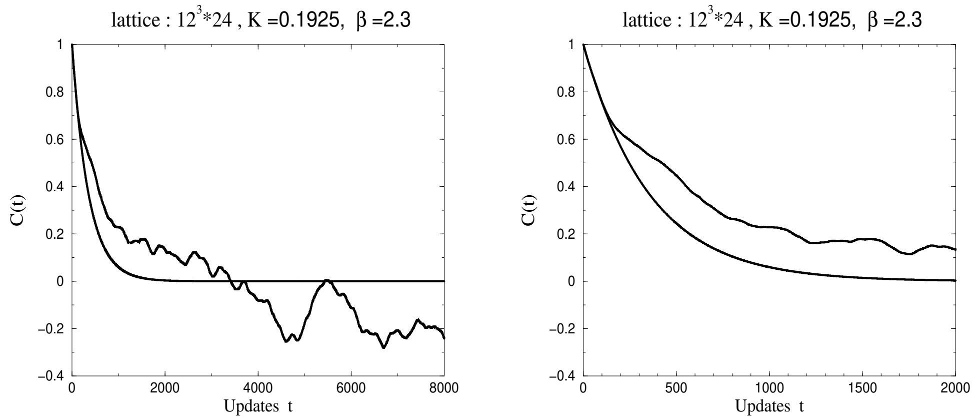

Figure 3.5: *Autocorrelation of the plaquette, with an exponential fit. The right graph shows the data in a smaller interval.*

We then calculated

$$\sum_{t=1}^{\hat{t}} C^{plaq}(t) \tag{3.43}$$

and took this value as an estimate of τ_{int}. We expect this procedure only to lead to an order of magnitude estimate for the integrated autocorrelation. The typical behavior for the autocorrelation function of the plaquette together with the exponential fit can be observed in Figure 3.5. In this example the cutoff $\hat{t}$ has been chosen at about $\hat{t} \sim 3500$ updates since at this point $C^{plaq}(t)$ is clearly dominated by its noise. The final result for τ_{exp} and τ_{int} have been obtained by averaging over all nine lattices run in parallel, and can be found in Table 3.3.

	τ_{exp}	τ_{int}
a-η'	≤ 150	-
gluino-glue	620(60)	1100(200)
plaquette	378(37)	675(43)

Table 3.3: *Autocorrelation and integrated autocorrelation of the propagators and the plaquette on* $12^3 \times 24$ *lattice at* $\beta = 2.3$ *and* $K = 0.1925$.

3.3 The low-lying spectrum

In this Section we will present the numerical methods and the results for the extraction of the lowest masses of the supermultiplet. These include the a-f_0 ($J^P = 0^+$), the a-η' ($J^P = 0^-$), the χ and the $J^P = 0^+$ glueball. The $J^P = 0^-$ glueball has not been analyzed, and the results quoted here are taken from [12]. In the supersymmetric limit at zero gluino mass $m_{\tilde{g}} = 0$ the different states are expected to occur in supermultiplets. For non-zero gluino mass the supersymmetry is softly broken and the masses are supposed to be analytic functions of $m_{\tilde{g}} = 0$ (see Chapter 1.2).
The following analysis is meant as a step towards the verification of the above scenario on the lattice.
The general strategy in calculating the different masses will be to determine the time-slice correlation functions as described in Chapter 2.2 of the interpolating fields discussed in Section 2.2.1 to Section 2.2.3. The relevant time-slice correlators $C(t)$ are calculated on the configurations of Table 3.2 that were produced by the above explained algorithm [6].
From the time-slice correlators $C(t), t \in [0, 23]$ we always calculate the symmetrized time-slice correlation function defined by [7]

$$C_{symm}(t) = \frac{1}{2}\left[C(t) + C(\frac{T}{2}+t)\right], \quad t \in [0, 12]. \tag{3.44}$$

As a first step in the determination of the mass we calculate in each case the effective mass from the symmetrized time-slice correlation function $C_{symm}(t)$. This is in all cases achieved by fitting $C_{symm}(t)$ with the symmetric function

$$\Gamma_1(t) = c_1 \cosh\left[m(\frac{T}{2}-t)\right], \tag{3.45}$$

in the interval $[t-1, t], t \in [1, 12]$, where T is the time extension of the lattice. The hope is that if a single state dominates we can observe that at some time-slice t the effective mass stabilizes and fluctuates within a small error for all later times. In this case we take the effective mass as a first orientation and try to estimate the mass of the lowest state by performing a one mass fit with the function (3.45) in the interval $[t_i, t_f]$ in which the effective mass gave stable results.
The reliability of this result is then checked, if the data allows this, by performing this one mass fit in the intervals $[t_i + 1, t_f], ..., [t_f - 1, t_f]$. If we can again observe that the mass extracted from these fits in the different intervals is stable and fluctuates only within a reasonable error we conclude that the mass of the lowest lying state has been isolated.
This situation however will only be realized if the influence of higher states is small at the time-slices considered.
To take into account also the contribution of higher states in the time-slice correlator we carry out a two mass fit according to

$$\Gamma_2(t) = c_1 \cosh\left[m_1(\frac{T}{2}-t)\right] + c_2 \cosh\left[m_2(\frac{T}{2}-t)\right]. \tag{3.46}$$

[6] For all that follows this is the only set of configurations our analysis is based on. For this reason in the following we will not explicitly refer to the lattice size or the run parameters. Unless stated otherwise the statistics used is always the one of Table 3.2.

[7] Since all of the correlation functions that turn out to be relevant for our analysis are symmetric we do not have to consider the case of anti-symmetrization.

However for a two mass fit with the above function to lead to stable results with a reasonable error the projection onto the lowest state by the interpolating operators must be very good. Hence it is not reasonable in all cases to perform a two mass fit.
Nevertheless if the correlator is not too noisy we can carry out a two mass fit and check the reliability of the results obtained by the one mass fit.
The tow mass fit is done in the interval $[t_i, 12]$ for t_i that varies from 1 to 9. The lowest mass can be considered reliable if it agrees with the one obtained from the one mass fit within the error for all t_i.
For t_i large it might also happen that the two mass fit becomes effectively a one mass fit, with both masses m_1 and m_2 equal.
In the detailed analysis that follows we discuss for each projecting operator seperately how the mass calculation was carried out. In case of the a-η' we will find data that is good enough to allow for the two mass fit in the above described manner, and we will also struggle with the a-f_0 which gives data that is so noisy, only a rough estimate of the mass can be given.
For the glueball and the gluino-glueball we find that smearing is essential in order to calculate the lowest mass. To optimize the signal and enhance the projection onto the lowest state we used Ape-smeared links for the glueball. It is well known from pure gauge theory that smearing is necessary if one wants to investigate glueball masses.
In case of the gluino-glueball, as it is a bound state consisting of a gluon and a gluino, we also used Ape-smeared links, and performed Jacobi smearing on the gluino fields. All errors in the following have been obtained by standard jackknifing
After the individual mass calculation we compare and summarize our results for the $12^3 \times 24$ lattice at $\beta = 2,3$ and $K = 0.1925$ with previously obtained masses at different K values and on different lattices [12]. We comment on the emerging particle scenario and on the formation of supermultiplets.
Finally we discuss the chiral limit in the context of the vanishing a-π mass and the a-η' correlator in the critical region of the hopping parameter.

3.3.1 The 0^+ Glueball

Glueball states and the techniques to compute their masses are well known from pure gauge theory (see [37] for a review).
The lightest state is the $J^P = 0^+$ glueball. the projecting operator we use to extract its mass has been introduced in Section 2.2.1. In order to optimize the signal and enhance the projection of the lightest state usually blocked or smeared links instead of the original ones are used.
In our case Ape smearing was performed since it gave smaller and more stable masses than Teper-blocking. The smearing parameters N_{APE} and ϵ_{APE} were fixed to the value, $N_{APE} = 20$ and $\epsilon_{APE} = 0.185$ that were also found in [43] for smaller lattices. We calculate the effective mass m_{eff} by fitting the correlation function (2.19) with $S(t) = S_{0^+}(t)$ of equation (2.23) with the symmetric function (3.45) in the interval $[t-1, t]$ with $t \in [1, 12]$. The result can be seen in Figure 3.6.
From $t = 9$ on the signal becomes too noisy for a determination of the effective mass m_{eff}. Notice that m_{eff} decreases with increasing t. This probably signals the presence of a higher mass state in the time-slice correlator. However, at $t = 3$ the effective mass has already stabilized and fluctuates for larger values of t within errors. Unfortunately we

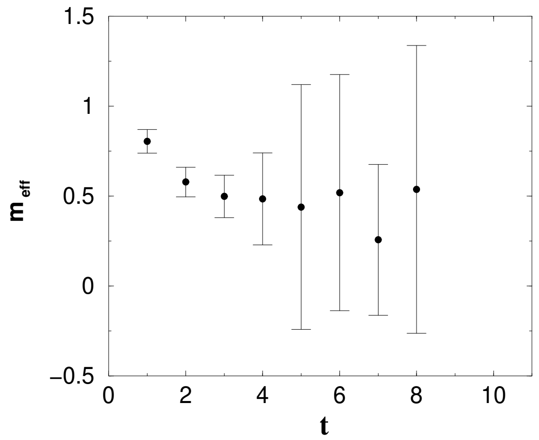

Figure 3.6: *Effective mass of the* 0^+ *glueball as a function of* t*.*

can also conclude from Figure 3.6 that a two mass fit will not be feasible since the signal is too noisy at later times.
Because we found the effective mass to have stabilized in the interval $[3, 8]$ we perform a one mass fit in this interval and quote as our best estimate

$$am_{glue} = 0.53 \pm 0.1. \tag{3.47}$$

3.3.2 Gluinoballs

We will now explain how we estimate the masses for the scalar and the pseudoscalar particle described in the Veneziano-Yankielowicz multiplet (see Section 1.2). Their wave functions are

- $\phi = \bar{\lambda}\lambda \quad (a\text{-}f_0)$,
- $\phi_p = \bar{\lambda}\gamma_5\lambda \quad (a\text{-}\eta')$.

Recall from Section 2.2.2 that the correlators formed from these wave functions consist of a connected and a disconnected part

$$C(t) = -2C(t)_{conn} + C(t)_{disconn}. \tag{3.48}$$

In QCD, $C(t)_{conn}$ gives rise to the π-mass and $C(t)$ to the η'-mass. In our model we only have one type of gluino flavor and hence the pion does not exist. However we will consider the "would be" pion in our model, that we denote by a-π whose two point correlation function is given by $C(t)_{conn}$.
Analogously to QCD we expect that as we approach the critical hopping parameter the mass of the a-π extracted from the decay of the connected part $C(t)_{conn}$ should vanish [31]. The total correlation function $C(t)$ should as $K \to K_{cr}$ become ever more dominated by the disconnected contribution.
The analysis of this third unphysical particle, the a-π is however postponed to Section 3.4.1 where we discuss the chiral limit. In the case of the gluinoballs no smearing has been done.

Let us now turn to the masss analysis of the two gluinoballs.

The a-η' particle :

As for the glueballs we proceed for the a-η' by calculating first the effective mass as a function of t. We fit (3.45) to the symmetrized time-slice correlator of (2.27) with $\Gamma = \gamma_5$ in the interval $[t-1, t]$ where t goes from 1 to $T/2 = 12$. The results are displayed in Figure 3.7. For t larger than 6, m_{eff} has stabilized and fluctuates within the error. So the

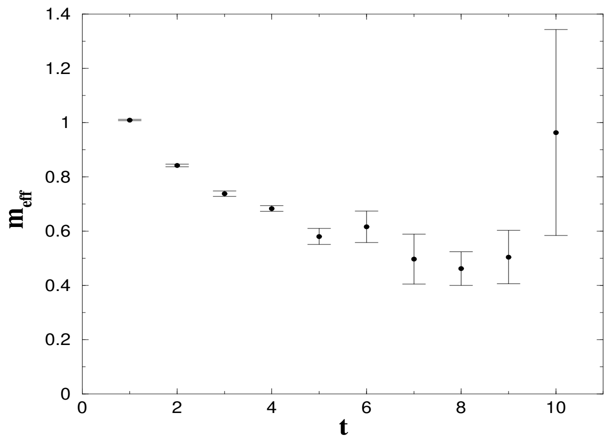

Figure 3.7: *Effective mass of the a-η' as a function of t.*

effective mass gives a good first orientation where the lowest lying state is located. The fact that with increasing t the effective mass decreases signals the presence of a higher state.
Since the effective mass is rather well determined up to time-slice $t = 9$ we can isolate also the next higher mass, performing a two mass fit with the function (3.46).
In Table 3.4 (upper row) we show the result of this two-state fit in the interval $[t_i, 12]$ as a function of t_i. Since from $t_i = 1$ on the results for the lower mass are fluctuating

$[t_i, 12]$	$t_i = 1$	$t_i = 2$	$t_i = 3$	$t_i = 4$	$t_i = 5$	$t_i = 6$	$t_i = 7$	$t_i = 8$	$t_i = 9$
am	0.56(3)	0.52(5)	0.51(8)	0.53(7)	0.53(7)	0.52(5)	0.52(5)	0.56(10)	0.66(18)
am	0.92(2)	0.76(2)	0.67(2)	0.61(2)	0.56(3)	0.54(5)	0.52(6)	0.56(10)	0.66(12)

Table 3.4: *Low-lying masses for the a-η' particle obtained from a two mass fit (upper row) and a one mass fit (lower row) in the interval* $[t_i, 12]$.

within the error, we can isolate the lowest state. It seems that since the lower mass is well determined from $t = 1$ on that the two state fit is sufficient to extract the influence of higher states on the correlation function. This conclusion is supported by the fact that with both masses equal within the error, the two mass fit turned from time-slice $t = 7$ on into an effective one mass fit.
As a further test we also performed a one state fit to the data in the same intervals. From

time-slice $t_i = 4$ on the results from a two mass and a one mass fit agree within the error (see Table 3.4). This justifies the conclusion that the lowest mass has been isolated and we quote as our best estimate

$$am_{a-\eta'} = 0.52 \pm 0.05. \tag{3.49}$$

The mass of the next higher state we estimate from the two mass fit in the interval $[2, 12]$ and quote as best estimate

$$a\tilde{m}_{a-\eta'} = 1.09 \pm 0.05. \tag{3.50}$$

The a-f_0 particle :

In contrast to the interpolating field for the a-η the operator $\phi = \bar{\lambda}\lambda$ which is used for the a-f_0 has a non zero vacuum expectation value, which is the gluino condensate $\langle\bar{\lambda}\lambda\rangle \neq 0$. This makes it more difficult to extract the mass from the time-slice correlation function, since the exponential decay sits on top of a large constant, $c_0 = |\langle\bar{\lambda}\lambda\rangle|^2$. It is difficult to determine this constant with reasonable errors since it fluctuates strongly [43]. This difficulty reflects itself in the effective mass of the a-f_0 (see Figure 3.8).
Note that the a-f_0 correlator has the general form

$$\Gamma(t) = c_0 + c_1 \cosh\left[m(\frac{T}{2} - t)\right]. \tag{3.51}$$

To determine the effective mass m_{eff} we calculate the additive constant $c_0 = |\langle\bar{\lambda}\lambda\rangle|^2$ from the disconnected contribution to the total propagator and subtract it from the correlation function.
The effective mass is then calculated by fitting the subtracted data to the symmetric function (3.45), in the interval $[t-1, t], t \in [1, 12]$. In Figure 3.8 we present the results for the effective mass of the a-f_0.

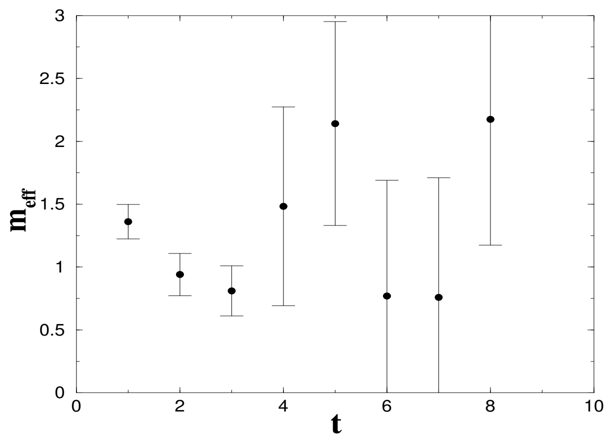

Figure 3.8: *Effective mass for the a-f_0 as a function of t.*

As m_{eff} from the fourth time-slice on has a large error ($\Delta m_{eff} > 1$ in lattice units) and is fluctuating strongly, the effective mass can not be used for a determination of the lowest mass. Furthermore we conclude that a one mass fit to the complete time-slice correlator

with (3.51) can only be carried out for small t. Otherwise the error in the mass will increase beyond the point of a reasonable estimate.
The mass value determined by a fit according to (3.51) can be found in Table 3.5. As best estimate we take the mass from fitting in the interval $[1, 3]$,

$$am_{a-f_0} = 1.00 \pm 0.13. \tag{3.52}$$

It must however be understood that since the fit interval used in the determination of the mass is at small t, contributions from higher masses can not be excluded. This means that our determination of am_{a-f_0} gives us an upper bound for the true mass of the state. It may very well be that there is yet another a-f_0 state with a lower mass, which is hidden in the noise at large t. The consistency of this result was checked by subtracting the constant

fit interval $[1, t_f]$	$t_f = 3$	$t_f = 4$	$t_f = 5$
m_{eff}	1.00(13)	1.01(14)	0.99(16)

Table 3.5: *Masses for the a-f_0 particle obtained from a one mass fit.*

c_0 from the complete propagator, as was done for the effective mass, and carrying out the fitting according to (3.45) afterwards.
The results obtained with the latter method were consistent with those from the former.

3.3.3 The gluino-glueball

The gluino-glueball is the spin 1/2 Majorana fermion occurring in the Veneziano-Yankielowicz multiplet. It is a bound state of a gluon and a gluino.
In order to calculate its mass we start by studying the correlator $C^{\alpha\beta}(t)$ of equation (2.31) with local sources (no smearing).
Recall (see Section 2.3.4) that $C^{\alpha\beta}(t)$ takes in the limit of infinite statistics the form

$$C^{\alpha\beta}(t) = C_1(t)\delta^{\alpha\beta} + C_2(t)\gamma_4^{\alpha\beta}. \tag{3.53}$$

We determine the two components C_1 and C_2 by taking the traces in Dirac space of the correlator (2.31)

$$C_1(t) = \frac{1}{4}\mathrm{Tr}[C(t)], \quad C_2(t) = \frac{1}{4}\mathrm{Tr}[C(t)\gamma_4]. \tag{3.54}$$

They can in principle be used for an independent determination of the lowest mass.
Before we calculate the effective mass, an inspection (see Figure 3.9) of the two components C_1 and C_2 of the correlation function (3.53) calculated on the configurations of Table 3.2 shows that the extraction of the lowest mass from local sources is a hopeless task. Note that the two components are displayed up to $t = 23$ and we have not made use of the boundary conditions to symmetrize or anti-symmetrize the correlator. Large statistical fluctuations spoil the signal and even the symmetry properties of C_1 and C_2 (see equation (2.33)) are washed out. This situation can be improved by smearing.
Since the gluino-glue is a bound state consisting of a gluon and a gluino we used APE [36] and Jacobi smearing [34] as was discussed in Chapter 2.2.6. Smearing was done on the

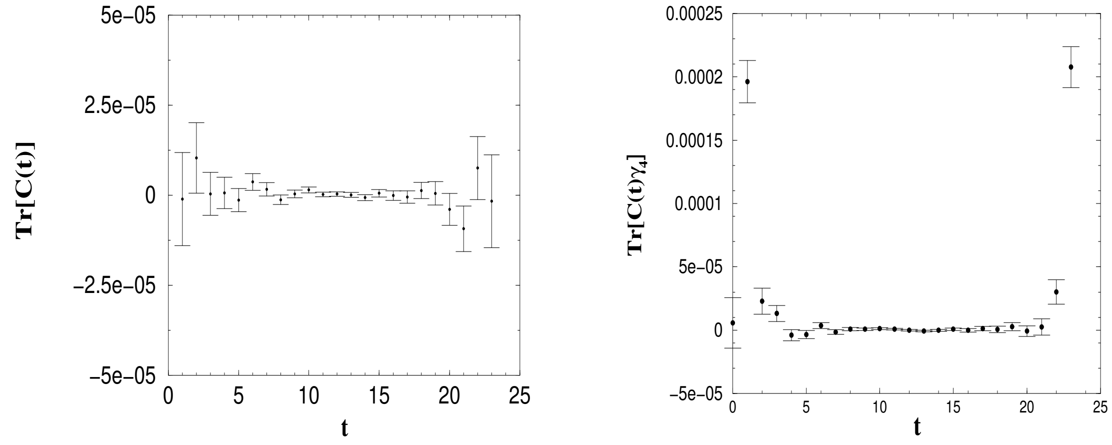

Figure 3.9: *Gluino-glue correlator as a function of the time distance t. The left graph shows the component C_1, and the right one the component C_2. To improve the readability of the plot the point at t=0 containing contact terms has been left out.*

source as well as on the sink of the propagator. Each algorithm introduces two parameters that have to be tuned to their optimal value. For the sink and the source the same parameters were used. Technical details concerning the numerical implementation of the smearing and the inversion can be found in Appendix C.
The problem of finding smearing parameters that model a wave function which gives a good projection onto the ground state and a signal to noise ratio that allows the determination of the lowest mass is very time consuming. For lattices up to the size $8^3 \times 16$ this has been done in [43], and for our optimization we have used the parameters found in this reference as a starting point. Note however that the projecting operators in [12, 43] have

N_{APE}	ϵ_{APE}	N_{JAC}	K_{JAC}
9	0.3	18	0.2
9	0.5	18	0.2
9	0.1	18	0.2
9	0.1	18	0.22
9	0.3	18	0.22
4	0.5	18	0.2
8	0.7	10	0.4
8	0.3	19	0.22
9	0.3	9	0.4

Table 3.6: *Trial parameters for the optimization of the smearing. The choice of the parameters is based on the study in [12, 43].*

a different spin structure than (2.29) which is used in this work.
To optimize the parameters of the smearing algorithms we calculated the effective mass of the gluino-glue on 500 configurations which is roughly 10% of the available statistics (see

Table 3.2). The optimization was done by finding the set among the parameters listed in Table 3.6 which gave the smallest mass and error.
We confronted the effective masses of both components C_1 and C_2 for the different parameters and found the optimal parameter values to be

$$N_{APE} = 9, \quad \epsilon_{APE} = 0.5, \qquad N_{JAC} = 18, \quad K_{JAC} = 0.2. \tag{3.55}$$

To appreciate the improvement that has taken place in going from point-like to smeared sources, the correlators for the above set of smearing parameters is shown in Figure 3.10. By pure inspection of these graphs we can see that the signal to noise ratio has improved by orders of magnitude and we can now attempt to isolate the lowest mass for the gluino-glueball.

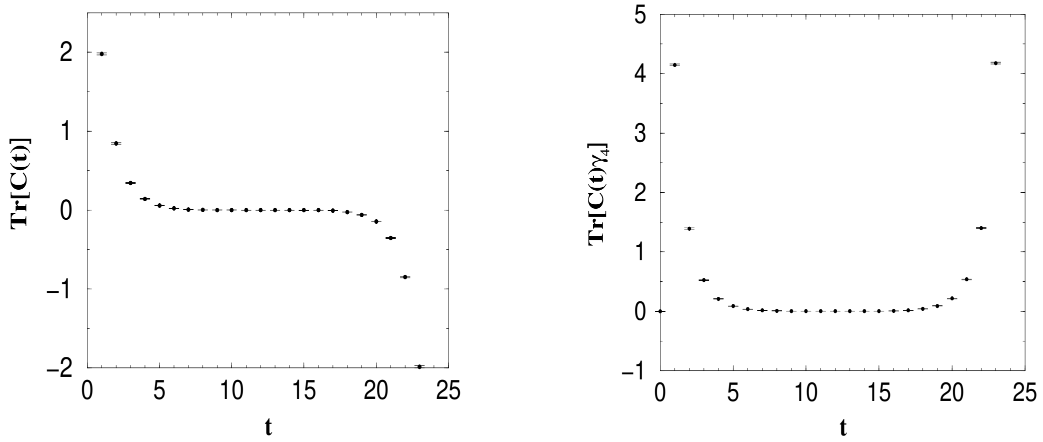

Figure 3.10: *Smeared gluino-glue correlator as a function of the time distance t. For comparison with the point-like sources the plots are not displayed logarithmically. Note that the symmetry properties of both components C_1 and C_2 emerge beautifully.*

As before first we calculate the effective masses. We can do this for the two components C_1 and C_2 of (3.53) seperately and should obtain an independent estimate of the mass from each of them. The best projection onto the lowest state was however always achieved by the component $C_2 = \mathrm{Tr}[C(t)\gamma_4]$ of the gluino-glue correlator and our analysis will only focus on this term. The analysis of C_1 always gave consistent results, but with larger errors.
Since the component C_2 is symmetric we can use (3.45) for the calculation of the effective mass m_{eff}. The result for m_{eff} is shown in Figure 3.11. The lowest state that could be found previously with a different projecting operator [12] had a mass of $am_{\tilde{g}g} = 0.93 \pm 0.08$. Figure 3.11 shows that the new operator (2.30) along with the retuning of the smearing parameters with respect to [12, 43] projects onto a state with a lower mass. The sudden drop that occurs from the seventh to the eighth time-slice clearly indicates the presence of a higher and a lower state, where the former of the two has roughly the mass of the gluino-glue state reported in [12]. Unfortunately the effective mass is not sufficient to isolate this lower state.
Qualitatively the signal seems not good enough to proceed directly with a two mass fit, in order to extract the contribution of the higher state.

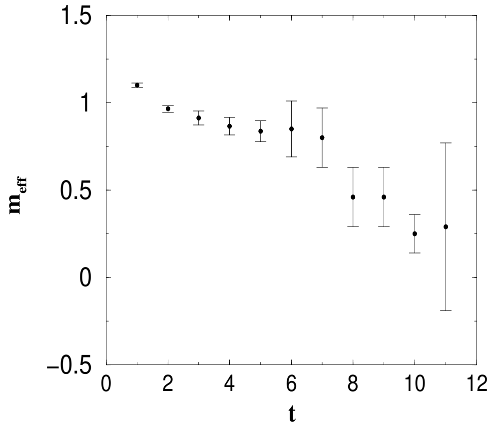

Figure 3.11: *Effective masses for the gluino-glue with smeared sources and sinks.*

Thus we perform a one mass fit according to (3.45) in the interval $[t_i, 12]$, where t_i runs from 1 to 11. In this way we want to observe that for larger t_i the mass stabilizes and begins to fluctuate within the error. This behavior would then allow us to estimate the lowest mass. These fits can be observed as a function of t_i in Figure 3.12.

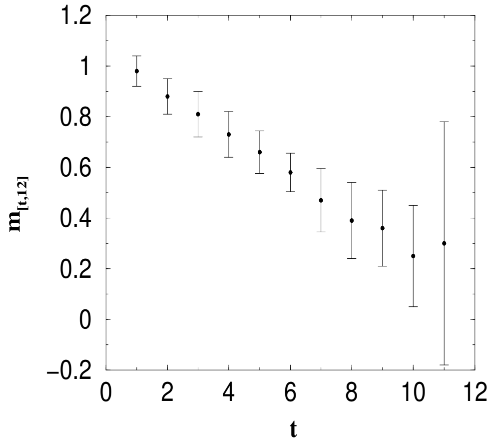

Figure 3.12: *One mass fits of the gluino-glue correlator in the interval* $[t, 12]$.

Unfortunately the signal does not stabilize, but drops steadily. This drop may signal the contribution of higher mass states that persists even for larger t. On the other hand since the drop remains within the error from time-slice 6 on it may also be a statistical coincidence for the later time-slices. This makes an isolation of the lowest mass difficult. Although the effective mass of Figure 3.11 seems a little too noisy, to take into account the contribution of a higher mass in the correlator we carry out a two mass fit with the function (3.46).
Again by fitting in the interval $[t_i, 12]$, for $t_1 = 1...9$ we hope to see the lower mass stabilize at a certain t_i and then fluctuate within reasonable small error. However as we can see from Table 3.7 where we report the results for the two mass fit the data does not allow for

a stable two mass fit. Nevertheless we see that from $t_i = 7$ on the two masses determined by the fit are equal. This is further strong evidence for the presence of a low-lying gluino-glue state which was missed in a previous analysis.

$[t_i, 12]$	$t_i = 1$	$t_i = 2$	$t_i = 3$	$t_i = 4$	$t_i = 5$	$t_i = 6$	$t_i = 7$	$t_i = 8$	$t_i = 9$
am_1	1.10(9)	0.95(10)	0.90(5)	0.90(07)	0.92(13)	0.98(26)	0.47(8)	0.45(8)	0.36(24)
am_2	0.51(10)	0.23(50)	0.01(60)	0.01(80)	0.01(80)	0.01(240)	0.47(8)	0.45(8)	0.36(24)

Table 3.7: *Higher (upper row) and lower mass (lower row) from the two mass fit to the smeared gluino-glue correlator in the interval* $[t_i, 12]$.

As best estimate for the lowest mass and the next higher state we take the results from the two mass fit in the interval $[1, 12]$. This takes on one hand the presence of a higher mass into account, and on the other hand the maximal amount of information that the correlation function offers is used. Hence we quote as our best estimate for the mass of the lowest gluino-glue state

$$am_{\tilde{g}g} = 0.51 \pm 0.10. \tag{3.56}$$

As a last check for the masses we subtracted from the correlator the contribution of the higher mass obtained from the two mass fit in the interval $[1, 12]$, and performed a one mass fit over the remaining data. The result of this one mass fit was in every fit interval consistent within the error with the one quoted above.

3.3.4 The low-lying multiplet

After the detailed analysis of the masses of the members of the Veneziano-Yankielowicz multiplet and possible glueball states, together with the previously obtained results from [12] we can study the multiplet structure as a function of the hopping parameter. In Table 3.8 you can find a summary of the masses of the light bound states at $\beta = 2.3$ in lattice units. Our results are summarized in the last two lines. The masses are shown as a function of $1/K$ in Figure 3.13. As one can see, for K approaching the shaded region where zero gluino mass and supersymmetry are expected [16] the particle masses are decreasing. This can be viewed as evidence for the formation of supermultiplets.

For the lightest gluino mass (highest K) the bound states form two groups. The lightest group which is found at $K = 0.1925$ with masses around $am \sim 0.5$ consists of the a-η' gluinoball, the spin $\frac{1}{2}$ gluino-glue and the 0^+ glueball. The fact that the 0^+ glueball is in the lighter group is in agreement with a theorem by West [19]. The heavier group at $K = 0.1925$ with masses around $am \sim 1.0$ consists of the a-f_0 gluinoball, the 0^- glueball and the heavier gluino-glue state. For small gluino mass and to lowest order we expect the masses of the multiplet to depend linearly on the gluino mass [20, 59]. Extrapolating to the region where the critical hopping parameter is expected, we see that both groups have a non-vanishing mass. This is further evidence for the expectation that the model has a QCD-like chiral behavior [5, 9].

In the low energy effective action of [6] there is a possible non-zero mixing between the states in the two light supermultiplets. The mixing of the 0^+ glueball with the a-f_0

lattice: L, T	K	$am_{gg}^{0^+}$	$am_{gg}^{0^-}$	$am_{\tilde{g}\tilde{g}}^{0^+}$	$am_{\tilde{g}\tilde{g}}^{0^-}$	$am_{\tilde{g}g}$
6,12	0.18	0.95(10)	-	1.49(13)	1.155(11)	1.93(5)
6,12	0.185	0.85(6)	1.5(3)	1.11(17)	0.941(8)	1.39(8)
8,16	0.19	0.75(6)	-	1.20(22)	0.725(20)	0.87(13)
8,16	0.1925	0.63(5)	1.1(1)	0.81(17)	0.551(17)	0.82(18)
12,24	0.1925	0.53(10)	-	1.00(13)	0.52(5)	0.51(10)
12,24	0.1925	-	-	-	1.09(5)	1.10(9)

Table 3.8: *Masses of the light bound states at $\beta = 2.3$ in lattice units. The last row shows the next higher mass for the particles of the supermultiplet that could be determined on the $12^3 \times 24$ lattice. Note that the gluino-glue masses determined on the $12^3 \times 24$ lattice have been calculated using a different operator than those of the $8^3 \times 16$ and the $6^3 \times 12$ lattice.*

gluinoball was analyzed in [12], and there was found to be none.
To estimate the mass of the gluino-glueball it was necessary to introduce Ape and Jacobi smearing and perform extensive tuning of the smearing parameters.
The introduction of the new gluino-glue operator (2.31) has revealed the presence of a gluino-glue state in the lower-mass group. This operator is a pure spin 1/2 state, while the formerly used operator (see [12]) is a sum of spin 1/2 and spin 3/2 states. So both operators have a projection on the same spin 1/2 state, but the numerical signal of (2.31) is less disturbed by the contribution of other, probably higher states. This is the reason why in the previous analysis the lower spin 1/2 component was missed.
Both mass groups are possible candidates for a supermultiplet from the point of view of their particle content. Note however that the particle structure of the groups is quite different from the one that has been predicted by effective actions (see Chapter 1.2).
The reasons for this may be various. In that respect we have to mention the mass analysis of the a-f_0 gluinoball.
Since its mass could only be extracted from a one mass fit on the first few time-slices it is probable that contributions from higher mass states are also present. This situation calls for bigger lattices and a proper smearing algorithm to isolate the lowest mass.
We might also not yet have come close enough to the supersymmetric limit with our numerical simulations and hence the spectrum does not exhibit weakly broken supersymmetry. One might also argue that finite volume effects and the presence of lattice artifacts spoil the signal of supersymmetry in our data. To exclude these possibilities simulations on larger lattices and closer to the chiral limit are under way. For a final analysis it will also be necessary to investigate the continuum limit by performing simulations at different values of the coupling β.
Let us comment on our strategy of parameter tuning in the lattice action. We started our simulations from the lower end of approximate scaling in pure $SU(2)$ gauge theory at $\beta = 2.3$. Due to the difference of the Callan-Symanzik β-function with and without light gluinos it is expected that the introduction of light dynamical fermions decreases the lattice spacing with respect to the quenched model.
The hopping parameter K was chosen around $K = 0.18$ during the first simulations [50],

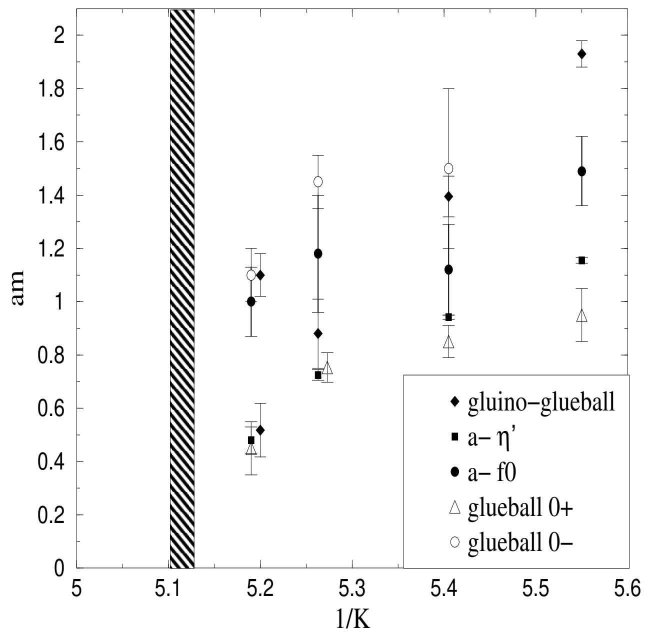

Figure 3.13: *The lightest bound state masses in lattice units as a function of the hopping parameter* $1/K$*. In the shaded area zero gluino mass and supersymmetry are expected [16].*

which is in the vicinity of the perturbative one loop estimate of the critical hopping parameter. K was then increased gradually and the spectrum was monitored. As mentioned before we expect that approaching the chiral limit the approximate restoration of supersymmetry will manifest itself through the formation of multiplets in the spectrum. We have now at $\beta = 2.3$ and $K = 0.1925$ observed the formation of two multiplets, but the projection onto the lowest mass state is not satisfactory for all particles considered.

Furthermore in the next Section discussing the chiral limit we will find evidence that we are not yet close enough to the chiral limit.

In simulations that were performed on $6^3 \times 12$ lattices at K values up to $K = 2.0$ evidence was found for a first order phase transition to occur at $K = 0.1955 \pm 0.05$ which is the best estimate of the critical hopping parameter.

Approaching K_c simulations become increasingly difficult from the algorithmic point of view, because the smallest eigenvalue of the fermion matrix decreases. Attempts to extract any of the masses on a $6^3 \times 12$ lattice at $K = 0.195$, $K = 0.196$, $K = 0.1975$ and $K = 0.2$ have failed. At the present K we can nevertheless conclude that our algorithm worked well. First tests seem to indicate that this is also the case at $K = 0.194$, and $\beta = 2.3$ on a $12^3 \times 24$ lattice.

As there is no physical quantity that has been measured in experiment which can be connected to our lattice simulation we cannot estimate the physical size of our lattice.

For a crude estimate however QCD units can be used. The string tension at $\beta = 2.3$ and $K = 0.1925$ has on our $12^3 \times 24$ lattice been measured to be [12] $a\sqrt{\sigma} = 0.17 \pm 0.01$. With L=12$a$, and $\sqrt{\sigma}_{QCD} = 0.44$ GeV we arrive at a lattice length in space of about L=1 fm. This seems not large enough for finite volume effects to be absent. Nevertheless the qualitative behavior of the spectrum is encouraging.

3.4 The chiral limit

As discussed in Chapter 1.1 a gluino mass $m_{\tilde{g}} \neq 0$ breaks chiral and supersymmetry. An appropriate tuning of the hopping parameter to its critical value K_{cr} can however restore chiral symmetry.

In Section 2.1.2 we mentioned different methods of how to extrapolate to the critical K_{cr}, and what behavior we expect for different quantities in the vicinity of $K = K_{cr}$. For convenience we list them again.

- The mass of the a-π should be small at $K \sim K_{cr}$, according to the PCAC relation

$$m_\pi^2 = A\left(\frac{1}{K} - \frac{1}{K_{cr}}\right). \qquad (3.57)$$

- At zero gluino mass the a-η' is believed to remain massive [5], and thus the correlation function of the a-η' must be dominated by its disconnected contribution (see (3.3.2)).

- At $K = K_{cr}$ a first order phase transition is expected to occur, which manifests itself in a jump of the value of the gluino condensate $\langle\bar{\lambda}\lambda\rangle$.

- At the critical point the renormalized gluino mass in the chiral and the supersymmetric Ward identities has to vanish.

In the next two Sections we want to discuss the first two of the above points numerically in detail. For the third point we refer to [16] where numerical evidence for a first order phase transition has been found. By observing a jump in the chiral condensate as the hopping parameter K is increased up to the value $K = 2.0$ an estimate of the region in which K_{cr} is expected to be found could be given.

Let us comment on the fourth item of the above list. The breaking of supersymmetry by a non-zero gluino mass makes itself manifest in the renormalized Ward identity (2.83) through the term

$$(m_0 - \bar{m}) \sum_{\vec{x} \in V} \langle D_S(x) \mathcal{O}(0) \rangle . \qquad (3.58)$$

Approaching the chiral limit the factor $(m_0 - \bar{m})$ stemming from the supersymmetry breaking by the gluino mass should vanish.

Vice versa the vanishing of $(m_0 - \bar{m})$ as a function of K can be used to define K_{cr} where supersymmetry is restored [9]. This way to define the supersymmetric limit provides us with an additional method to tune our simulations to $K = K_{cr}$.

Within the framework of our numerical analysis only ratios of renormalization coefficients can be calculated, such as $(m_0 - \bar{m})/Z_S$. Since perturbatively $Z_S = 1 + O(g_0^2)$ and $Z_T = O(g_0^2)$ we will divide by Z_S. In principle, a numerical determination of $(m_0 - \bar{m})/Z_S$ as a function of K can show if the critical hopping parameter K_{cr} estimated with the other above mentioned methods is consistent with the vanishing of $(m_0 - \bar{m})/Z_S$.

It is important to check if the different ways in which the supersymmetric limit of the lattice theory is approached give a self-consistent picture.

In Section 3.5 we show that it is possible to determine numerically the ratios Z_T/Z_S and $(m_0 - \bar{m})/Z_S$ to a precision which should allow to monitor the tuning of K to K_{cr} via the ratio $(m_0 - \bar{m})/Z_S$.

3.4.1 Vanishing of the a-π mass.

Recall that the correlator of the a-η' consists of a connected and a disconnected contribution (See (2.27) for the exact form)

$$C(t) = -2C(t)_{conn} + C(t)_{disconn}. \tag{3.59}$$

The connected term corresponds to the pion in QCD. Since in $N = 1$ Super Yang-Mills

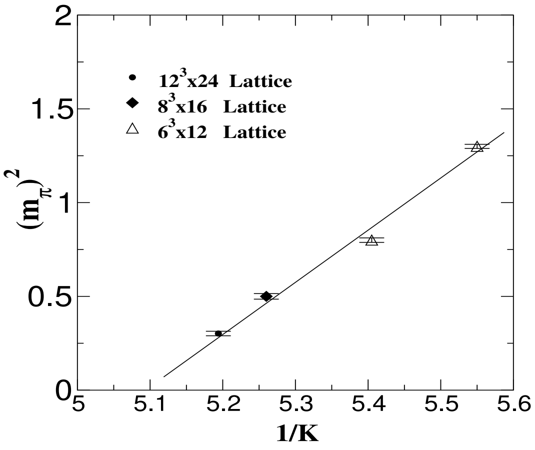

Figure 3.14: *The pion mass squared as a function of the inverse hopping parameter* $\frac{1}{K}$.

theory we have only one type of gluino flavor the a-π is not a physical state. Nevertheless we expect in analogy to QCD that the mass of the a-π vanishes in the chiral limit [5, 31]. We have calculated the mass of the a-π with the usual configurations at $\beta = 2.3$, and $K = 0.1925$ on the $12^3 \times 24$ lattice. To display the dependence of m_π^2 on $1/K$ which can be found in Figure 3.14 we have also used results from [43] on different lattices and at different K. Extrapolating linearly according to the PCAC relation (3.57) we find roughly $K_{cr} \simeq 0.1960(5)$ which is in good agreement with [16]. In the context of the quenched approximation [60] using the same approach $K_{cr} = 0.2151(3)$ has been found. We attribute the difference to the effects of dynamical gluinos.
Comparing at $K = 0.1925$ the values of the a-π mass ($am_{a-\pi} = 0.52 \pm 0.015$) and the mass of the a-η' ($am_{a-\eta'} = 0.48 \pm 0.05$) we see that they agree within errors. Both masses are of the same order, but close to the chiral limit we expect the a-π mass to vanish, while the a-η' should remain massive. Hence we can conclude that further simulations at higher K values are needed to approach chiral and supersymmetry.

3.4.2 The a-η' in the critical region.

Since we expect the a-π mass to decrease as we are approaching K_{cr} while the a-η' remains massive, the ratio

$$R(t) = \frac{C(t)}{C(t)_{disconn}} \tag{3.60}$$

as a function of $\frac{1}{K}$ is also expected to decrease. We plot $R(t)$ in Figure 3.15. For $K = 0.1925$ and $K = 0.196$ we observe that indeed $R(t)$ demonstrates the expected QCD-like behavior. The configurations at $K = 0.196$ are taken from [16]. They were produced

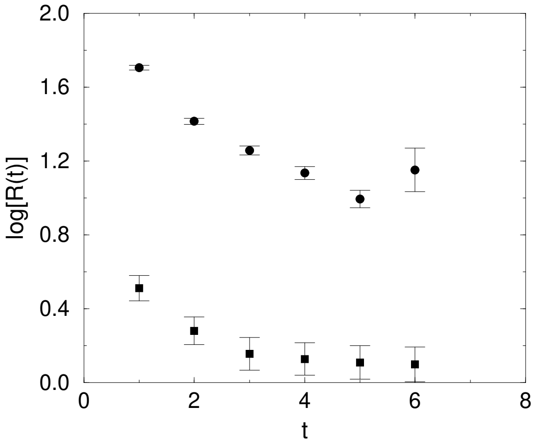

Figure 3.15: $R(t)$ *as defined in the text at* $K = 0.1925$ *(circles) and* $K = 0.196$ *(squares).*

on a $6^3 \times 12$ lattice at $\beta = 2.3$, and the statistics used at this point is the same as for $K = 0.1925$ (see Table 3.2). Unfortunately for K values higher than $K = 0.1925$ we were not able to determine the a-π and the a-η' mass with sufficient accuracy. For this reason we could not compare the masses directly, but carried out the above analysis instead.

3.5 Numerical investigation of the SUSY Ward identity on the lattice

In this Section we are going to describe in detail how we determine the ratios of the renormalization coefficients Z_T/Z_S and $(m_0 - \bar{m})/Z_S$ of the Ward identity (2.83) in a numerical simulation. It is not a new idea to use lattice Ward Identities for a non-perturbative determination of renormalization constants [44, 61–65].

In QCD on the basis of chiral Ward identities the renormalization constants Z_A and Z_V of the lattice vector and axial vector currents, as well as the ratio Z_P/Z_S of the renormalization constants of the scalar and the pseudoscalar density have been determined [66].

Another illustration of the same idea is the determination of the renormalization factor relating the renormalization group invariant quark mass to the bare quark mass of lattice QCD. The calculation is based on the PCAC relation and has been performed in the framework of the Schrödinger functional [64].

More recently Ward identities have also been used to calculate lattice mixing renormalization constants of composite operators in QCD [67].

In our case we calculate the ratios of the renormalization coefficients Z_T/Z_S and $(m_0 - \bar{m})/Z_S$ from the SUSY Ward identity (2.83). We do this to establish on one hand the validity of (2.83) within our numerical accuracy. A non-perturbative calculation of this kind can contribute to the question of supersymmetric anomalies.

On the other hand, determining $(m_0 - \bar{m})/Z_S$ is the first step towards a non-perturbative tuning of the bare gluino mass to the critical point where the restoration of SUSY and

chiral symmetry is expected.
The SUSY Ward identity on the lattice was found to have the form

$$\nabla_4^d \sum_{\vec{x}\in V} \left\{ \left\langle S_4^d(x)\mathcal{O}_i(0)\right\rangle + \frac{Z_T^d}{Z_S^d}\left\langle T_4^d(x)\mathcal{O}_i(0)\right\rangle \right\} = \frac{(m_0-\bar{m})}{Z_S^d}\sum_{\vec{x}\in V}\langle D_S(x)\mathcal{O}_i(0)\rangle + O(a). \tag{3.61}$$

The superscript d stands for the different lattice forms that we have discussed for the current $S_\mu^d(x)$, the mixing operator $T_\mu^d(x)$ and the lattice derivative ∇_μ^d. The index i enumerates the different operators $\mathcal{O}$.
To begin a numerical study of (3.61) we are basically confronted with two questions. First of all we have to find a lattice discretization of the current $S_\mu(x)$, the mixing operator $T_\mu(x)$ and the breaking term $D_S(x)$. Since the Ward identity (3.61) holds only up to order $O(a)$ there is a large arbitrariness in the choice of these operators involved. This freedom can in principle be used to choose operators such that the numerical determination of the matrix elements is least affected by statistical noise. Unfortunately it is not clear for what kind of operator this is going to be the case.
In the numerical analysis that follows we have chosen different discretizations. One choice is an ultra local form, and has been inspired by simplicity arguments only. The other discretization is based on lattice SUSY transformations and has a point-split form.
The different lattice operators were chosen such that among one pair of current and mixing operator the transformation properties under $\mathcal{P}$ and $\mathcal{T}$ where the same. In this way extra $O(a)$ effects are reduced.
In the beginning of our numerical simulations the hope was that at least one of the two forms leads to an accurate numerical signal. We will see that as a matter of fact both choices give good results, and there is no clear advantage of one over the other in numerical simulations.
The other question that has to be addressed is what kind of projecting operator $\mathcal{O}$ is to be used in the numerical analysis. It is important, as it is for the current, to choose the projecting operators in such a way that the matrix elements are well determined with a small error.
Fortunately for the projecting operator we have more freedom than for the current. They are in principle completely arbitrary constrained only by the fact that their matrix elements in (3.61) must not vanish. In Chapter 2.3.4 we have found two simple independent operators of the gluino-glue form that can be used as projecting operators.
Inserting these operators in their local form of equation (2.91) and (2.96) will probably not lead to a signal with a high signal to noise ratio as we have seen in case of the gluino-glue operator.
However we can apply the same techniques that allowed us to calculate the mass of the gluino-glueball. Since $\mathcal{O}$ is arbitrary we can use Ape and Jacobi smearing on $\mathcal{O}$ in order to enhance the projection onto intermediate states and to reduce the noise in the signal.
It must be stressed that the smearing can only be applied to the inserted operator $\mathcal{O}$ and not to the current or any other operator appearing in the Ward identity.
As expected using a local non-smeared operator as insertion in the Ward identity does not lead to a satisfactory determination of the ratios of the renormalization coefficients.
Only when smearing is performed on the projecting operators a determination of Z_T/Z_S and $(m_0-\bar{m})/Z_S$ with good accuracy becomes possible.

Before we start our analysis, in the next Section we will summarize the different currents and projecting operators, as well as the numerical technique we use to solve the Ward identity for the relevant ratios of the renormalization coefficients.
We then turn to the evaluation of Z_T/Z_S and $(m_0 - \bar{m})/Z_S$ with local operator insertions. After concluding that local operators do not lead to a satisfactory determination of the ratios of the renormalization coefficients we employ smearing on these operators.
As in the case of the gluino-glueball smearing enhances the projection onto the intermediate states and reduces the noise to such an extend that finally Z_T/Z_S and $(m_0 - \bar{m})/Z_S$ can be calculated with good accuracy.
In the last Section of this Chapter we will discuss the results of the analysis of the SUSY Ward identity and draw our conclusions.

3.5.1 Currents and projecting operators

In this section for completeness we summarize the different lattice discretizations of the current $S_\mu(x)$ the mixing operator $T_\mu(x)$ and the breaking term $D_S(x)$. We also list the different projecting operators, and discuss in detail how we solve the Ward identity (3.61) for Z_T/Z_S and $(m_0 - \bar{m})/Z_S$.
One lattice discretization of the supersymmetric current S_μ is the point-split current originating from a lattice SUSY transformation[8] with a mixing operator T_μ of analogous structure and the lattice derivative to the right. They were found to have the form

$$\begin{aligned}
S^d_\mu(x) &= S^{ps}_\mu(x) \\
&= -\frac{1}{2}\sum_{\rho\sigma}\sigma_{\rho\sigma}\gamma_\mu \mathrm{Tr}\Big[P_{\rho\sigma}(x)U^\dagger_\mu(x)\lambda(x+\hat{\mu})U_\mu(x) + P_{\rho\sigma}(x+\hat{\mu})U_\mu(x)\lambda(x)U^\dagger_\mu(x)\Big], \\
T^d_\mu(x) &= T^{ps}_\mu(x) \\
&= \sum_\nu \gamma_\nu \mathrm{Tr}\Big[U_\mu(x)P_{\mu\nu}(x)U^\dagger_\mu(x)\lambda(x+\hat{\mu}) + U^\dagger_\mu(x)P_{\mu\nu}(x+\hat{\mu})U_\mu(x)\lambda(x)\Big], \\
\nabla^d_\mu &= \nabla^r_\mu f(x) = f(x) - f(x-\hat{\mu}).
\end{aligned} \tag{3.62}$$

The other choice we have considered is a local current together with a local mixing operator and a symmetric lattice derivative

$$\begin{aligned}
S^d_\mu(x) &= S^l_\mu(x) = -\sum_{\rho\sigma}\sigma_{\rho\sigma}\gamma_\mu \mathrm{Tr}\Big[P_{\rho\sigma}(x)\lambda(x)\Big], \\
T^d_\mu(x) &= T^l_\mu(x) = 2\sum_\nu \gamma_\nu \mathrm{Tr}\Big[P_{\mu\nu}(x)\lambda(x)\Big], \\
\nabla^d_\mu &= \nabla^{symm}_\mu f(x) = \frac{1}{2}(f(x+\hat{\mu}) - f(x-\hat{\mu})).
\end{aligned} \tag{3.63}$$

These operators have the same naive continuum limit as $a \to 0$ as the point-split ones, but differ in this limit by terms of the order $O(a)$. Since the lattice Ward identity (3.61) holds up to the order $O(a)$ the local operators are a priori as suited as the point-split

[8]The transformation we refer to is that of equation (2.42) and is only a SUSY transformation up to order $O(a)$.

operators. It is important to note that for different currents and mixing operators also the renormalization coefficients Z_S and Z_T will differ. The operator

$$D_S(x) = \sum_{\rho\sigma} \sigma_{\rho\sigma} \mathrm{Tr}\Big[P_{\rho\sigma}(x)\lambda(x)\Big] \tag{3.64}$$

giving rise to the mass renormalization is not changed, and hence the term $M_R = (m_0 - \bar{m})$ which will also be referred to as the subtracted gluino-mass is the same in both cases. Note that M_R and the physical gluino mass differ by a multiplicative renormalization [9].
Let us now turn to the operators $\mathcal{O}_i$ that can be inserted in (3.61). Our discussion was limited to those operators that have the $P_{\mu\nu}\lambda$ gluino-glue structure. We found that there are two suitable independent operators, namely

$$\begin{aligned}
\mathcal{O}_1^{\alpha}(y) = \bar{\chi}_s^{\alpha} &= \sum_{ij} \mathrm{Tr}[P_{ij}(y)\overline{\lambda}^{\beta}(y)]\sigma_{ij}^{\beta\alpha}, \\
\mathcal{O}_2^{\alpha}(y) = \bar{\chi}_t^{\alpha} &= \sum_{k} \mathrm{Tr}[P_{4k}(y)\overline{\lambda}^{\beta}(y)]\sigma_{4k}^{\beta\alpha}.
\end{aligned} \tag{3.65}$$

The expectation values in (3.61) have two independent components with either of the above operators, namely one proportional to the identity $\mathbb{1}$, and the other proportional to γ_4. In all of our numerical simulations we will use for the operator $\bar{\chi}_s$ instead of the clover plaquette $P_{\mu\nu}$ the simple plaquette in $U_{\mu\nu}$. This does not alter any of the conclusions drawn in Chapter 2.3.4 since in the $a \to 0$ limit the only difference between the two choices are extra $O(a)$ terms. However for the operator $\bar{\chi}_t$ we stick with the clover plaquette since otherwise we would be left with a non-symmetric correlator in the time direction. The simple plaquette leads to an asymmetry in the time variable t of time-slice correlation functions, such that (2.98) does not hold any more.
For either current this leaves us with an overdetermined system of four independent equations for every time-slice. These can be used in a linear fit to determine the ratios of the renormalization coefficients in (3.61).
Before we proceed with the calculation of the ratios of the renormalization coefficients with local operator insertions let us discuss in detail how the numerical analysis is going to be carried out. For definiteness let us consider the case of the local current, the corresponding operator mixing, and the symmetric lattice derivative (3.63). Inserting the operator $\mathcal{O}_1$ of (3.65) every time-slice correlation function $C(t)$ in (3.61) has two components that can be isolated by taking $\mathrm{Tr}[C(t)]$ or $\mathrm{Tr}[C(t)\gamma_4]$.
Defining now

$$x_1 = \mathrm{Tr}\left[\sum_{\vec{x}} \nabla_4 \left\langle T_4^l(x)\mathcal{O}_1\right\rangle\right], \quad y_1 = \mathrm{Tr}\left[\sum_{\vec{x}} \langle D_S(x)\mathcal{O}_1\rangle\right], \quad z_1 = \mathrm{Tr}\left[\sum_{\vec{x}} \nabla_4 \left\langle S_4^l(x)\mathcal{O}_1\right\rangle\right],$$

$$x_2 = \mathrm{Tr}\left[\sum_{\vec{x}} \nabla_4 \left\langle T_4^l(x)\mathcal{O}_1\right\rangle\gamma_4\right], y_2 = \mathrm{Tr}\left[\sum_{\vec{x}} \langle D_S(x)\mathcal{O}_1\rangle\gamma_4\right], z_2 = \mathrm{Tr}\left[\sum_{\vec{x}} \nabla_4 \left\langle S_4^l(x)\mathcal{O}_1\right\rangle\gamma_4\right],$$

$$a = Z_T/Z_S, \quad b = (m_0 - \bar{m})/Z_S,$$

we have two independent equations for every time-slice, which are of the form

$$-ax_i + by_i = z_i. \tag{3.66}$$

These can be solved for a and b (see Appendix A) for every fixed time-slice t. Since the renormalization coefficients in (3.61) are time independent, with an accurate enough determination of the expectation values a plateau must develop for a and b as a function of the time-slice t, which then determines the ratios a and b and their error.
The best estimate for a and b is determined by fitting simultaneously all $2 \times n_t$ equations of the form (3.66), where n_t is the number of time-slices considered. The fitting algorithm we used in this work is described in Appendix A.
The same analysis can be carried out for the operator $\mathcal{O}_2$ of (3.65). If the supersymmetric Ward identity holds the resulting ratios should agree with the ones obtained from inserting O_1 within errors up to $O(a)$.
In a first step we analyze the Ward identity (3.61) seperately for $\mathcal{O}_1$ and $\mathcal{O}_2$ as described above. If the results for the ratios of the renormalization coefficients from the two operators are consistent we can consider all four equations stemming from the two operators $\mathcal{O}_1$ and $\mathcal{O}_2$ together and perform a fit to find the best estimate of a and b. We do this first for every time-slice seperately. After we have established that a plateau develops all time-slices can be simultaneously fitted. This means that we fit all $4 \times n_t$ equations of the form (3.66) according to the fit procedure described in Appendix A.
The method described above can be applied to point-like and to smeared sources. Certainly on the basis of prior experience it is improbable that point-like sources will give a clear enough signal in order to determine the above ratios with reasonable accuracy. It is however worthwhile to consider local sources first, as we have to consider ratios of correlation functions and the noise that we have for example encountered in the local gluino-glue correlator might cancel to a sufficient degree.
So in a first attempt we will consider (3.61) with the local operators (3.65) inserted.

3.5.2 Local sources

To evaluate the Ward identity (3.61) with local sources we distinguish between the two different types of currents, namely the point-split current, and the local current.
We will start the numerical investigation, by considering (3.61) with the point-split current (3.62) and the local operator $\bar{\chi}_s$ of (3.65) inserted. Numerically we have to evaluate the three time-slice correlations

$$\sum_{\vec{x}} \nabla_4^r \left\langle (S_4^{ps})^\alpha(x) \mathcal{O}_1^\beta(y_s) \right\rangle = \sum_{\vec{x},\rho,\sigma,i,j} -\frac{1}{2}\sigma_{\rho\sigma}^{\alpha\gamma'}\gamma_4^{\gamma'\alpha'} \Big\{$$

$$\Big[\mathrm{Tr}\left[P_{\rho\sigma}(x+\hat{\mu}_4)U_4(x)\frac{\sigma_a}{2}U_4^\dagger(x)\right] - \mathrm{Tr}\left[P_{\rho\sigma}(x-\hat{\mu}_4)U_4^\dagger(x-\hat{\mu}_4)\frac{\sigma_a}{2}U_4(x-\hat{\mu}_4)\right]\Big] \Delta_{xa\alpha'}^{y_s b\beta'}$$

$$+\mathrm{Tr}\left[P_{\rho\sigma}(x)U_4^\dagger(x)\frac{\sigma_a}{2}U_4(x)\right]\Delta_{(x+\hat{\mu}_4)a\alpha'}^{y_s b\beta'} - \mathrm{Tr}\left[P_{\rho\sigma}(x)U_4(x-\hat{\mu}_4)\frac{\sigma_a}{2}U_4^\dagger(x-\hat{\mu}_4)\right]\Delta_{(x-\hat{\mu}_4)a\alpha'}^{y_s b\beta'}$$

$$\Big\}\mathrm{Tr}\left[P_{ij}(y_s)\frac{\sigma_b}{2}\right]\sigma_{ij}^{\beta'\beta},$$

$$\sum_{\vec{x}} \nabla_4^r \left\langle (T_4^{ps})^\alpha(x) \mathcal{O}_1^\beta(y_s) \right\rangle = \sum_{\vec{x},\nu,i,j} \gamma_\nu^{\alpha\alpha'} \Big\{$$

$$\Big[\mathrm{Tr}\left[P_{4\nu}(x+\hat{\mu}_4)U_4(x)\frac{\sigma_a}{2}U_4^\dagger(x)\right] - \mathrm{Tr}\left[P_{4\nu}(x-\hat{\mu}_4)U_4^\dagger(x-\hat{\mu}_4)\frac{\sigma_a}{2}U_4(x-\hat{\mu}_4)\right]\Big]\Delta_{xa\alpha'}^{y_s b\beta'}$$

$$
+\mathrm{Tr}\left[P_{4\nu}(x)U_4^\dagger(x)\frac{\sigma_a}{2}U_4(x)\right]\Delta^{y_s b\beta'}_{(x+\hat\mu_4)a\alpha'} - \mathrm{Tr}\left[P_{4\nu}(x)U_4(x-\hat\mu_4)\frac{\sigma_a}{2}U_4^\dagger(x-\hat\mu_4)\right]\Delta^{y_s b\beta'}_{(x-\hat\mu_4)a\alpha'}
$$

$$
\Big\}\mathrm{Tr}\left[P_{ij}(y_s)\frac{\sigma_b}{2}\right]\sigma_{ij}^{\beta'\beta},
$$

$$
\sum_{\vec x}\Big\langle (D_S(x))^\alpha(x)\mathcal{O}_1^\beta(y_s)\Big\rangle = \sum_{\vec x,\mu,\nu,i,j}\sigma_{\mu\nu}^{\alpha\alpha'}\Big\{\mathrm{Tr}\left[P_{\mu\nu}(x)\frac{\sigma_a}{2}\right]\Delta^{y_s b\beta'}_{xa\alpha'}\mathrm{Tr}\left[P_{ij}(y_s)\frac{\sigma_b}{2}\right]\sigma_{ij}^{\beta'\beta}\Big\}. \tag{3.67}
$$

The coordinate y_s is fixed, for example at the origin. The two components of these expectation values were calculated on the configurations listed in Table 3.2. The numerical results for the above time-slice correlators are shown in Figure 3.16. We display them to give an idea of the quality of the numerical signal.

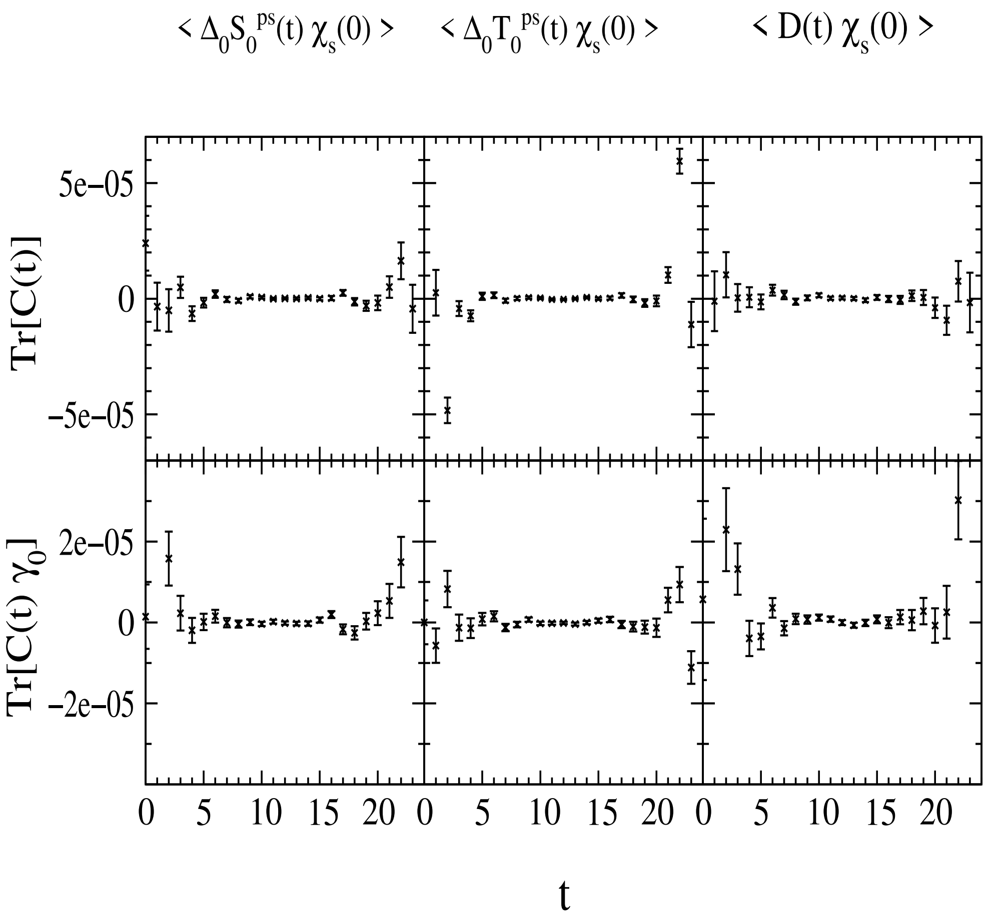

Figure 3.16: *Numerical results for the two components $\propto \mathbb{1}$ and $\propto \gamma_4$ of the time-slice correlation functions of (3.67).*

Qualitatively it is clear by inspection that the signal is dominated by noise. However, when solving the arising system of homogeneous equations for Z_T/Z_S and M_R/Z_S as explained in the last section we have to calculate the ratios of these correlators on every time-slice, and a large part of the noise could cancel. Thus we proceed with our analysis,

even though the correlators do not look encouraging.
Since for each correlator we have two components, we can solve exactly for the ratios Z_T/Z_S and $(m_0 - \bar{m})/Z_S$ on every time-slice as described in the previous Section.
The result is shown in the left graph of Figure 3.17. Because the current $\nabla_4 S_4^{ps}$ as well as the operator $\nabla_4 T_4^{ps}$ overlaps for small distances with the operator $\bar{\chi}_s$ there are contact terms up to the time distance $t = 2$, and down to $t = 22$. So the physical signal can be expected between time-slice $t = 3$ and $t = 21$. Unfortunately we see immediately that the data is too noisy to allow a determination of M_R/Z_S that is accurate enough to investigate the approach of the chiral limit as $K \to K_{cr}$.

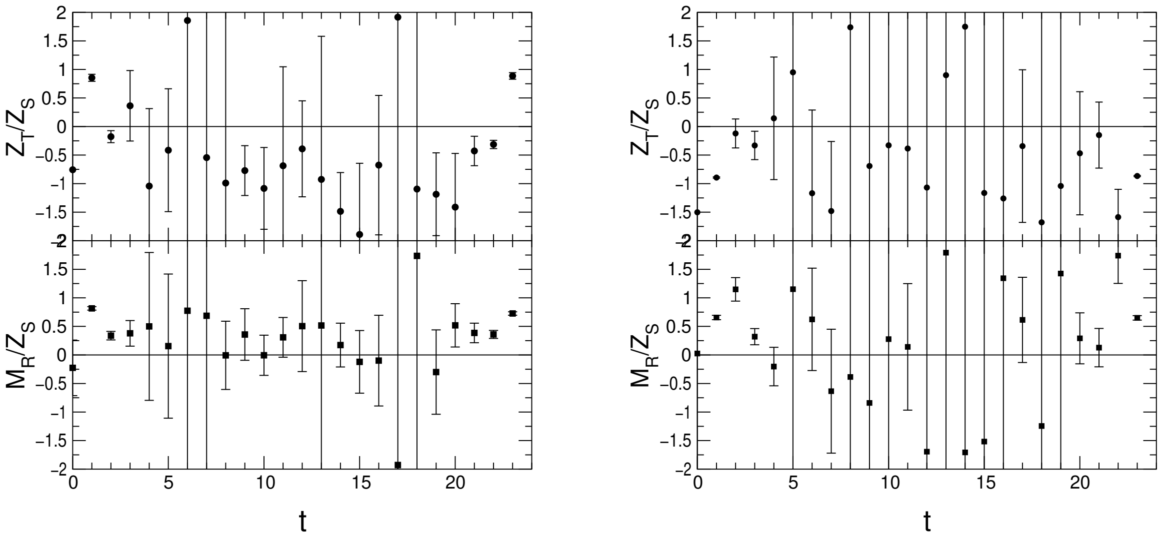

Figure 3.17: *Results for the two ratios Z_T/Z_S and $M_R = (m_0 - \bar{m})/Z_S$ as a function of the time-slice t for the point-split current. The left graph shows the evaluation of the ratios with the operator $\mathcal{O}_i = \bar{\chi}_s$ inserted in (3.61). The right graph shows the results for $\mathcal{O}_i = \bar{\chi}_t$.*

However, we can still do the same analysis for the operator $\bar{\chi}_t$ of (3.65), and finally perform a fit over all data. This could in principle improve the situation, since we double the statistics involved. Note that for the operator $\bar{\chi}_t$ the contact terms are present up to $t = 3$ and $t = 21$, since the time-like plaquette extends one lattice spacing in the time direction. The three time-slice correlators of (3.61) with $\mathcal{O} = \bar{\chi}_t$ inserted change only in so far, as the sum over the spatial indices (ij) in (3.67) is substituted by a sum over $(4i), i \in [1, 2, 3]$. For this case we do not display the numerical values of the different time-slice correlators, since they are qualitatively the same as those of Figure 3.16.
The results for the ratios of the renormalization coefficients Z_T/Z_S and $M_R/Z_S = (m_0 - \bar{m})/Z_S$ obtained from the operator insertion $\mathcal{O} = \bar{\chi}_t$ can be found in in the right graph of Figure 3.17. Unfortunately they fluctuate in the same way as the ones we obtained using $\mathcal{O} = \bar{\chi}_s$ as inserted operator.
Nevertheless assuming that (3.61) is valid we analyze the total of the data that we have

from inserting the two operators $\bar{\chi}_s$ and $\bar{\chi}_t$. Since every operator insertion has two independent components we arrive at four equations for every time-slice. Hence we have an overdetermined system of the form (3.66), and we carry out a linear fit. This gives us a best estimate for the ratios Z_T/Z_S and $M_R/Z_S = (m_0 - \bar{m})/Z_S$ for every time-slice using the described local operators as insertions in (3.61).

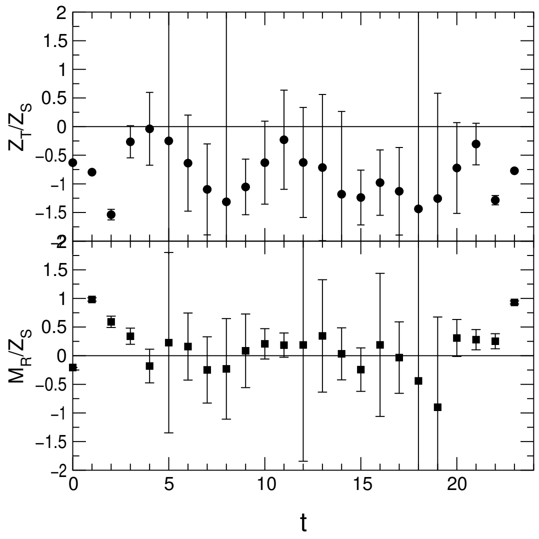

Figure 3.18: *Results for the ratios Z_T/Z_S and $M_R/Z_S = (m_0 - \bar{m})/Z_S$ for the point-split current as a function of the time-slice t. A linear fit has been performed on the four equations resulting from the two insertions $\mathcal{O}_i = \bar{\chi}_t$ and $\mathcal{O}_i = \bar{\chi}_s$.*

The result can be seen in Figure 3.18. Unfortunately considering all the data together does not improve the situation substantially, and we conclude that by using local operators $\mathcal{O}$ of the above form and the point-split current S_μ^{ps} and the operator T_μ^{ps} of equation (3.62) we cannot determine non-perturbatively the ratios Z_T/Z_S and $M_R/Z_S = (m_0 - \bar{m})/Z_S$ accurately enough for our purposes.
The local choice (3.63) for the current S_μ and the operator T_μ could improve the situation. We will now repeat the same analysis as we have carried out above, for the Ward identity (3.61), but use the local current as in (3.63). The time-slice correlators are given explicitly by

$$\sum_{\vec{x}} \nabla_4^{symm} \left\langle (S_4^l)^\alpha(x) \mathcal{O}_1^\beta(y_s) \right\rangle = \sum_{\vec{x},\rho,\sigma,i,j} -\frac{1}{2}\sigma_{\rho\sigma}^{\alpha\gamma'} \gamma_4^{\gamma'\alpha'} \Bigg\{$$

$$\mathrm{Tr}\left[P_{\rho\sigma}(x+\hat{\mu}_4)\frac{\sigma_a}{2}\right] \Delta^{y_s b\beta'}_{(x+\hat{\mu}_4)a\alpha'} - \mathrm{Tr}\left[P_{\rho\sigma}(x-\hat{\mu}_4)\frac{\sigma_a}{2}\right] \Delta^{y_s b\beta'}_{(x-\hat{\mu}_4)a\alpha'} \Bigg\} \mathrm{Tr}\left[P_{ij}(y_s)\frac{\sigma_b}{2}\right] \sigma_{ij}^{\beta'\beta},$$

$$\sum_{\vec{x}} \nabla_4^{symm} \left\langle (T_4^l)^\alpha(x) \mathcal{O}_1^\beta(y_s) \right\rangle = \sum_{\vec{x},\nu,i,j} \gamma_\nu^{\alpha\alpha'} \Bigg\{$$

$$\mathrm{Tr}\left[P_{4\nu}(x+\hat{\mu}_4)\frac{\sigma_a}{2}\right]\Delta^{y_s b\beta'}_{(x+\hat{\mu}_4)a\alpha'} - \mathrm{Tr}\left[P_{4\nu}(x-\hat{\mu}_4)\frac{\sigma_a}{2}\right]\Delta^{y_s b\beta'}_{(x-\hat{\mu}_4)a\alpha'}\Bigg\}\mathrm{Tr}\left[P_{ij}(y_s)\frac{\sigma_b}{2}\right]\sigma^{\beta'\beta}_{ij},$$

$$\sum_{\vec{x}}\left\langle (D_S(x))^{\alpha}(x)\mathcal{O}^{\beta}_1(y_s)\right\rangle = \sum_{\vec{x},\mu,\nu,i,j}\sigma^{\alpha\alpha'}_{\mu\nu}\left\{\mathrm{Tr}\left[P_{\mu\nu}(x)\frac{\sigma_a}{2}\right]\Delta^{y_s b\beta'}_{xa\alpha'}\mathrm{Tr}\left[P_{ij}(y_s)\frac{\sigma_b}{2}\right]\sigma^{\beta'\beta}_{ij}\right\}. \tag{3.68}$$

Instead of solving for the ratios Z_T/Z_S and $M_R/Z_S = (m_0 - \bar{m})/Z_S$ seperately for the two possible insertions $\mathcal{O} = \bar{\chi}_s$ and $\mathcal{O} = \bar{\chi}_t$ we proceed directly with a linear fit to all 4 equations on every time-slice coming from both operators. The results are displayed in Figure 3.19.

In case of the local current there are also contact terms present up to $t = 2$ and down to $t = 22$ for $\mathcal{O}_i = \bar{\chi}_s$ and up to $t = 3$ and down to $t = 21$ for $\mathcal{O}_i = \bar{\chi}_t$. With respect to the point-split current the extension of these contact terms has not been reduced, since the symmetric derivative for the local current has the same extension as the right-derivative for the point-split current. However again we see clearly that the data is far too noisy.

We conclude that for the local projecting operators we have not been able to obtain numerical data that allowed the determination of the ratios of the renormalization coefficients. Nevertheless since the operators $\mathcal{O}$ that can be inserted in (3.61) are arbitrary to a large extent we can use smearing techniques that we have already used for the time-slice correlators of the gluino-glue particle to improve the signal.

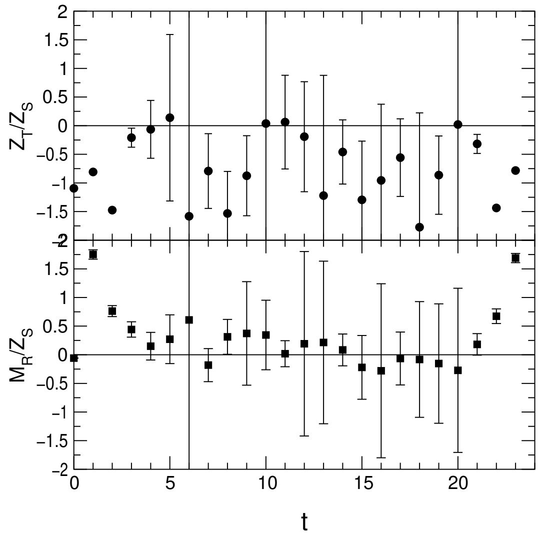

Figure 3.19: *Results for the two ratios Z_T/Z_S and $M_R = (m_0 - \bar{m})/Z_S$ for the local current as a function of t. A linear fit has been performed on the four equations resulting from the two operators $\mathcal{O}_i = \bar{\chi}_t$ and $\mathcal{O}_i = \bar{\chi}_s$.*

3.5.3 Smeared sources

As we have seen in Chapter 3.3.3 using Ape and Jacobi smearing improved the gluino-glue correlator to such a great extent that from a totally unusable signal we arrived at correlation functions that allowed a reasonable determination of the lowest mass. When we consider projecting operators for states of which we want to calculate the mass, we can smear on both, the source and the sink. In the case of the Ward identity (3.61) the situation is different. Here we can only smear the operators $\mathcal{O}$ that we wish to insert in the expectation values.
The operators $\mathcal{O}_i$ we found as possible candidates for insertion in (3.61) are either exactly the gluino-glue projecting operator (χ_s) or have the same structure, but with a summation over only the time-like Lorentz-indices. For this reason we can use the same smearing techniques used before on the gluino-glueball.
A priori it is not clear if we have to retune the smearing parameters with respect to the tuning done for the gluino-glue correlator (see Chapter 3.3.3) to find a set which is optimal for the Ward identity. Nevertheless, since the operators that occur in the Ward identity have the same quantum numbers as the gluino-glueball, we expect that the previously found optimal set (see (3.55)) will also be reasonable for use in the Ward identity.
The optimal set of smearing parameters should then work for both choices of the currents, as the smearing is carried out on the sources only. To find an optimal set of smearing parameters we start from the pool of parameters in Table 3.6 that was used for the gluino-glueball.
For every set of parameters we calculated the renormalization coefficients Z_T^{ps}/Z_S^{ps} and M_R/Z_S^{ps} of the Ward identity (3.61), with the point-split current S_μ^{ps} and the corresponding mixing operator T_μ^{ps} as defined in (3.62). As described in the last Section we did this for every time-slice t. Instead of analyzing the Ward identity seperately for the insertion of the smeared versions of $\bar{\chi}_s$ and $\bar{\chi}_t$ of equation (3.65) we performed a linear fit for every time-slice to the complete data to estimate the ratios.
To decide which of the smearing parameters was suited best we fitted the two ratios Z_T^{ps}/Z_S^{ps} and M_R/Z_S^{ps} as a function of the time-slice t to a straight line between $t = 4$ and $t = 20$.[9] Leaving out one time-slice at a time and subsequently performing the fit we can monitor how the values of Z_T^{ps}/Z_S^{ps} and M_R/Z_S^{ps} behave. The set of parameters which gave the most stable results on the ratios was then chosen to be the optimal set. However, different sets seemed equally well suited, and the decision was not as clear as for

N_{APE}	ϵ_{APE}	N_{JAC}	K_{JAC}
9	0.1	18	0.2
9	0.5	18	0.2
9	0.3	9	0.4

Table 3.9: *Smearing parameters which gave equally good results for the determination of the ratios Z_T^{ps}/Z_S^{ps} and M_R/Z_S^{ps}.*

[9] Remember that in the correlations appearing in the Ward identity (3.61) for each choice of current there are contact terms up to time-slice $t = 3$. Because of the boundary conditions these terms reach also down to $t = 21$.

the gluino-glueball mass. The parameters of Table 3.9 show those sets which gave equally good results. Since the propagators $\Delta = Q^{-1}$ for the second set in Table 3.9 were already calculated for the gluino-glueball we decided to stick in a first step with this set also for the analysis of the Ward identity.
To give a qualitative impression of the improvement the smearing of the source has done on the correlators we show in Figure 3.20 the time-slice correlation functions of (3.67) with the smeared version of the operator $\mathcal{O}_i = \bar{\chi}_s$ inserted[10].

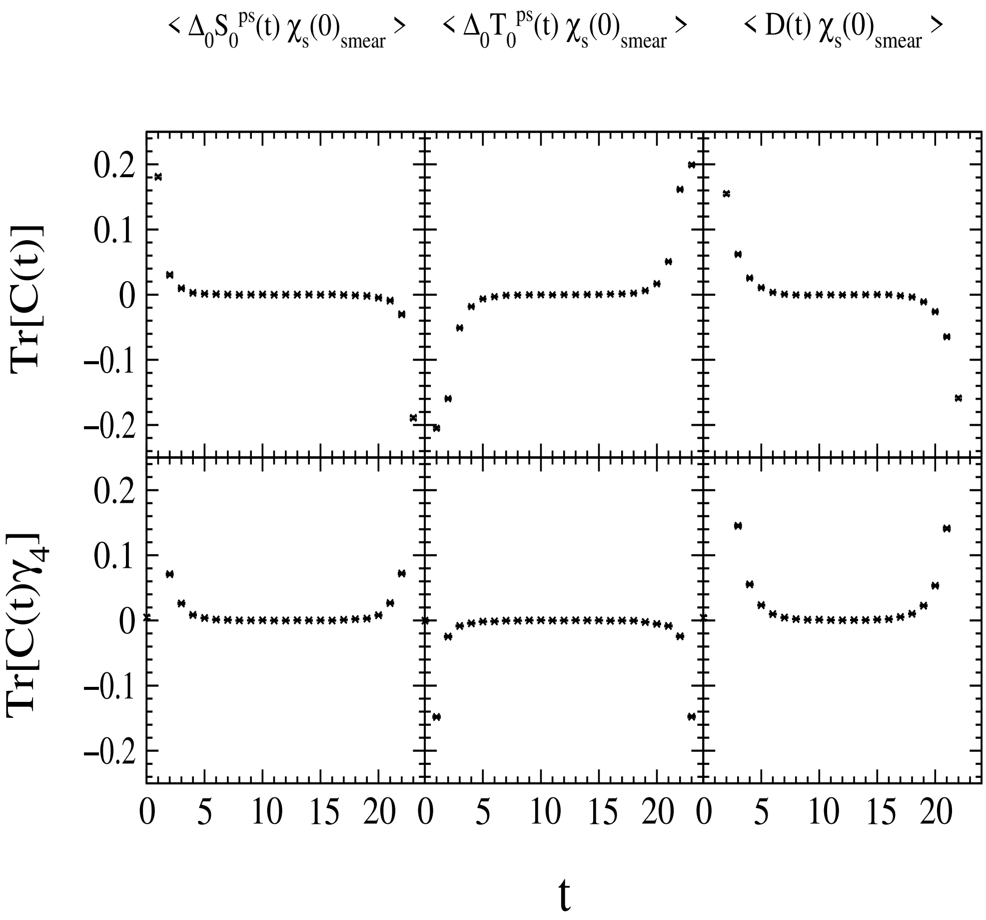

Figure 3.20: *Numerical results for the two components $\propto \mathbb{1}$ and $\propto \gamma_4$ of the time-slice correlation functions of (3.67) with smeared sources $\mathcal{O}_i = \bar{\chi}_s$.*

It can be seen at once that the improvement is dramatic, though not as strong as in the case of the gluino-glue. The smeared correlators show beautifully the symmetry properties of their components, analyzed in Section (2.3.4).
Carrying out our analysis as in the last Section, we first find Z_T^{ps}/Z_S^{ps} and M_R/Z_S^{ps} as a function of t for $\mathcal{O}_i = \bar{\chi}_s$ and $\mathcal{O}_i = \bar{\chi}_t$ seperately by resolving the arising system of equations.

[10] In this Section for the simplicity of notation we write $\bar{\chi}_s$ and $\bar{\chi}_s$ when we refer to their smeared versions.

The result is displayed in Figure 3.21, where we have made use of the symmetry and anti-symmetry properties of the correlation functions involved, and thus the ratios are displayed for $t \in [0, 12]$.

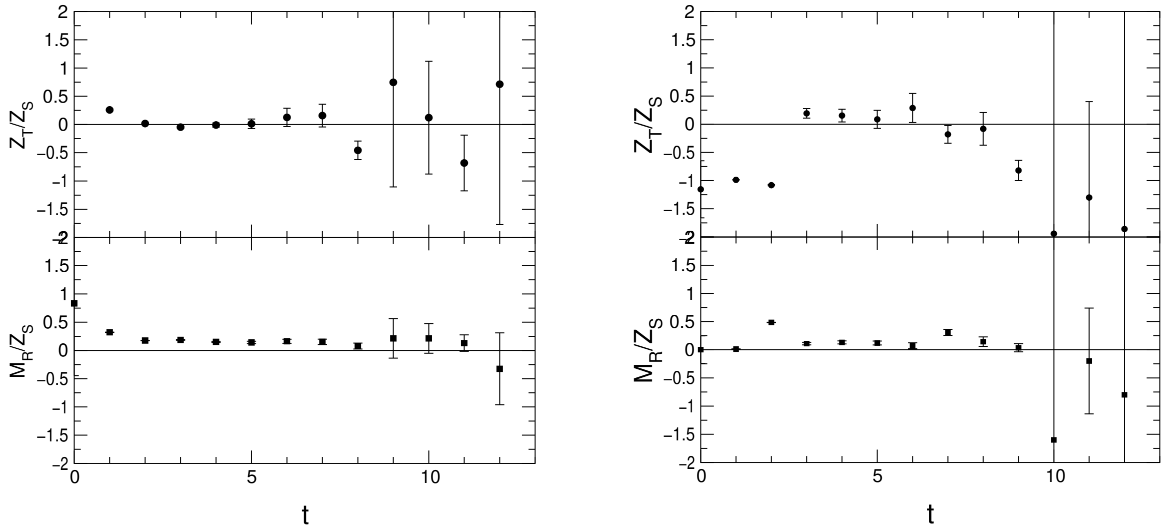

Figure 3.21: *Results for the two ratios Z_T^{ps}/Z_S^{ps} and $M_R = (m_0 - \bar{m})/Z_S^{ps}$ as a function of t for the point-split current and the smeared operator insertion $\mathcal{O}_i = \bar{\chi}_s$ (left graph), and $\mathcal{O}_i = \bar{\chi}_t$ (right graph).*

In all cases the ratios display a plateau-like behavior. For Z_T^{ps}/Z_S^{ps} and $\mathcal{O}_i = \bar{\chi}_s$ this can be observed between time-slice $t = 3$ and $t = 8$ and respectively between $t = 4$ and $t = 9$ for $\mathcal{O}_i = \bar{\chi}_t$. For large t the error grows and the signal starts to fluctuate.
The ratio M_r/Z_S^{ps} is better behaved, as the relative errors are much smaller. For the insertion $\mathcal{O}_i = \bar{\chi}_s$ the plateau extends between $t = 3$ and $t = 12$, while for $\mathcal{O}_i = \bar{\chi}_t$ we observe a plateau between $t = 4$ and $t = 9$.
Generally the signal is much better determined in case of the insertion $\mathcal{O}_i = \bar{\chi}_s$. This is not surprising, since the smearing algorithm we used has been designed for space-like operators. Furthermore the optimization has been done for the operator $\bar{\chi}_s$.
For each insertion $\bar{\chi}_s$ and $\bar{\chi}_t$ we can now obtain a best estimate of Z_T^{ps}/Z_S^{ps} and M_R/Z_S^{ps} by fitting seperately over all time-slices from $t = 3$, respectively $t = 4$ on. The result is shown in Table 3.10. We see that for M_R/Z_S^{ps} the two insertions $\bar{\chi}_s$ and $\bar{\chi}_t$ give results that differ by three standard deviations.

	$\mathcal{O}_i = \bar{\chi}_s$	$\mathcal{O}_i = \bar{\chi}_t$
Z_T^{ps}/Z_S^{ps}	-0.043(16)	0.11(7)
M_R/Z_S^{ps}	0.182(6)	0.132(16)

Table 3.10: *The ratios Z_T^{ps}/Z_S^{ps} and M_R/Z_S^{ps} for different operator insertions and the point-split current.*

If, however (3.61) holds any operator inserted in the Ward identity should lead to the same ratios of renormalization coefficients.
The reasons for this discrepancy can be various. A possible scenario might be that when renormalizing the Ward identity an additional term arises, and our form of the renormalized Ward identity (3.61) does not hold.
This would be a systematic effect which we should then observe also in the analysis of the Ward identity with the local current S^l_μ and the local mixing operator T^l_μ. We see in Table 3.11 however that the ratios of the renormalization coefficients pertaining to the local operators are compatible. Hence we conclude that the presence of an additional anomalous term in the renormalized Ward identity is an unlikely scenario.
It is much more probable that the difference of three standard deviations is caused by statistical fluctuations and order $O(a)$ effects.
Certainly (3.61) must hold for any operator $\mathcal{O}_i$ that is inserted regardless of its structure in terms of fundamental fields. Nevertheless different operators lead to different $O(a)$ effects. In this context note that the operator $\mathcal{O}_i = \bar{\chi}_s$ is formed with the simple plaquette, while for $\mathcal{O}_i = \bar{\chi}_t$ the clover plaquette was used. The clover plaquette has a higher degree of symmetry than the simple plaquette. The different behavior under parity for example introduces in the $O(a)$ term of (3.61) additional terms of the order $O(a)$ themselves, for the simple plaquette.

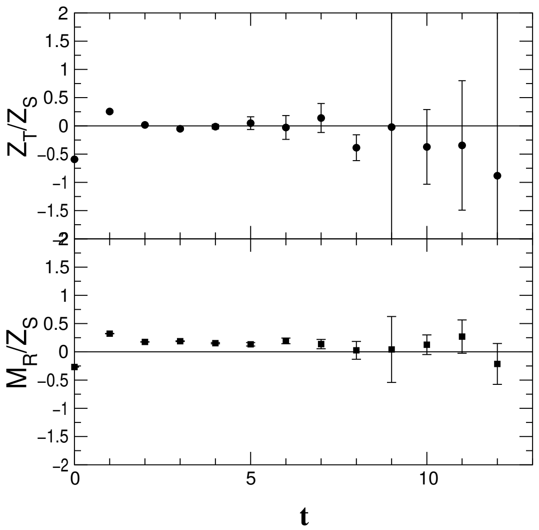

Figure 3.22: *Results for a fit to the complete data, for the two ratios Z^{ps}_T/Z^{ps}_S and $M_R/Z^{ps}_S = (m_0 - \bar{m})/Z^{ps}_S$ as a function of t for the point-split current and the smeared operator insertions.*

So in principle the insertion of $\mathcal{O}_i = \bar{\chi}_s$ with the simple plaquette introduces also stronger $O(a^2)$ effects than $\mathcal{O}_i = \bar{\chi}_s$ with the clover plaquette. These effects are probably small, but they can contribute to the discrepancies between the two operator insertions. This question is currently under investigation in the DESY-Münster-Rome collaboration.
We can now analyze the data that we have from both operator insertions $\bar{\chi}_s$ and $\bar{\chi}_t$ si-

multaneously. Every operator insertion has two independent components, and we arrive at four linear equations on every time-slice. For this overdetermined system we carry out a linear fit. First we do this for every time-slice seperately, and the result can be seen in Figure 3.22. Again using the symmetry properties of the correlators we display the ratios in the interval $t \in [0, 12]$. It can clearly be seen that both ratios have a plateau like behavior.

Finally we fitted the complete data over all time-slices from t=3 on (respectively from t=4) to the linear form of (3.66). As our best estimate of Z_T^{ps}/Z_S^{ps} and M_R/Z_S^{ps} we quote

$$Z_T^{ps}/Z_S^{ps} = 0.11(7), \qquad M_R/Z_S^{ps} = 0.135(20). \tag{3.69}$$

We can conclude that Z_T^{ps}/Z_S^{ps} is compatible with zero. Unfortunately we can not determine the ratio accurately enough to establish its sign. Note that in the final analysis the value of Z_T^{ps}/Z_S^{ps} coming from the operator $\mathcal{O}_i = \bar{\chi}_t$ is dominant.

We speculate that this behavior is due to its much larger error with respect to the determination of Z_T^{ps}/Z_S^{ps} from $\mathcal{O}_i = \bar{\chi}_s$.

Furthermore we see that M_R/Z_S^{ps} has been determined with a 15% error. This is sufficient to monitor its change in future simulations at different values of the hopping parameter. We can conclude that the numerical investigation of the Ward identity (3.61) has lead to results that are accurate enough to monitor the approach of the chiral limit as defined through them.

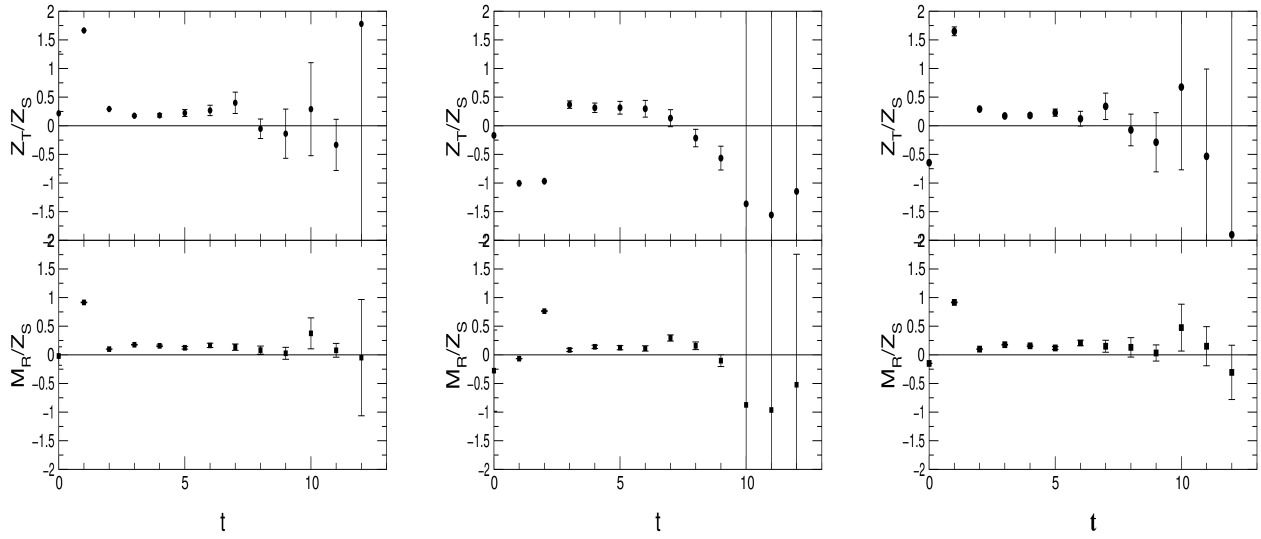

Figure 3.23: *Results for the two ratios Z_T^l/Z_S^l and $M_R = (m_0 - \bar{m})/Z_S^l$ as a function of t for the local current and the smeared operator insertion $\mathcal{O} = \bar{\chi}_s$ (left graph), and $\mathcal{O} = \bar{\chi}_t$ (middle graph). The right graph shows the fit over the complete data.*

The same analysis was carried out for the Ward identity (3.61) with smeared sources, but the local current S_μ^l and the operator T_μ^l.

The results for the ratios of the renormalization coefficients seperately for the insertion of $\bar{\chi}_s$ and $\bar{\chi}_t$ as a function of t can be found in the left and middle graph of Figure 3.23.

The best estimate of Z_T^l/Z_S^l and M_R/Z_S^l for each insertion seperately is shown in Table 3.11. It has been obtained as in the case of the point-split current by fitting the data from each insertion seperately over all physically relevant time-slices. We see that both ratios agree for both operator insertions within the error, as expected if (3.61) holds.

	$\mathcal{O}_i = \bar{\chi}_s$	$\mathcal{O}_i = \bar{\chi}_t$
Z_T^l/Z_S^l	0.176(14)	0.29(6)
M_R/Z_S^l	0.173(6)	0.144(18)

Table 3.11: *The ratios Z_T^l/Z_S^l and M_R/Z_S^l for different operator insertions and the local current.*

To arrive at a best estimate we fitted the complete data from the insertion of $\bar{\chi}_s$ and $\bar{\chi}_t$ for every time-slice t as before to the form of the Ward identity (3.61). The result can be seen in the right graph of Figure 3.23.
Finally we performed a linear fit over all time-slices from $t = 3$, respectively $t = 4$ on. Our best estimate for the ratios is

$$Z_T^l/Z_S^l = 0.27(6), \qquad M_R/Z_S^l = 0.147(23) \tag{3.70}$$

It seems that with a sufficient degree of confidence we can conclude that Z_T^l/Z_S^l is positive. Furthermore we see that M_R/Z_S^l is determined as accurately as M_R/Z_S^{ps}. Nevertheless, for different operator insertions $\mathcal{O}_i$ the local current seems to be less affected by $O(a)$ effects.

3.5.4 Discussion

The motivation for the above analysis has been twofold. On one hand we wanted to check numerically whether the Ward identity (3.61) holds, and on the other hand by a determination of M_R/Z_S we wanted to take a first step towards a non-perturbative tuning of the hopping parameter K to its critical value where supersymmetry is expected.
For both purposes it is necessary to obtain a good precision on the ratios. Especially M_R/Z_S must be well determined since in the supersymmetric limit $M_R/Z_S \to 0$ is expected.
We have seen that to attain this precision it has been decisive to perform smearing on the operators $\mathcal{O}_i$ that have to be inserted in the Ward identity (3.61). Without smearing we can conclude directly from Figure 3.18 and Figure 3.19 that for either choice of the current $S_\mu^d(x)$ a determination of Z_T/Z_S and M_R/Z_S is not possible with the required accuracy.
The results for the ratios of the renormalization coefficients obtained in the previous Section are summarized in Table 3.12. Before we discuss the numbers in detail let us comment on another important point. For all of the numerical analysis we have worked with operators that behaved in the same manner under the discrete symmetries $\mathcal{P}$ and $\mathcal{T}$. We mentioned this already in Chapter 2.3.3 when we chose the mixing operator T_μ^{ps} for the point-split current.
As a first orientation certainly one tries to choose the lattice operators such that their transformation properties are those of the continuum operators [11]. In this way we hoped

[11] See for example the definition of the plaquette (2.17).

operators $\mathcal{O}_i$	Z_T^l/Z_S^l	M_R/Z_S^l	Z_T^{ps}/Z_S^{ps}	M_R/Z_S^{ps}
$\bar{\chi}_s$	0.176(14)	0.173(6)	-0.043(16)	0.182(6)
$\bar{\chi}_t$	0.29(6)	0.144(18)	0.11(7)	0.132(16)
$\bar{\chi}_s$, $\bar{\chi}_t$	0.27(6)	0.147(23)	0.11(7)	0.135(20)

Table 3.12: *Fitted values of M_R/Z_S and Z_T^l/Z_S^l for different operator insertions.*

to reduce effects of the order $O(a)$. Furthermore since our analysis is carried out in a first step on every time-slice seperately and the lattice extension in the time direction is relatively small (T=24 at $\beta = 2.3$) it is important that the behavior under time reversal $\mathcal{T}$ of the different point-split or local lattice operators is the same.
If this is not the case on every time-slice there will be extra order $O(a)$ effects that spoil the symmetry of the signal and would make the determination of Z_T/Z_S and M_R/Z_S much more noisy. Thus for the above analysis it has been important to respect the discrete symmetries $\mathcal{P}$ and $\mathcal{T}$.
Let us comment on the numerical results reported in Table 3.12. Observing M_R/Z_S^{ps} as determined from the different operators $\bar{\chi}_s$ and $\bar{\chi}_t$ we see that the values are compatible only within three standard deviations. This may be caused either by order $O(a)$ effects from the insertions of the two different operators $\bar{\chi}_s$ and $\bar{\chi}_t$, or one might also speculate that the form (3.61) of the SUSY Ward identity does not hold due to a supersymmetric anomaly.
In the latter case our solution of the homogeneous system (3.66) arising from the Ward identity would be invalid, and this could explain the above disagreement. However this effect should be systematic and also be observable for the other ratios of Table 3.12. Furthermore in Figure 3.21 to Figure 3.23 the formation of a plateau in t should not be observable. Since this is not the case we attribute the difference in M_R/Z_S^{ps} for the two operator insertions $\bar{\chi}_s$ and $\bar{\chi}_t$ to order $O(a)$ effects.
Hence we conclude that within our numerical accuracy the supersymmetric Ward identity of equation (3.61) holds. Nevertheless for different operator insertions $\mathcal{O}_i$ the local current seems to be less affected by order $O(a)$ effects.
We can conclude furthermore that the precision with which M_R/Z_S could be determined for either the point-split or the local current is sufficient to take the next step and perform another analysis at a value of K closer to K_c and to investigate the chiral limit.
Certainly a complete analysis must also include an investigation of the β dependence, hence numerical simulations performed at different values of the bare coupling β (for example $\beta = 2.2$, $\beta = 2.3$ and $\beta = 2.4$). This could then be used for an extrapolation to the continuum limit, where the expectation is that $Z_T/Z_S \sim O(g_0^2)$ becomes small. Performing these numerical simulations on lattice sizes of $12^3 \times 24$ and $16^3 \times 32$ should be enough to keep final volume effects under control.
Using the results on the ratio M_R/Z_S of Table 3.12 and $K_{cr} = 0.1955(5)$ from [16] we can give a rough estimate of Z_S.
By using $M_R = m_0 - \bar{m} = 1/(2K) - 1/(2K_{cr})$[12], with $K = 0.1925$ and $K_{cr} = 0.195$ we find $M_R = 0.033$ and hence $Z_S = 0.24$. This is roughly of the perturbative order of Z_S given in [9].

[12] This is certainly only an approximation to M_R, since we calculate m_0 and $\bar{m}$ at different values of K. The subtracted mass $M_R = m_0 - \bar{m} = m_0(K) - \bar{m}(\beta, K)$ is a function of K where both coefficients depend on K.

Chapter 4

Conclusion

In this thesis we have studied numerically the lattice formulation of $SU(2)$ $N=1$ Super Yang-Mills theory of reference [9]. The masses of those states that are believed to make up the low-lying multiplets [5, 6] were numerically determined. Furthermore the breaking of supersymmetry of the lattice formulation was studied through the lattice SUSY Ward identity. The ratios of the renormalization coefficients of the SUSY Ward identity have been calculated non-perturbatively in a numerical simulation.

In order to study the structure of the states that are believed to be part of the low-lying multiplet of $N=1$ Super Yang-Mills theory, we have proposed different projecting operators, and discussed how their time-slice correlation function can be evaluated in a numerical simulation. In case of the gluino-glue particle a new kind of operator has been proposed and studied thoroughly. This operator carrying spin 1/2 differs from the one previously used [12, 43] in its Dirac structure.

The proposed low-lying multiplets do not contain a "baryonic" state built out of three gluinos. Nevertheless it is an interesting question where such a state enters in the mass hierarchy. We have proposed a three-gluino state, determined its time-slice correlator and devised a method to determined it numerically.

The masses of the particles that are believed to be a part of the low-lying multiplet have been determined in a Monte Carlo simulation. As can be seen in Figure 3.13 where the results for the spectrum are summarized, at the lightest gluino mass m_0 (highest hopping parameter) the bound state masses fall into two groups. With respect to previously performed simulations [43, 51] the introduction of the new gluino-glue operator has revealed the presence of a lower spin 1/2 state.

The lightest states are the 0^- gluinoball (a-η'), the 0^+ glueball, and the spin 1/2 gluino-glueball. In lattice units these masses are at $K = 0.1925$ close to $am = 0.5$. The higher group consisting of the 0^+ gluinoball (a-f_0), the 0^- glueball and the heavier spin 1/2 gluino-glueball is at $K = 0.1925$ clustered around $am = 1.0$. Both multiplets do not display the structure that has been advocated by either of the investigations based on effective actions [5, 6]. However, glueballs neglected by [5] seem to play a role in the multiplet structure of the low-lying states.

When comparing the results of [5, 6] to our numerical simulation one has to keep in mind some important facts.

For some of the states we have investigated the accuracy of the determination of the mass is not yet satisfactory. Especially the 0^+ gluinoball (a-f_0) has to be mentioned. It was

shown in Chapter 3.3.2 that without smearing the mass of this state can only be extracted from the first three time-slices of the correlation function. In this region almost certainly the influence of higher excited states will be present.
To attain a sufficient degree of confidence on the structure of the low-lying states in weakly broken $N = 1$ SYM theory by numerical simulations it is important to calculate the a-f_0 mass to satisfactory precision. To do so in a future simulation bigger lattices with a larger time extension are needed and a proper smearing algorithm for the a-f_0 must be developed.
In Chapter 3.3.4 we calculated the spatial lattice extension in QCD units of our $12^3 \times 24$ lattice at $\beta = 2.3$ and $K = 0.1925$ to about $1fm$. This is probably not large enough for finite volume effects to be absent which is a further argument to consider bigger lattices in future simulations.
By means of the supersymmetric Ward identity on the lattice we studied the breaking of supersymmetry introduced by the lattice formulation of $N = 1$ SYM theory we have used. With the help of a lattice supersymmetry transformation [1] the bare SUSY Ward identity has been derived in the usual way. The lattice regularization breaks supersymmetry explicitly and the lattice Ward identity acquires additional breaking terms. The renormalization conditions can however be fixed by requiring that the renormalized Ward identities have a form which differs from the continuum ones only by terms that vanish in the continuum- respectively the chiral limit.
On the lattice the renormalized Ward identity holding up to $O(a)$ consists of three terms: the current S_μ renormalized multiplicatively by Z_S, the mixing operator T_μ also renormalized multiplicatively, by Z_T, and the mass term D_S which is multiplied with the subtracted mass M_R.
To determine the renormalization coefficients numerically we have made use of two different forms of the current S_μ and the mixing operator T_μ differing only by order $O(a)$ terms in the continuum limit. Our choice has been a point-split version of these operators as proposed in [46] and a local version [22, 47].
As possible operators $\mathcal{O}_i$ to be inserted in the SUSY Ward identity we have identified two independent operators of the gluino-glue type structure.
Since the Ward identity leads to a homogeneous system of equations only ratios of the renormalization coefficients can be determined.
For the insertion of local operators $\mathcal{O}_i$ it was found that the ratios of the renormalization coefficients Z_T/Z_S and M_R/Z_S could not be calculated with the required accuracy.
To determine the ratios Z_T/Z_S and M_R/Z_S to a satisfactory degree it was necessary to insert smeared operators $\mathcal{O}_i$ in the supersymmetric Ward identity. Since the operators we used have the gluino-glue structure the same smearing techniques as for the mass determination of the gluino-glueball could be applied.
Furthermore to keep $O(a)$ effects under control it was important to choose lattice discretizations of the point-split and the local operators for the current and the operator insertion that behaved for each set in the same way under time-reversal $\mathcal{T}$.
The numerical determination of the ratios Z_T/Z_S coming from different independent operators agreed for the local and the point-split current seperately within the error. Differences in the ratio of M_R and Z_T for different operator insertions are attributed to $O(a)$

[1] The transformation we refer to is that of equation (2.42) and is only a SUSY transformation up to order $O(a)$.

and higher symmetry breaking effects. Hence we conclude that with our numerical accuracy the SUSY Ward identity (3.61) holds. However for different operator insertions the local form of the current S_μ and the mixing operator T_μ seems to be less affected by order $O(a)$ effects. In particular the chiral- and supersymmetric limit defined by the vanishing of the subtracted mass M_R as we approach $K \to K_{cr}$ in our simulation can be investigated numerically.
In this way also the consistency of different methods to determine the critical hopping parameter can be established. For future investigations it is also interesting to determine the ratios of the renormalization constants using yet another independent operator, such as the three gluino operator proposed in Chapter 2.2.4.
On the basis of the analysis of the low-lying spectrum and the supersymmetric Ward identity it seems an important step to increase both, the lattice size and the hopping parameter in future simulations. This task is getting more difficult from the algorithmic point of view as the smallest eigenvalue of the fermion matrix decreases further.
However as preliminary studies at $K = 0.194$ on a $12^3 \times 24$ lattice have shown, the multi-bosonic algorithm with the two step variant still performs well, and the algorithmic difficulties are under control. Increasing K at fixed β is also expected to decrease the lattice spacing.
Since we expect our lattice extension to be small already, a calculation of the spectrum at higher K might be strongly influenced by finite volume effects. However since finite volume effects do not enter in the Ward identity a simulation at higher K and fixed β is an important next step.
In a final analysis also the continuum limit must be investigated. This makes future simulations at various β values necessary. For an extrapolation to the continuum limit simulations at $\beta = 2.2$, $\beta = 2.3$ and $\beta = 2.4$ could be performed. Lattice sizes of $12^3 \times 24$ and $16^3 \times 32$ should be enough to keep finite volume effects under control.

Appendix A

Notation, conventions and tools

In this Appendix we list the conventions and the definitions that were used throughout this work.

Generalities

The number of colors has been denoted by N_c. In this work for the specific numerical calculations we work in the adjoint representation of SU(2), hence $N_c = 2$. Color in the adjoint representation is labeled by Latin lower indices of the form $a, b, c... = 1, ..., N_c^2 - 1$. Greek lower case indices or primed lower case indices from the beginning of the alphabet such as $\alpha, \alpha', \beta, \beta', ... = 1, ..., 4$ label the spin. Greek lower case letters from the middle of the alphabet such as $\mu, \nu, \rho, \sigma, ... = 1, ..., 4$ denote Lorentz space-time components (in Euclidean space-time).
Latin lower case indices of the form $i, j, k, l, ... = 1, 2, 3$ label Lorentz spatial components.

SU(N) group

Elements of the Lie-algebra $su(N)$ of the gauge group $SU(N)$ are denoted by T^a with $a \in \{1, ..., N_C^2 - 1\}$ as an $N \times N$ matrix in the fundamental representation. The algebra itself reads

$$[T^a, T^b] = i f^{abc} T^c. \tag{A.1}$$

The generators are normalized according to

$$\mathrm{Tr}[T^a T^b] = \frac{1}{2}\delta^{ab}. \tag{A.2}$$

The completeness relation for the generators is

$$(T^a)^{AB}(T^a)^{CD} = \frac{1}{2}\delta^{AD}\delta^{BC} - \frac{1}{2N}\delta^{AB}\delta^{CD}, \tag{A.3}$$

where A, B, C, D are indices running from 1 to N. The element V^{ab} in the adjoint representation and U of the fundamental representation associated to the same group element

$g \in SU(N_c)$ are related by

$$V^{ab} = \frac{1}{2}\mathrm{Tr}[U^\dagger T^a U T^b]. \tag{A.4}$$

Pauli and Euclidean Dirac matrices

The Pauli matrices σ^a are defined by

$$\sigma_1 = \begin{pmatrix} 0 & 1 \\ 1 & 0 \end{pmatrix}, \quad \sigma_2 = \begin{pmatrix} 0 & -i \\ i & 0 \end{pmatrix}, \quad \sigma_3 = \begin{pmatrix} 1 & 0 \\ 0 & -1 \end{pmatrix}. \tag{A.5}$$

The Dirac matrices γ_μ in the Weyl representation in Euclidean space-time are given in terms of the three Pauli matrices by

$$\gamma_4 = \begin{pmatrix} 0 & \mathbb{1} \\ \mathbb{1} & 0 \end{pmatrix}, \qquad \gamma_k = -i \begin{pmatrix} 0 & \sigma_k \\ -\sigma_k & 0 \end{pmatrix}. \tag{A.6}$$

For the gamma matrices $\gamma_\mu^\dagger = \gamma_\mu$ holds, and they fulfill the anticommutation relation

$$\{\gamma_\mu, \gamma_\nu\} = 2\delta_{\mu\nu}\mathbb{1}. \tag{A.7}$$

We also define the following matrices

$$\gamma_5 = \gamma_1\gamma_2\gamma_3\gamma_4 = \begin{pmatrix} \mathbb{1} & 0 \\ 0 & -\mathbb{1} \end{pmatrix}, \quad C = \gamma_4\gamma_2 = \begin{pmatrix} i\sigma_2 & 0 \\ 0 & -i\sigma_2 \end{pmatrix}, \quad \sigma_{\mu\nu} = \frac{1}{2}[\gamma_\mu, \gamma_\nu]. \tag{A.8}$$

The matrix γ_5 has the following useful properties

$$\{\gamma_5, \gamma_\mu\} = 0, \qquad \gamma_5\gamma_5 = 1, \qquad \gamma_5^\dagger = \gamma_5. \tag{A.9}$$

The charge conjugation matrix C and the tensor $\sigma_{\mu\nu}$ fulfill the following relations

$$C^{-1} = -C = C^T, \;\; \gamma_\mu^T = -C^{-1}\gamma_\mu C, \;\; -C^{-1}\sigma_{\mu\nu}C = \sigma_{\mu\nu}^T, \;\; \sigma_{\mu\nu}^\dagger = -\sigma_{\mu\nu}. \tag{A.10}$$

For the antisymmetric tensor $\epsilon_{\mu\nu\rho\sigma}$ we take the sign convention $\epsilon_{4123} = 1$.

Lattice notations

A hypercubical space-time lattice Λ is defined by the set

$$\Lambda = \{x = (\vec{x}, t) = (x_1, x_2, x_3, t) \in \mathbb{Z}^4; 0 \le x_\mu < L_\mu, \mu = 1, ..., 4, L_\mu \in \mathbb{N}\}. \tag{A.11}$$

The summation over this lattice is denoted by

$$\sum_x = \prod_{\mu=1}^{4} \sum_{x_\mu}^{L_\mu - 1}. \tag{A.12}$$

The extension of the lattice is the same in all space directions $L_s = L_1 = L_2 = L_3$, while T is the time extension of the lattice. The spatial volume of the lattice is given by $V = L_s^3$, and the total number of lattice points is $\Omega = VT$. The four orthogonal directions are labeled by $\mu = 1, ...4$, and the unit vector in direction μ is $\hat{\mu}$. The sum over the four positive directions is written as

$$\sum_{\mu=1}^{4} . \tag{A.13}$$

When summing over negative and positive directions we write

$$\sum_{\mu} = \sum_{\mu=\pm 1}^{\pm 4} . \tag{A.14}$$

The sum over the spatial lattice points at fixed time is denoted by

$$\sum_{\vec{x}} . \tag{A.15}$$

The lattice gauge field $[U]$ is given by the link variables $[U] = \{U_\mu(x) = U(x+\hat{\mu}, x) \quad \in SU(N_c), \forall x \in \Lambda, \mu \in \{1,2,3,4\}\}$ The smallest closed path formed from the link variables, the plaquette is defined by

$$\begin{aligned} U_P &= U(x, x+\hat{\nu})U(x+\hat{\nu}, x+\hat{\nu}+\hat{\mu})U(x+\hat{\mu}+\hat{\nu}, x+\hat{\mu})U(x+\hat{\mu}, x) \\ &= U_\nu^\dagger(x)U_\mu^\dagger(x+\hat{\nu})U_\nu(x+\hat{\mu})U_\mu(x). \end{aligned}$$

The clover plaquette is defined by

$$\begin{aligned} &P_{\mu\nu}(x) = \frac{1}{4}\sum_{i=1}^{4} \frac{1}{2ig}\left(U_{\mu\nu}^{(i)}(x) - U_{\mu\nu}^{(i)\dagger}(x)\right), \\ &U_{\mu\nu}^{(1)}(x) \equiv U_{\mu\nu}(x) = U_\nu^\dagger(x)U_\mu^\dagger(x+\hat{\nu})U_\nu(x+\hat{\mu})U_\mu(x), \\ &U_{\mu\nu}^{(2)}(x) = U_\mu^\dagger(x)U_\nu(x-\hat{\nu}+\hat{\mu})U_\mu(x-\hat{\nu})U_\nu^\dagger(x-\hat{\nu}), \\ &U_{\mu\nu}^{(3)}(x) = U_\nu(x-\hat{\nu})U_\nu(x-\hat{\nu}-\hat{\mu})U_\mu^\dagger(x-\hat{\nu}-\hat{\mu})U_\mu^\dagger(x-\hat{\mu}), \\ &U_{\mu\nu}^{(4)}(x) = U_\mu(x-\hat{\mu})U_\nu^\dagger(x-\hat{\mu})U_\mu^\dagger(x+\hat{\nu}-\hat{\mu})U_\nu(x). \end{aligned}$$

The sum over all plaquettes is defined as the sum where each plaquette is only counted with the positive orientation

$$\sum_{pl} = \sum_{x} \sum_{1 \le \mu \le \nu \le 4} . \tag{A.16}$$

Majorana fermions and the inverse fermion matrix

The Majorana fermion field (gluino) in the continuum and on the lattice is denoted by $\lambda_a^\alpha(x)$. The Majorana condition for a spinor reads,

$$\lambda^C = \lambda = C\bar{\lambda}^T \leftrightarrow \bar{\lambda} = \lambda^T C. \tag{A.17}$$

We also use $\lambda^\alpha(x) = \lambda_a^\alpha T^a$. The fermion matrix is defined by

$$Q_{ab}^{\alpha\beta}(x,y) = \delta_{ab}\delta_{xy}\delta^{\alpha\beta} - K\sum_{\mu=1}^{4}\left[\delta_{y,x+\hat{\mu}}(1+\gamma_\mu)^{\alpha\beta}V_{\mu,ab}(x) + \delta_{y+\hat{\mu},x}(1-\gamma_\mu)^{\alpha\beta}(V^T)_{\mu,ab}(y)\right]. \tag{A.18}$$

It has the following properties

$$\begin{aligned} C^{-1}QC &= Q^T, \\ \gamma_5 Q^\dagger \gamma_5 &= Q. \end{aligned}$$

These relations also hold for the inverse Q^{-1} and we can use them to specify the form of the inverse fermion matrix. Making use of the above relations we see that the inverse fermion matrix for fixed space-time and color does not have $16 = 4 \times 4$ independent components, but that only the first and the third column are independent. The general form of Q^{-1} is therefore

$$\Delta = (Q^{-1}) = \begin{pmatrix} a^{11} & (-a^{21})^* & a^{13} & (-a^{23})^* \\ a^{21} & (a^{11})^* & a^{23} & (a^{13})^* \\ a^{31} & (-a^{41})^* & a^{33} & (-a^{43})^* \\ a^{41} & (a^{31})^* & a^{43} & (a^{33})^* \end{pmatrix}. \tag{A.19}$$

This is very useful, since it reduces the necessary inversions with the conjugate gradient algorithm by a factor of 2.

Numerical representation of $SU(2)$

In the fermionic interaction the adjoint representation of $SU(2)$ is used. Since the numerical implementation of the fundamental and the adjoint representation can be carried out in a number of equivalent ways we want to present the numerical representation that we have used in our programs.

The gauge configuration is saved as a sequence of double precision numbers in xdr format. Every link matrix is saved in four real numbers a, b, c, d that represent two complex numbers which determine the $SU(2)$ matrix entirely. The matrix associated with these numbers is

$$U = \begin{pmatrix} a+ib & c+id \\ -c+id & a-ib \end{pmatrix}, \text{with} \quad \mathrm{a}^2+\mathrm{b}^2+\mathrm{c}^2+\mathrm{d}^2 = 1. \tag{A.20}$$

For every lattice point there are four links, which makes a total of 16 numbers per lattice point. For each site the first four numbers in the file containing one gauge configuration pertain to the x-direction the second set to the y-direction and the third and fourth group to the z and t-direction respectively. The different sites, each a block of four link matrices are saved according to

$$N = n_x + L(n_y - 1) + L^2(n_z - 1) + L^3(n_t - 1), \tag{A.21}$$

where N is the number of the site, n_x, n_y, n_z and n_t are the site coordinates and L is the spatial lattice extension. For example the links pertaining to the site with the coordinates $(1, 2, 2, 1)$ are to be found after the 156'th block of 16 real numbers each representing the links of one lattice site. The last two numbers in the file represent the correction factor of the configuration and its plaquette.

The adjoint representation used in the fermionic action is calculated in the programs from the above form of the fundamental representation. It is defined by

$$V_{ab,\mu}(x) = \frac{1}{2}\mathrm{Tr}\left[U_\mu^\dagger(x)\sigma_r U_\mu(x)\sigma_s\right], \tag{A.22}$$

where the σ are the Pauli spin matrices.

Linear fit

To solve the Ward identity (3.61) for the ratios Z_T/Z_S and M_R/Z_T we have to perform a linear fit. In Chapter 2.3.4 two independent operators were identified that can be used as projecting operators $\mathcal{O}$, each having two independent components. This leaves us with a total of four equations and two unknowns for every time-slice. We can also collect the equations from different time-slices and fit simultaneously for all time-slices that are physically permitted (no contact terms). This overdetermined system has the form

$$ax_i + by_i = z_i, \qquad i = 1, ..., 4, \tag{A.23}$$

where a, b, are defined by

$$a = -\frac{Z_T}{Z_S}, \quad b = (m_0 - \bar{m})Z_S, \tag{A.24}$$

and x_i, y_i and z_i are the different components of the correlation functions

$$x \sim \sum_{\vec{x}} \nabla_4^d \left\langle T_4^d(x)\overline{\mathcal{O}}_1\right\rangle, \qquad y \sim \textstyle\sum_{\vec{x}} \left\langle D_S(x)\overline{\mathcal{O}}_1\right\rangle, \qquad z \sim \displaystyle\sum_{\vec{x}} \nabla_4^d \left\langle S_4^d(x)\overline{\mathcal{O}}_1\right\rangle,$$

that can be formed by taking $\mathrm{Tr}[C(t)]$ or $\mathrm{Tr}[C(t)\gamma_4]$ [1] with either of the two independent projecting operators. To determine a and b we minimize

$$\chi = \sum_i (ax_i + by_i - z_i)^2. \tag{A.25}$$

With the conditions

$$\frac{\partial\chi}{\partial a} = 2\sum_i x_i(ax_i + by_i - z_i) = 0$$

$$\frac{\partial\chi}{\partial b} = 2\sum_i y_i(ax_i + by_i - z_i) = 0$$

and the definition

$$\sum_i = x_i y_i =< x, y >$$

a and b are given by

$$a = \frac{< x, z >< y, y > - < y, z >< x, y >}{< x, x >, < y, y > - < x, y >^2},$$

$$b = \frac{< x, x >< y, z > - < x, y >< x, z >}{< x, x >, < y, y > - < x, y >^2}.$$

[1] $C(t)$ stands here for any of the above correlation functions.

Appendix B

Symmetries on the lattice

In this appendix following [31] we list the properties under discrete symmetry transformations of the gluino field λ and $\bar{\lambda}$, the gauge field $U_\mu(x)$ and the lattice field tensor $P_{\mu\nu}$ defined with the clover plaquette.
The properties under symmetry transformations of more complex objects build out of these fundamental variables can then be derived easily. Under parity $\mathcal{P}$ we have the following transformation properties:

$$
\begin{aligned}
(\vec{x},t) &\rightarrow (\vec{x}^{\mathcal{P}},t^{\mathcal{P}}) = (-\vec{x},t), \\
\lambda(x) &\rightarrow \lambda^{\mathcal{P}}(x^{\mathcal{P}}) = \gamma_4\lambda(-\vec{x},t), \\
\bar{\lambda}(x) &\rightarrow \bar{\lambda}^{\mathcal{P}}(x^{\mathcal{P}}) = \bar{\lambda}(-\vec{x},t)\gamma_4, \\
U_4(x) &\rightarrow U_4^{\mathcal{P}}(x^{\mathcal{P}}) = U_4(-\vec{x},t), \\
U_k(x) &\rightarrow U_k^{\mathcal{P}}(x^{\mathcal{P}}) = U_{-k}(-\vec{x},t) = U_k^{\dagger}(x-\hat{k}), \\
P_{4k}(x) &\rightarrow P_{4k}^{\mathcal{P}}(x^{\mathcal{P}}) = -P_{4k}(-\vec{x},t), \\
P_{lk}(x) &\rightarrow P_{lk}^{\mathcal{P}}(x^{\mathcal{P}}) = P_{lk}(-\vec{x},t).
\end{aligned}
$$

Under time reversal $\mathcal{T}$ the fields transform according to

$$
\begin{aligned}
(\vec{x},t) &\rightarrow (\vec{x}^{\mathcal{T}},t^{\mathcal{T}}) = (\vec{x},-t), \\
\lambda(x) &\rightarrow \lambda^{\mathcal{T}}(x^{\mathcal{T}}) = \gamma_4\gamma_5\lambda(\vec{x},-t), \\
\bar{\lambda}(x) &\rightarrow \bar{\lambda}^{\mathcal{T}}(x^{\mathcal{T}}) = \bar{\lambda}(\vec{x},-t)\gamma_5\gamma_4, \\
U_4(x) &\rightarrow U_4^{\mathcal{T}}(x^{\mathcal{T}}) = U_{-4}(\vec{x},-t) = U_4^{\dagger}(x-\hat{4}), \\
U_k(x) &\rightarrow U_k^{\mathcal{T}}(x^{\mathcal{T}}) = U_k(\vec{x},-t), \\
P_{4k}(x) &\rightarrow P_{4k}^{\mathcal{T}}(x^{\mathcal{T}}) = -P_{4k}(\vec{x},-t), \\
P_{lk}(x) &\rightarrow P_{lk}^{\mathcal{T}}(x^{\mathcal{T}}) = P_{lk}(\vec{x},-t).
\end{aligned}
$$

These two discrete symmetries can be used to derive the following relations for the gluino propagator, that hold on a single gauge configuration,

$$
\begin{aligned}
\Delta(x,y,U_\mu(x)) &= \gamma_4\Delta(x^{\mathcal{P}},y^{\mathcal{P}},U_\mu^{\mathcal{P}}(x^{\mathcal{P}}))\gamma_4, \\
\Delta(x,y,U_\mu(x)) &= \gamma_5\gamma_4\Delta(x^{\mathcal{T}},y^{\mathcal{T}},U_\mu^{\mathcal{T}}(x^{\mathcal{T}}))\gamma_4\gamma_5.
\end{aligned}
$$

Explicit form of the breaking term X_S

The explicit SUSY breaking term X_S of (2.45) is given by a sum of four terms

$$X_S(x) = X_S^{(1)}(x) + X_S^{(2)}(x) + X_S^{(3)}(x) + X_S^{(4)}(x) \tag{B.1}$$

with

$$\begin{aligned} X_S^{(1)}(x) &= \sum_{\mu\rho\sigma} r\sigma_{\rho\sigma} \mathrm{Tr}\Big[P_{\rho\sigma}(x)\Big(\lambda(x) - \frac{1}{2}\Big(U_\mu^\dagger(x)\lambda(x+\hat{\mu})U_\mu(x)\Big) \\ &\quad -\frac{1}{2}\left(U_\mu(x-\hat{\mu})\right)\lambda(x-\hat{\mu})U_\mu^\dagger(x-\hat{\mu})\Big)\Big], \end{aligned} \tag{B.2}$$

$$\begin{aligned} X_S^{(2)}(x) &= \sum_{\mu\nu\rho\sigma} \frac{1}{2}\epsilon_{\mu\nu\rho\sigma}\gamma_\nu\gamma_5 \mathrm{Tr}\Big[U_\mu(x)\lambda(x)U_\mu^\dagger(x)P_{\rho\sigma}(x+\hat{\mu}) \\ &\quad -U_\mu^\dagger(x-\hat{\mu})\lambda(x)U_\mu(x-\hat{\mu})P_{\rho\sigma}(x-\hat{\mu})\Big], \end{aligned} \tag{B.3}$$

$$\begin{aligned} X_S^{(3)}(x) &= \sum_{\mu\nu} \gamma_\nu \mathrm{Tr}\Big[U_\mu^\dagger(x-\hat{\mu})\lambda(x)U_\mu(x-\hat{\mu})H_{\mu\nu}(x-\hat{\mu}) + U_\mu(x)\lambda(x)U_\mu^\dagger(x)H_{\mu\nu}(x+\hat{\mu}) \\ &\quad -2\lambda(x)H_{\mu\nu}(x)\Big], \end{aligned} \tag{B.4}$$

$$\begin{aligned} X_S^{(4)}(x) &= -\frac{1}{2}ig\sum_\mu\Big[\left(\gamma_\mu\lambda_a(x)\right)\bar{\lambda}_b(x)\left(-r+\gamma_\mu\right)\lambda_c(x+\hat{\mu})\mathrm{Tr}\left[\left[T^a,T^b\right]U_\mu^\dagger(x)T^cU_\mu(x)\right] \\ &\quad +\left(\gamma_\mu\lambda_a(x)\right)\bar{\lambda}_b(x)\left(r+\gamma_\mu\right)\bar{\lambda}_c(x-\hat{\mu})\mathrm{Tr}\left[\left[T^a,T^b\right]U_\mu(x-\hat{\mu})T^cU_\mu^\dagger(x-\hat{\mu})\right]\Big], \end{aligned} \tag{B.5}$$

where $H_{\mu\nu}$ is given by a subtraction between the clover leafs,

$$\begin{aligned} H_{\mu\nu}(x) &= \frac{1}{8ig}\Big(\Big(U_{1,\mu\nu}^\dagger(x) - U_{1,\mu\nu}(x)\Big) + \Big(U_{4,\mu\nu}^\dagger(x) - U_{4,\mu\nu}(x)\Big) \\ &\quad - \Big(U_{2,\mu\nu}^\dagger(x) - U_{2,\mu\nu}(x)\Big) - \Big(U_{3,\mu\nu}^\dagger(x) - U_{3,\mu\nu}(x)\Big)\Big). \end{aligned} \tag{B.6}$$

Note that $X_S^{(2)}$, $X_S^{(3)}$ are the breaking terms originating from the pure gauge part. The terms $X_S^{(1)}$, $X_S^{(4)}$ arise from the gluino action. Especially $X_S^{(1)}$ is given by transforming the gluino field in the Wilson term.

Fierz identities

With the definitions

$$\begin{aligned}
O_S &= \mathrm{Tr}\left[(\bar{\psi}(x)\psi(x))\psi(x)\right], \\
O_P &= \mathrm{Tr}\left[(\bar{\psi}(x)\gamma_5\psi(x))\gamma_5\psi(x)\right], \\
O_V &= \mathrm{Tr}\left[(\bar{\psi}(x)\gamma_\mu\psi(x))\gamma_\mu\psi(x)\right], \\
O_A &= \mathrm{Tr}\left[(\bar{\psi}(x)\gamma_5\gamma_\mu\psi(x))\gamma_5\gamma_\mu\psi(x)\right], \\
O_T &= \mathrm{Tr}\left[(\bar{\psi}(x)\sigma_{\mu\nu}\psi(x))\sigma_{\mu\nu}\psi(x)\right],
\end{aligned}$$

where ψ is any four component Dirac spinor, the following identities known as Fierz identities hold:

$$O_V(x) = -O_A(x) = O_S(x) - O_P(x), O_T(x) = -O_S(x) - O_P(x). \tag{B.7}$$

If the spinor is a Majorana field it is easy to show that

$$O_S(x) = O_P(x) = O_A(x) = 0 \tag{B.8}$$

holds.

Appendix C

The conjugate gradient with preconditioning

On different occasions throughout this work we had to calculate matrix elements of the inverse fermion matrix $\Delta_{xa\alpha}^{yb\beta} = (Q^{-1})_{xa\alpha}^{yb\beta}$. For this task a conjugate gradient algorithm (see for example [68]) and even-odd preconditioning of the fermion matrix have been implemented.
The conjugate gradient algorithm is a minimization algorithm. To use it for the calculation of matrix elements of the inverse fermion matrix we have to reformulate this problem in terms of a minimization problem. This can be achieved by noticing that solving the linear system

$$Az = b, \tag{C.1}$$

where A is a hermitian positive definite $N \times N$ matrix is equivalent to minimizing the functional

$$f(z) = \frac{1}{2} \langle z, Az \rangle - bz. \tag{C.2}$$

Starting from the functional

$$g(z) = Az - b, \tag{C.3}$$

with an initial vector z_1, the initial residuum $r_1 = b - Az_1$ and the search-direction $p_1 = r_1 = -g(z)$ the algorithm is defined by the iteration

$$\begin{aligned}
\alpha_i &= \frac{< r_i, r_i >}{< p_i, Ap_i >}, \quad z_{i+1} = z_i + \alpha_i p_i, \\
r_{i+1} &= r_i - \alpha_i A p_i, \quad \beta_i = \frac{< r_{i+1}, r_{i+1} >}{< r_i, r_i >}, \\
p_{i+1} &= r_{i+1} + \beta_i p_i.
\end{aligned}$$

In our case the matrix A is the fermion matrix Q which is neither hermitian nor positive definite. Remembering however that $\tilde{Q} = \gamma_5 Q$ is hermitian, we can multiply (C.1) by $Q^\dagger$. We arrive at

$$Q^\dagger Q z = \tilde{Q}^2 z = Q^\dagger b, \tag{C.4}$$

and can apply the conjugate gradient to the above equation to solve for z. Note that this introduces an extra multiplication with the adjoint fermion matrix.
The rate at which the conjugate gradient algorithm converges depends on the condition number of the matrix Δ, which is the ratio of its largest and smallest eigenvalue $k(\Delta) = \lambda/\epsilon$. The closer $k(\Delta)$ is to one the faster is the convergence of the algorithm [69].
To accelerate the inversion of the fermion matrix Q we invert instead the preconditioned matrix $\bar{Q}$ which has an eigenvalue spectrum with the eigenvalues closer to each other. Even-odd preconditioning in multi-bosonic algorithms has been introduced in [70]. To define the preconditioned matrix, first we rearrange the space-time lattice points in even and odd sites according to $\sum_{\mu=1}^{4} x_\mu$,

$$\lambda = \begin{pmatrix} \lambda_{even} \\ \lambda_{odd} \end{pmatrix} \rightsquigarrow Q = \begin{pmatrix} 1\!\!1 & KM_{even-odd} \\ -KM_{odd-even} & 1\!\!1 \end{pmatrix}, \tag{C.5}$$

where $\lambda_{even(odd)}$ corresponds to the Majorana field on the even (odd) sites. The next step is to decompose the Matrix Q according to

$$Q = L\bar{Q}U = \begin{pmatrix} 1\!\!1 & 0 \\ -KM_{oe} & 1\!\!1 \end{pmatrix} \begin{pmatrix} 1\!\!1 & 0 \\ 0 & 1\!\!1 - K^2 M_{oe} M_{eo} \end{pmatrix} \begin{pmatrix} 1\!\!1 & -KM_{eo} \\ 0 & 1\!\!1 \end{pmatrix}. \tag{C.6}$$

The inverse matrices of U and L are given by

$$L^{-1} = \begin{pmatrix} 1\!\!1 & 0 \\ KM_{oe} & 1\!\!1 \end{pmatrix}, \quad U^{-1} = \begin{pmatrix} 1\!\!1 & KM_{eo} \\ 0 & 1\!\!1 \end{pmatrix}. \tag{C.7}$$

To show now how we perform the inversion with the preconditioned matrix we start with equation (C.1) where $A = Q$, and where we have multiplied with γ_5

$$\begin{aligned} \gamma_5 Q z = \gamma_5 b \quad &\Leftrightarrow \quad \gamma_5 L\bar{Q}U z = \gamma_5 b \\ &\Leftrightarrow \quad \gamma_5 L\bar{Q}\gamma_5\gamma_5 U z = \gamma_5 b \\ &\Leftrightarrow \quad \gamma_5 L\tilde{\bar{Q}}\gamma_5 U z = \gamma_5 b \\ &\Leftrightarrow \quad z = U^{-1}\gamma_5 \tilde{\bar{Q}}^{-1} L^{-1} b. \end{aligned}$$

In the above calculation we have written $\tilde{\bar{Q}} = \bar{Q}\gamma_5$, which is hermitian like $\tilde{Q} = \gamma_5 Q$ [1]. Since the conjugate gradient algorithm allows only positive definite hermitian matrices we have to modify the last of the above equations by the insertion of $1\!\!1 = \tilde{\bar{Q}}^{-1}\tilde{\bar{Q}}$. Finally we get

$$z = U^{-1}\gamma_5 (\tilde{\bar{Q}}^2)^{-1} \tilde{\bar{Q}} L^{-1} b. \tag{C.8}$$

In this form we can now for a given vector b solve $Qz = b$, by inverting $\tilde{\bar{Q}}^2$ using the conjugate gradient and multiplying with L^{-1} ,U^{-1} and $\tilde{\bar{Q}}$ which are known.

[1] Note that the hermitian form of the preconditioned matrix $\tilde{\bar{Q}}$ is defined by multiplying with γ_5 from the right, while for the simple fermion matrix we multiply with γ_5 from the left. This is merely a convention and the reason for this difference lies in the way in which the first software for our project was designed.

Preconditioning in the above manner introduces extra matrix multiplications which amount to three additional fermion matrix multiplications. However, the rate of convergence of the conjugate gradient is much better in the case of the preconditioned matrix and the overall saving in CPU-time is about a factor of two [43].
For suitable choices of the vector b the solution vector z can be any column of the matrix A^{-1} or any linear combination of different columns. Choosing for example the vector b as $b = \delta_{xa\alpha}^{\tilde{y}\tilde{b}\tilde{\beta}}$ for a fixed $\tilde{y}$, $\tilde{b}$ and $\tilde{\beta}$ projects out exactly the column $\tilde{y}\tilde{b}\tilde{\beta}$ of the matrix A^{-1} of (C.1). Because the fermion matrix has the form (A.19) to find the inverse for a fixed space-time point (which we refer to as a local or a point-like source in this work) 2 (spin) $\times 3$ (color) inversions are necessary. This means that six applications of the conjugate gradient algorithm are enough to allow a calculation of matrix elements with a fixed source and spin and color indices that are summed over.
To determine for example the connected part of the gluinoball correlator (2.27) the inverse of the fermion matrix was calculated in this way with a randomly chosen source $\tilde{x}$ for all configurations that were available on the $12^3 \times 24$ lattice (see table (3.2)). This was also tried out on the gluino-glueball and for the correlators involved in the Ward identity, but the results achieved were not satisfactory in either of these cases.
When Jacobi smearing is involved the source b must be chosen in a different way. Applying the smearing in case of the gluino-glueball and the expectation values in the Ward identity we had to calculate expressions of the form

$$\Delta_{xa\alpha}^{yb\beta'} F^{bb'}(y, y_s) \mathrm{Tr}[U_{kl}(y_s)\sigma^{b'}]\sigma_{kl}^{\beta'\beta}, \tag{C.9}$$

for fixed y_s. The matrix $F^{bb'}(y, y_s)$ represents here the Jacobi smearing-matrix defined in Chapter 2.2.6. To calculate this expression we proceed as follows. We start with a point source for b of (C.1) as described in the last paragraph. The lattice site y_s this source is at is chosen randomly, and we define

$$b_{\tilde{x}\tilde{a}\tilde{\alpha}}^{kl} = \delta_{\tilde{x}}^{y_s} \delta_{\tilde{\alpha}}^{\beta'} \mathrm{Tr}[U_{kl}(y_s)\sigma^{\tilde{a}}] \tag{C.10}$$

for fixed y_s and fixed β' and a fixed pair of (kl). This source vector is then multiplied with the Jacobi matrix $F^{bb'}(y, y_s)$ and the product is taken as source for the inversion. To calculate the typical correlators of the form (2.31) we need to apply the conjugate gradient six times, for each spatial index pair $(kl) \in \{12, 23, 13\}$ and the spin indices $\beta' = 1, \beta' = 3$ [2].

[2] Because of equation (A.19) the indices $\beta' = 2$ and $\beta' = 4$ can be left out.

Bibliography

[1] K. Wilson, *Phys. Rev.* **D 10** (1974) 2445.

[2] N. Seiberg and E. Witten, *Nucl. Phys.* **B 431** (1994) 484.

[3] N. Seiberg and E. Witten, *Nucl. Phys.* **B 426** (1994) 19.

[4] N. Seiberg, *Nucl. Phys.* **B 435** (1995) 129.

[5] G. Veneziano and S. Yankielowicz, *Phys. Lett.* **B 113** (1982) 231.

[6] G. R. Farrar, G. Gabadadze and M. Schwetz, *Phys. Rev.* **D 58** (1998) 15009.

[7] M. Lüscher, *Phys. Lett.* **B 428** (1998) 342.

[8] M. Lüscher, *Nucl. Phys.* **B 549** (1999) 295.

[9] G. Curci and G. Veneziano, *Nucl. Phys.* **B 292** (1987) 555.

[10] M. Lüscher, *Nucl. Phys.* **B 418** (1994) 637.

[11] I. Montvay, *Nucl. Phys.* **B 466** (1996) 259.

[12] I. Campos, A. Feo, R. Kirchner, I. Montvay, K. Spanderen *et al.*, *Eur. Phys. J.* **C 11** (1999) 507.

[13] L. Girardello and M. T. Grisaru, *Nucl. Phys.* **B 194** (1982) 65.

[14] A. Kovner and M. Shifman, *Phys. Rev.* **D 56** (1997) 2396.

[15] D. Amati, K. Konishi, Y. Meurice, G. Rossi and G. Veneziano, *Phys. Rep.* **162** (1988) 169.

[16] R. Kirchner, S. Luckmann, I. Montvay, K. Spanderen and J. Westphalen, *Phys. Lett.* **B 446** (1999) 209.

[17] J. Wess and J. Bagger, *Supersymmetry and Supergravity*, Princeton University Press, 2nd ed., 1992.

[18] V. A. Novikov, M. A. Shifman, A. I. Vainshtein and V. I. Zakharov, *Nucl. Phys.* **B 229** (1983) 381.

[19] G. West, *Phys. Rev. Lett.* **77** (1996) 2622.

[20] N. Evans, D. Hsu and M. Schwetz, *hep-th/9707260* (1997).

[21] K. Fujikawa, *Phys. Rev. Lett.* **42** (1979) 1195.

[22] T. Galla, Supersymmetrische und Chirale Ward-Identitäten in einer diskretisierten N=1-SUSY-Yang-Mills-Theorie, *Diploma Thesis, Universität Münster* (1999).

[23] H. Nicolai and P. Dondi, *Nuovo Cim.* **41 A** (1977) 1.

[24] S. Elitzur, E. Rabinovici and A. Schwimmer, *Phys. Lett.* **B 119** (1982) 165.

[25] T. Banks and P. Windey, *Nucl. Phys.* **B 198** (1982) 226.

[26] J. Bartels and G. Kramer, *Z. Phys.* **C 20** (1983) 159.

[27] J. Bartels and J. B. Bronzan, *Phys. Rev.* **D 28** (1983) 818.

[28] H. B. Nielsen and M. Ninomiya, *Phys. Lett.* **B 105** (1981) 219, *Nucl. Phys.* **B 185** (1981) 20 [E: **B 195** (1982) 541], *ibid.* **B 193** (1981) 173.

[29] E. Witten, *Phys. Lett.* **B 117** (1982) 324.

[30] I. Montvay and G. Münster, *Quantum Fields on the lattice*, Cambridge University Press, 1994.

[31] A. Donini, M. Guagnelli, P. Hernandez and A. Vladikas, *Nucl. Phys.* **B 523** (1998) 529.

[32] S. Sharpe and N. Shoresh, *Nucl. Phys. Proc. Suppl.* **83-84** (2000) 968.

[33] M. Teper, *Phys. Lett.* **B 183** (1986) 345.

[34] C. R. Allton, C. T. Sachrajda, R. Baxter, S. Booth, C. Bowler *et al.*, *Phys. Rev.* **D 47** (1993) 5128.

[35] S. Güsken, U. Löw, K. Mütter, R. Sommer, A. Patel *et al.*, *Nucl. Phys. Proc. Suppl.* **B 17** (1990) 361.

[36] M. Albanese, F. Costantini, G. Fiorentini, F. Flore, M. Lombardo *et al.*, *Phys. Lett.* **B 192** (1987) 163.

[37] M. J. Teper, *hep-th/9812187* .

[38] B. Berg and A. Billoire, *Nucl. Phys.* **B 221** (1983) 109.

[39] Y. Kuramashi, M. Fukugita, H. Mino, M. Okawa and U. Ukawa, *Phys. Rev. Lett.* **72** (1994) 3448.

[40] E. Elitzur, *Phys. Rev.* **D 12** (1975) 3978.

[41] E. Gabrielli, A. Gonzalez-Arroyo and C. Pena, *Int. J. Mod. Phys.* **A 15** (2000) 553.

[42] W. Rarita and J. Schwinger, *Phys. Rev. Lett.* **60** (1941) 61.

[43] K. Spanderen, Monte Carlo Simulationen von SU(2) Yang-Mills Theorien mit dynamischen Gluinos, *PhD Thesis, Universität Münster* (1998).

[44] M. Bochicchio, L. Maiani, G. Martinelli, G. Rossi and M. Testa, *Nucl. Phys.* **B 262** (1985) 331.

[45] L. Karsten and J. Smit, *Nucl. Phys.* **B 183** (1981) 103.

[46] Y. Taniguchi, *hep-lat/9906026 v2* (1999).

[47] A. Vladikas, The SUSY WIs on the lattice. A Memorandum on Strategies., (2000) unpublished.

[48] A. Donini and M. Guagnelli, *Phys. Lett.* **B 383** (1996) 301.

[49] D. Talkenberger, Monte-Carlo-Simulationen von Modellen der Elementarteilchenphysik mit dynamischen Fermionen., *PhD Thesis, Universität Münster* (1997).

[50] G. Koutsoumbas, I. Montvay, A. Pap, K. Spanderen, D. Talkenberger *et al.*, *Nucl. Phys. Proc. Suppl.* **B 63** (1998) 727.

[51] R. Kirchner, S. Luckmann, I. Montvay, K. Spanderen and J. Westphalen, *Nucl. Phys. Proc. Suppl.* **73** (1999) 828.

[52] A. Borelli, P. de Forcrand and A. Galli, *Nucl. Phys.* **B 477** (1996) 809.

[53] I. Montvay, *Comput. Phys. Commun.* **109** (1998) 144.

[54] W. Schrörs, Private communication, (2000).

[55] R. Frezzotti and K. Jansen, *Phys. Lett.* **B 402** (1997) 328.

[56] D. Kaplan and M. Schmaltz, Talk given at Chiral '99 Taipei, September 13-18, *hep-lat/0002030* (2000).

[57] A. Sokal, Monte Carlo Methods in Statistical Mechanics: Foundations and New Algorithms, *Cours de Troisième Cycle de la Physique en Suisse Romande Lausanne* (1989).

[58] H. Flyvbjerg and H. Petersen, *J. Chem. Phys.* **91** (1989) 461.

[59] G. R. Farrar, G. Gabadadze and M. Schwetz, *Phys. Rev.* **D 60** (1999) 035002.

[60] G. Koutsoumbas and I. Montvay, *Phys. Lett.* **B 398** (1997) 130.

[61] A. Vladikas, *Nucl. Phys. Proc. Suppl.* **47** (1996) 84.

[62] G. Rossi, *Nucl. Phys. Proc. Suppl.* **53** (1997) 3.

[63] G. M. Divitiis and R. Petronzio, *Phys. Lett.* **B 419** (1998) 311.

[64] S. Capitani, M. Guagnelli, M. Lüscher, S. Sint, R. Sommer *et al.*, *Nucl. Phys. Proc. Suppl.* **63** (1998) 153.

[65] T. Bhattacharya, S. Chandrasekharan, R. Gupta, W. Lee and S. Sharpe, *Phys. Lett.* **B 461** (1999) 79.

[66] G. Martinelli, S. Petrarca, C. T. Sachrajda and A. Vladikas, *Phys. Lett.* **B 311** (1993) 241.

[67] A. Donini, V. Giménez, G. Martinelli, M. Talevi and A. Vladikas, *Eur. Phys. J.* **C 10** (1999) 121.

[68] T. Kalkreuter and H. Simma, *Comput. Phys. Commun.* **93** (1996) 33.

[69] A. Boriçi, Technical Report, Swiss Center for Scientific Computing, (1996).

[70] B. Jegerlehner, *Nucl. Phys. Proc. Suppl.* **B 53** (1997) 959.

Acknowledgments

First I would like to thank my supervisor Dr. István Montvay, who suggested the topic of this work to me, for his constant support his encouragement, and the many interesting and stimulating discussions we had.
Special thanks go to my collaborator Federico Farchioni. Discussing physics with him has always been a pleasure, a source of new fruitful ideas, and an opportunity to learn. I also owe my thanks to him for proofreading the first manuscript of this work.
In many stages of this work I profited from vivid and pleasurable conversations with Anastassios "Tassos" Vladikas. Through his precise questions and comments I had the opportunity to learn many things about spectroscopy, and Ward identities on the lattice. For his constant encouragement and the sharing of his view of physics I am greatly in debt to him.
I am grateful to Jörg Westphalen, who introduced me to C^{++} and the CRAY T3E.
It is a great pleasure to thank my friends and colleagues Oliver Bär and Matthias Bolz, who were never far, in the rougher and in the more quiet times we shared at DESY.
Special thanks go to my dear friend Konstantin von Achten for the great time we had. Life at Hamburg would not have been the same without him.
Furthermore I want to thank my brother Jochen, who even though far away gave me great support in completing this work.
I also thank Margarete Mühlleitner for her helpful comments on supersymmetry.
Finally I would like to thank all my colleagues at DESY, and the members of the theory group, in particular York Schröder, Frank Eberlein, Claus Gebert, Arndt Brandenburg and Francesco Vissani for the pleasant and stimulating atmosphere.
The numerical simulations presented here have been performed on the CRAY-T3E computers at NIC Jülich. I thank HLRZ and the staff for their kind and competent support.
Financial support by Deutsches Elektronen-Synchrotron (DESY) is gratefully acknowledged.